

# The role of the nucleotide-binding proteins FlhF and FlhG during flagellar biosynthesis

---



Doctoral Thesis

Submitted in Fulfilment of the Requirements

of a Doctoral Degree in Chemistry

(Dr. rer. nat.)

to the

Department of Chemistry,

Philipps-Universität Marburg

**Carina Knauer**

Unna (Nordrhein-Westfalen)

Marburg an der Lahn, 2016

Vom Fachbereich Chemie der Philipps-Universität Marburg (Hochschulkenziffer 1180) als  
Dissertation am 06.10.2016 angenommen.

Erstgutachter: Dr. Gert Bange (Fachbereich Chemie, Philipps-Universität Marburg)

Zweitgutachter: Prof. Dr. Peter Graumann (Fachbereich Chemie, Philipps-Universität Marburg)

Tag der Disputation:

Die Untersuchungen zur vorliegenden Dissertation wurden in der Zeit vom Oktober 2013 bis Juli 2016 unter der Leitung von Herrn Dr. Gert Bange an der Philipps-Universität Marburg durchgeführt.

## **ERKLÄRUNG**

(gemäß § 10, Abs. 1 der Promotionsordnung der Mathematisch-Naturwissenschaftlichen Fachbereiche und des Medizinischen Fachbereichs für seine mathematisch-naturwissenschaftlichen Fächer der Philipps-Universität Marburg vom 15.07.2009)

Ich versichere, dass ich meine vorgelegte Dissertation:

„The role of the nucleotide-binding proteins FlhF and FlhG during flagellar biosynthesis“

selbst und ohne fremde Hilfe verfasst, nicht andere als die in ihr angegebenen Quellen oder Hilfsmittel benutzt, alle vollständig oder sinngemäß übernommenen Zitate als solche gekennzeichnet sowie die Dissertation in der vorliegenden oder einer ähnlichen Form noch bei keiner anderen in- oder ausländischen Hochschule anlässlich eines Promotionsversuches oder zu anderen Prüfungszwecken eingereicht habe.

---

Ort, Datum

---

Carina Knauer

Die im Laufe meiner Promotion entstandenen Daten sind in folgenden Originalpublikationen veröffentlicht:

**1. The MinD-like ATPase FlhG effects location and number of bacterial flagella during C-ringassembly**

Schuhmacher JS, Rossmann F, Dempwolff F, Knauer C, Altegoer F, Steinchen W, Dörrich A, Klingl A, Stephan M, Linne U, Thormann K and Bange G (2015) PNAS, 112 (10), 3092-7

**2. The role of FlhF and HubP as polar landmark proteins in Shewanella putrefaciens CN-32.**

Rossmann F, Brenzinger S, Knauer C, Bubendorfer, S, Ruppert U, Bange G, Thormann K (2015). *Molecular Microbiology*, DOI: 10.1111/mmi.13152

**3. FlhG Employs Diverse Intrinsic Domains and Influences FlhF GTPase Activity to Numerically Regulate Polar Flagellar Biogenesis in Campylobacter jejuni.**

Gulbranson CJ, Ribardo DB, Balaban B, Knauer C, Bange G, Hendrixson DR (2015). *Molecular Microbiology*, doi: 10.1111/mmi.13231

# Abstract

Flagella are bacterial organelles of locomotion and present one the smallest motors in the living organisms. Their architecture can be divided into a cytoplasmic C-ring, the membrane-embedded basal body and the extracellular hook and filament structures. While flagellar structure and constituents are conserved among the bacterial species, number and localization of flagella at the bacterial cell surface are not. Instead, they appear in species-specific patterns that are characterized by defined number and places of the flagella. For example, *Shewanella putrefaciens* exhibits one flagellum at one cell pole (monotrichous), while the food-borne pathogen *Campylobacter jejuni* features one flagellum at both cell poles (amphitrichous). In contrast, the Gram-positive bacterium *Bacillus subtilis* shows approximately 25 flagella that are regularly spaced at the lateral sides and are absent from the cell poles (peritrichous). Importantly, these patterns are reproduced during each cycle of cell division and have been used as an early criterion for the taxonomic classification of bacteria. An essential question for understanding bacterial cell physiology is how these flagellation patterns are maintained? During the past decade, the two nucleotide-binding proteins FlhF and FlhG have been identified as key players for the spatial and numerical regulation of flagella. Most notably, both proteins are highly conserved but manage different types of flagellation patterns. The major aim of this work was to understand the function of FlhF and FlhG in regulating flagellation patterns. I could show that FlhF and FlhG form a regulatory unit in the monotrichous *Shewanella putrefaciens* and the amphitrichous *Campylobacter jejuni*. Similar to the situation in the peritrichous *B. subtilis*, the N-terminal fraction of FlhG stimulates the GTPase activity of the homodimeric GTPase FlhF via a conserved 'DQAxLR' motif (x = any amino acid). These findings suggest that the regulation of FlhF by FlhG is highly conserved among differently flagellated bacteria and does probably not account for the diversity FlhF/FlhG-dependent flagellation patterns. This notion is also supported by in-depth biochemical and structural analysis of the FlhG enzymes from *Shewanella putrefaciens* and *Campylobacter jejuni*. To better understand how the FlhF/FlhG unit can regulate different flagellation patterns, I next set out to identify interaction partners of FlhF and FlhG in the monotrichous *Shewanella putrefaciens* and the peritrichous *B. subtilis*. In *Shewanella putrefaciens*, I could show the FlhG interacts with the C-ring protein complex of FliM/FliN via the conserved 'EIDAL' motif of FliM. This is in contrast to the situation in *B. subtilis* where FlhG also interacts with the FliM/FliY complex, however, via a motif within the N-terminus of

FliY. This finding presents the first differences between FlhF/FlhG-dependent regulation of a monotrichous and peritrichous flagellation pattern. My search for interaction partners of FlhF showed that the protein interacts with ribosomes, the SRP-RNA and the FliM/FliN (FliY complex). In monotrichous *Shewanella putrefaciens*, the three-domain protein FlhF interacts via its N-terminal and natively unfolded B-domain with the ribosome, the SRP-RNA and the FliM/FliN. Definition of the binding sites showed that they localize within the first 40 amino acids of the protein and seem to partially overlap. However, further studies need to clarify the molecular details. Similarly, the B-domain of FlhF from the peritrichous *B. subtilis* also interacts with the C-ring protein complex FliM/FliY via the FliY protein. While many questions remain open, I would like to suggest a working hypothesis that combines and reflects the current knowledge about FlhF/FlhG with the data obtained in this work.

# Zusammenfassung

Das bakterielle Flagellum ermöglicht vielen Bakterien die Fortbewegung in ihrer Umgebung und repräsentiert einen der kleinsten Motoren in lebenden Organismen. Die Architektur des Flagellums kann in einen zytoplasmatischen C-Ring, einen in der Membran eingebetteten Basalkörper und in die extrazellulären Strukturen Hacken und Filament eingeteilt werden. Während die Struktur des Flagellums und deren Bestandteile innerhalb der Bakterien konserviert sind, variiert die Anzahl und die Lokalisation der Flagellen artspezifisch an der Bakteriellen Zelloberfläche. *Shewanella putrefaciens* besitzt beispielsweise nur ein Flagellum an einem Zellpol (monotrich), während die Lebensmittel übertragbaren Erreger *Campylobacter jejuni* ein Flagellum an beiden Zellpolen (amphitrich) aufweist. Im Gegensatz dazu findet man bei den Gram-positiven Bakterien *Bacillus subtilis* (peritrich) ca. 25 Flagellen, die entlang der Zelllänge regelmäßig angeordnet sind und dabei die Zellpole aussparen (peritrichous). Diese sogenannten Muster werden bei jedem Zellteilungs-Zyklus neu gebildet. Welcher regulatorische Mechanismus hinter der Aufrechterhaltung des artspezifischen Flagellen-Musters steckt, ist eine der wesentlichen Fragen in der bakteriellen Zellphysiologie. Während der letzten zehn Jahre wurden die beiden Nukleotid-bindenden Proteine FlhF und FlhG als wichtige Akteure für die räumliche und numerische Regelung der Flagellen identifiziert. Bemerkenswert dabei ist, dass diese hoch konservierten Proteine unterschiedliche Arten von Flagellierungs-Mustern verwalten. Das Hauptziel dieser Arbeit war es, die Funktion von FlhF und FlhG während der Regulierung von unterschiedlichen Flagellen Mustern zu verstehen. Ich konnte zeigen, dass FlhF und FlhG als regulatorische Einheit in dem monotrichen *Shewanella putrefaciens* und dem amphitrichen *Campylobacter jejuni* agieren. Das stimmt mit der Situation in dem peritrichen *B. subtilis* überein, wo der N-terminale Bereich von FlhG die GTPase-Aktivität der homodimeren GTPase FlhF über ein konserviertes „DQAxLR“ Motiv (x = beliebige Aminosäure) stimuliert. Diese Ergebnisse deuten darauf hin, dass die Regulation von FlhF durch FlhG in unterschiedlich flagellierten Bakterien hoch konserviert ist und somit wahrscheinlich nicht für die Vielfalt von FlhF/FlhG abhängigen Flagellen-Mustern verantwortlich ist. Diese Vermutung wird durch eingehende biochemische und strukturelle Analysen der FlhG Enzyme aus *Shewanella putrefaciens* und *Campylobacter jejuni* unterstützt. Für ein besseres Verständnis, wie FlhF/FlhG als Einheit unterschiedliche Flagellen Muster regulieren, sollten Interaktionspartner von FlhF und

FlhG im monotrichen *S. putrefaciens* und im peritrichen *B. subtilis* identifiziert werden. In *S. putrefaciens*, konnte ich zeigen, dass FlhG mit dem C-Ring-Protein-Komplex FliM/FliN über das konservierte „Eidal“ Motiv von FliM interagiert. Das steht im Gegensatz zur Situation in *B. subtilis*, wo FlhG auch mit dem FliM/FliY-Komplex interagiert, jedoch interagiert hier FlhG über ein Motiv innerhalb des N-Terminus von FliY. Diese Entdeckung ist einer der ersten Unterschiede zwischen einer FlhF/FlhG-abhängigen Regulierung eines monotrichen und peritrichen Flagellen-Musters. Die Suche nach Interaktionspartnern für FlhF, zeigt, dass FlhF mit Ribosomen, der SRP-RNA und mit FliM/FliN (FliY) interagiert. In *S. putrefaciens* interagiert das Drei-Domänen-Protein FlhF über seine N-Terminale nativ ungefaltete B-Domäne mit Ribosomen, SRP-RNA und dem FliM/FliN-Komplex. Untersuchungen der Interaktions-Bindestellen zeigten, dass diese innerhalb der ersten 40 Aminosäuren lokalisiert sind und teilweise überlappen. Des Weiteren konnte auch im peritrichen *B. subtilis* nachgewiesen werden, das FlhF mittels seiner B-Domäne mit dem C-Ring-Protein-Komplex FliM/FliY interagiert. In diesem Rahmen werden weitere Studien benötigt, um die molekularen Details zu klären. Während noch viele Fragen offen bleiben, schlage ich eine Arbeitshypothese vor, die das aktuelle Wissen um FlhF/FlhG und den hier gewonnenen Daten kombiniert und widerspiegelt.



# Table of contents

<b>1. Introduction .....</b>	<b>1</b>
<b>1.1 Bacterial motility .....</b>	<b>1</b>
<b>1.2 Bacterial Flagellum .....</b>	<b>2</b>
1.2.1 Architecture of the flagellum.....	4
1.2.2 C-ring.....	5
1.2.3 Flagella regulation .....	6
<b>1.3 Flagellation pattern .....</b>	<b>8</b>
1.3.1 Dual flagellation systems.....	9
<b>1.4 Regulation of flagellation pattern .....</b>	<b>10</b>
1.4.1 Landmark protein systems for localization of the flagella .....	12
<b>1.5 Regulation of flagellation patterns by FlhF and FlhG.....</b>	<b>13</b>
1.5.1 FlhF and FlhG.....	13
1.5.2 Role of FlhF and FlhG in polar flagellated bacteria.....	16
1.5.2.1 Monotrichous flagellation.....	16
1.5.2.2 Amphitrichous and lophotrichous flagellation .....	17
1.5.3 Role of FlhF and FlhG in peritrichous flagellated bacteria .....	18
<b>1.6 SRP-System.....</b>	<b>19</b>
1.6.1. Rearrangement of the SRP-System during the targeting process.....	20
<b>Aim of work .....</b>	<b>22</b>
<b>2. Results.....</b>	<b>23</b>
<b>2.1 The ATPase FlhG of <i>Shewanella putrefaciens</i> and <i>Campylobacter jejuni</i> .....</b>	<b>23</b>
2.1.1. Purification of FlhG from <i>S. putrefaciens</i> and <i>C. jejuni</i> .....	24
2.1.2 Crystallization of CjFlhG .....	25
2.1.2.1 Structure determination and refinement of CjFlhG.....	25
2.1.2.2 Crystal structure of the monomeric CjFlhG .....	25
2.1.2.3 Catalytic motifs and ADP coordination of monomeric CjFlhG .....	27
2.1.2.4 The C-terminal amphipathic helix of CjFlhG.....	28
2.1.3 ATPase activity of FlhG .....	29
<b>2.2 Interaction partners of FlhG.....</b>	<b>32</b>
2.2.1 FlhG interacts with FlhF and stimulates its GTPase activity .....	32
2.2.2 C-ring components of the polar and lateral Flagella system in <i>Shewanella putrefaciens</i> .	35

2.2.3 FlhG interacts with a component of the polar C-ring of <i>Shewanella putrefaciens</i> .....	36
2.2.4 Formation of the FlhG-FliM <sub>1</sub> /FliN <sub>1</sub> complex requires the ‘EIDALL’ motif .....	37
2.2.5 FlhG and C-ring components of <i>C. jejuni</i> .....	39
<b>2.3 Crystallization of SpFliN<sub>1</sub> from <i>S. putrefaciens</i> .....</b>	<b>41</b>
2.3.1 Structure determination and refinement of SpFliN <sub>1</sub> .....	41
2.3.1 Crystal structure of FliN <sub>1</sub> .....	42
<b>2.5 Characterization of FlhF .....</b>	<b>43</b>
2.5.1 Purification of FlhF from <i>S. putrefaciens</i> .....	44
2.5.2 The N-terminal region of FlhF from <i>S.putrefaciens</i> .....	44
2.5.3 The N-terminus of FlhF pulls interacts with ribosomes .....	46
2.5.4 FlhF associates with ribosomes .....	47
2.5.5 The N-terminal region of FlhF interacts with SRP-RNA.....	49
2.5.5.1 Ffh and FtsY modulate the interaction of FlhF-N32 with SRP-RNA .....	50
2.5.6 Interaction of FlhF with C-ring components in <i>B. subtilis</i> .....	51
2.5.6.1 The B-domain of <i>B. subtilis</i> FlhF interacts with the FliN-homology domain of the C-ring protein FliY .....	52
<b>3. Discussion .....</b>	<b>54</b>
<b>3.1 The nucleotide-binding proteins FlhF and FlhG.....</b>	<b>54</b>
<b>3.2 FlhG supports C-ring assembly .....</b>	<b>56</b>
3.2.1 Bifunctional role of FlhG .....	59
<b>3.3 The mysterious role of FlhF .....</b>	<b>61</b>
3.3.1 The B-domain of FlhF: a platform for multiple interactions.....	62
<b>3.4 Species independent and species dependent interaction partners of FlhG and FlhF .....</b>	<b>64</b>
<b>3.5 Conclusion &amp; Open questions .....</b>	<b>65</b>
<b>4. Material and methods .....</b>	<b>68</b>
<b>4.1 Materials .....</b>	<b>68</b>
4.1.1 Chemicals .....	68
4.1.2 Bacterial strains and plasmids. ....	68
4.1.2.1 Plasmids.....	68
4.1.3 Oligonucleotides.....	70
4.1.4. Enzymes and cloning equipment.....	72
4.1.5 Protein biochemistry.....	72
4.1.6 Crystallization.....	72
4.1.6.1 Data collection at the ESRF.....	73
4.1.7 Growth media and buffers .....	73
4.1.8 Antibiotics .....	74
4.1.9 Laboratory equipment.....	75

<b>4.2 Methods</b> .....	<b>76</b>
4.2.1 Molecular cloning .....	76
4.2.2 Isolation of plasmid DNA from <i>E. coli</i> .....	77
4.2.3 Agarose gel electrophoresis .....	77
4.2.4 Purification of recombinant proteins .....	77
4.2.5.1 Ribosome purification .....	78
4.2.5.2 Ribosome high and low salt wash .....	78
4.2.6 SDS-Page .....	79
4.2.7 Western blotting and immunodetection .....	79
4.2.8 Protein interaction assays .....	80
4.2.8.1 Glutathione-S-transferase (GST) .....	80
4.2.8.1 Ni-NTA affinity .....	80
4.2.9 Protein crystallization .....	80
4.2.9.1 Data collection .....	80
4.2.10 GTPase/ATPase assays .....	81
<b>5. Literatur</b> .....	<b>82</b>
<b>6. Apendix</b> .....	<b>90</b>
<b>Supplementary table</b> .....	<b>90</b>
<b>Table of figures</b> .....	<b>92</b>
<b>Abbreviations</b> .....	<b>94</b>
<b>Acknowledgments</b> .....	<b>97</b>
<b>Curriculum Vitae</b> .....	Fehler! Textmarke nicht definiert.

# 1. Introduction

## 1.1 Bacterial motility

For most bacteria, motility plays a key role for the survival under changing environmental conditions. To this end, bacteria have evolved remarkable motility systems during the course of evolution. The majority of motile bacteria move by rotating a long helical filament, the bacterial flagellum. The bacterial flagellum is an impressive nanomachine, which enables bacteria to move through liquids and highly viscous environments (swimming) or move in communities across surfaces (swarming) (**Figures 1A and B**, (1-3)). Flagella-mediated motility is not only responsible for locomotion, but also plays a central role in biofilm formation, virulence and antibiotic resistance (3–5). A special case is the unique flagella-mediated movement of the spirochetes. They possess periplasmic flagella, which are enclosed between the outer membrane and the peptidoglycan layer and are attached to each end of the protoplasmic cylinder. The rotation of these periplasmic flagella results in a serpentine movement of the whole cell body (6). Another way to crawl over surfaces without the aid of flagella is called twitching (**Figure 1C**). Bacteria which are moving by twitching motility (e.g.; *Neisseria gonorrhoeae* and *Pseudomonas aeruginosa*) use Type IV pili that are often extended from the cell poles (1). The cell propulsion accrues by pilus extension, attachment to a surface and pilus retraction resulting in a jerky movement. The fourth way to move is independent from flagella or pili and is known as gliding. Gliding motility results in a membrane protrusion at the cell pole and is dependent on a large set of proteins (**Figure 1D**). In brief, many flexible ‘legs’ composed of proteins project outside the cell and are supported by cytoskeletal structures from inside the cell (reviewed in (7)). The force resulting in repeated binding, pull and release of the ‘legs’ is generated by ATP hydrolysis of the intracellular compounds. However, under fast changing living conditions, flagella-mediated motility is the fastest and most effective way of movement for bacteria.

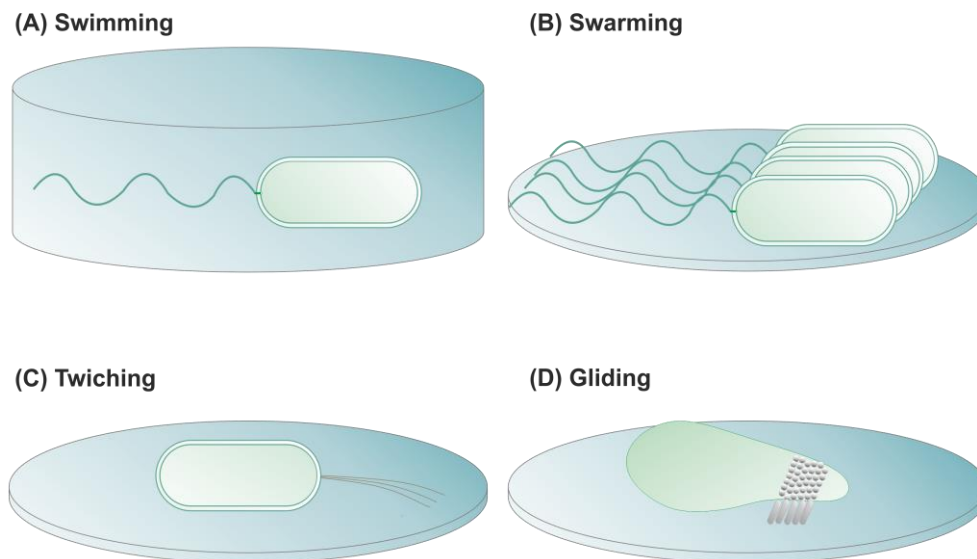


**Figure 1: Bacterial motility.** Flagella mediated motility includes (A) swimming through liquid medium and (B) swarming where cells move in communities over semi-solid surfaces. (C) Twitching motility is mediated by type IV pili and allows bacteria to crawl over surfaces. (D) Gliding motility on the example of the centipede model organism *Mycoplasma mobile*. Large cell surface proteins build the ‘legs’ close to the ‘neck’ of *M. mobile*. Conformational changes of the legs mediated by motor components in the cytoplasm or cytoplasmic membrane result in gliding cell movement. The image was adapted from ref. (1, 8).

## 1.2 Bacterial Flagellum

The bacterial flagellum represents one of the tiniest complex motors in the biosphere. Nevertheless, it generates an enormous power by rotating  $\sim 100.000$  times per minute (*Vibrio alginolyticus* (9)) driven by proton motor force (PMF) generated by the MotA/B complex of the flagellar basal body (**Figure 2B** and 1.2.1). By this, bacteria are able to attain a very high speed in proportion to their size with some species achieving  $\sim 200x$  of their body length per second (10). The flagella-mediated motility is based on a well-studied process named chemotaxis. This chemosensory system allows bacteria to change the direction of swimming depending on the presence of nutrients or repellents (reviewed in (11)). This sensory input is integrated by switching the rotation direction of the flagellum between counterclockwise (CCW) and clockwise (CW) resulting in swimming in one direction or a change of swimming direction by tumbling, respectively.

Core flagella components are fairly conserved across motile bacteria and can be divided into four major building parts (**Figure 2A**). Firstly, the membrane-spanning basal body, which generates the driving force and allows the secretion of the flagella subunits. Secondly, a rod, which traverses the cell membrane and cell wall and transfers the rotary motion to the outer flagella components. Of note, the rod slightly differs between Gram-positive and Gram-negative bacteria owing to the differing thickness of the peptidoglycan layer and the presence of an outer membrane. Thirdly, an extracellular hook serves as hinge to transfer motor generated rotation from the rod onto the filament. Last but not least, the filament consisting of more than 20,000 subunits of the protein flagellin pushes the cell through the environment.

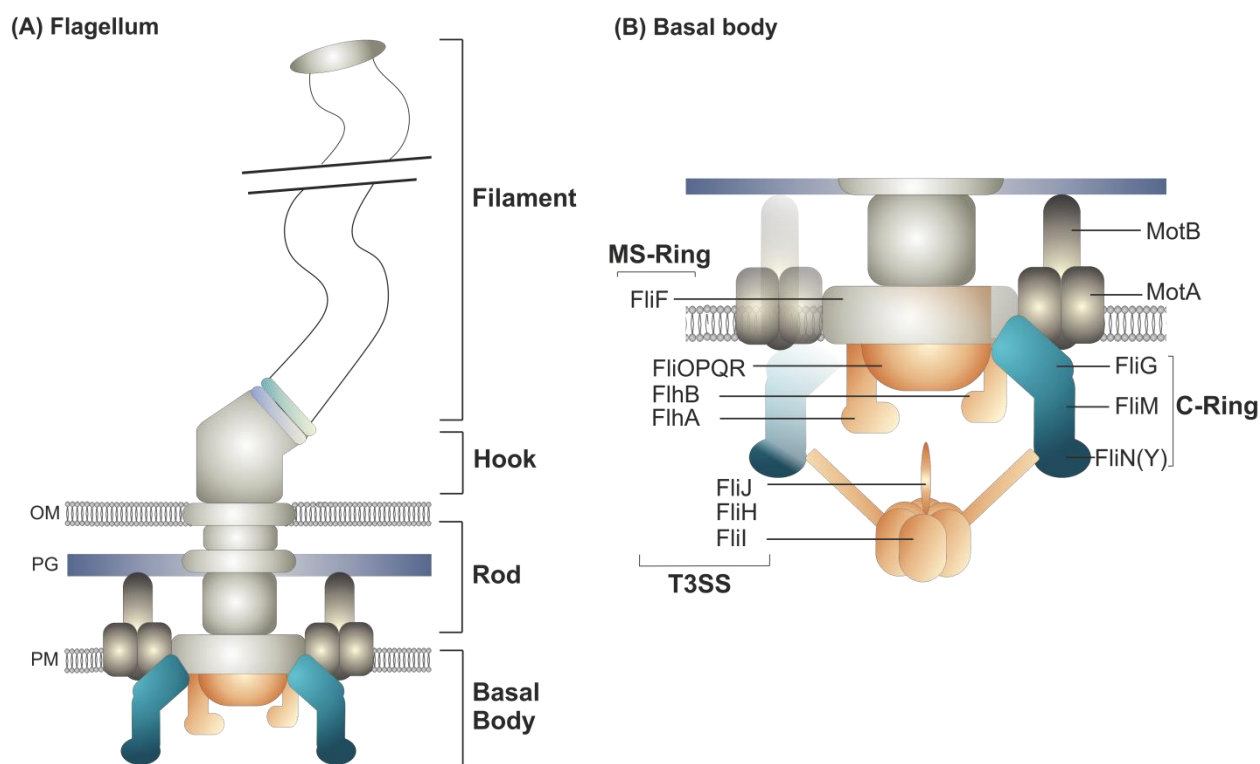


**Figure 2: Architecture of the bacteria.** (A) Scheme of a bacterial flagellum of a Gram-negative bacterium with the four major building blocks: basal body, rod, hook and filament. A detailed description is given in the text. The abbreviations are: PM: plasma membrane, PG: peptidoglycan, OM: outer membrane. (B) Detailed scheme of the membrane-embedded basal body consisting of the flagellar type III secretion system (fT3SS) in light brown, the C-ring in dark blue and the MS-ring in light grey. The motor components MotA/B are colored in dark grey. The figure was adapted from ref. (12).

### 1.2.1 Architecture of the flagellum

The general structure of the bacterial flagellum is well understood. Flagella biogenesis is executed in a highly hierarchical order and begins with the assembly of the basal body (**Figures 2A, B**). The earliest events in assembly involve the integral membrane components belonging to the flagellar type III secretion system (fT3SS) and a cytoplasmic membrane ring structure (MS-ring) (13–16). The fT3SS creates a central pore within the cytoplasmic membrane and is composed of six trans-membrane proteins (i.e.; FlhAB, FliOPQR) and three soluble components (i.e.; FliH, FliI, FliJ). The fT3SS mediates the export of extracellular flagellar building blocks and is essential for flagellar assembly (reviewed in (12, 17, 18)). The fT3SS is surrounded by the MS-ring, which consists of 26 copies of the FliF protein and serves as a mounting plate for the cytoplasmic ring structure (C-ring). The three proteins FliG, FliM and FliN (also named FliY in *Bacillus subtilis*) constitute the C-ring that is required for torque generation but also transmits chemosensory signals to change the rotary direction of the flagellum between CCW and CW allowing changes in swimming direction (see 1.1). Interaction of FliG with FliF and the motor protein complex MotA/B (**Figure 2B**) transduces the PMF generated by the latter onto the extracellular flagellar components (i.e.; the hook and filament) via the MS-ring (reviewed in (19)). The interaction of FliM with the phosphorylated component of the chemosensory system CheY leads to a change of FliG's conformational state thereby changing the direction of the flagellar rotary direction ((19–21), reviewed in (11)). Assembly of the flagellar rod is probably also dependent on the fT3SS, however it is still unknown whether other factors guiding rod assembly exist (22). The flagellar rod is less conserved among Gram-positive and Gram-negative bacteria due to the different architecture of the cell wall and cell membrane (22). The extracellular hook is composed of 120 subunits of the FlgE protein and transmits the torque from the basal body to the filament. The last step of flagella biosynthesis is the assembly of the filament, a long, hollow tube polymer composed of over 20000 copies of flagellin. The extracellular assembly of flagellin is mediated by the pentameric FliD cap structure present at the nascent end of the growing filament (reviewed in (12, 18)).

### 1.2.2 C-ring

The flagellar C-ring generates the torque and rotational switching and is important for flagellar assembly. The C-ring is composed of multiple copies of FliG (~26), FliM (~34) and FliN (~120) (**Figure 3A**, (22, 23)). The upper part of the C-ring is formed by FliG, which is directly involved in the torque generation and consists of three domains (**Figure 3B**). FliG establishes multiple protein-protein interactions with the motor complex, other proteins of the C-ring and the MS-ring. The N-terminal domain of FliG (FliG<sub>N</sub>) interacts with FliF while the C-terminal domain (FliG<sub>C</sub>) binds the membrane embedded MotA. Interaction of FliG with FliM is mediated by a hydrophobic part within FliG<sub>C</sub> and a conserved 'EHPQR' motif in its middle domain (FliG<sub>M</sub>) (24, 25). The second flagellar C-ring component is the three-domain protein FliM (**Figure 3B**). The middle domain of FliM binds through its conserved 'GGXG' motif to FliG (26–28). The N-terminal domain of FliM includes the high conserved 'EIDAL' motif which mediates binding of the phosphorylated form of the response regulator CheY, a member of the intracellular chemotaxis system (29–32). Upon binding of CheY to FliM, the interaction interface between FliG-MotA is rearranged leading to a switch of flagella rotation from CCW to CW (33–35). CCW rotation leads to cells which swim smoothly, whereas CW rotation causes cells to tumble and reorient (36, 37). The C-terminal domain of FliM interacts with FliN constituting the lower part of the C-ring. The domain architecture of FliN shows variations among the bacterial kingdom. While the FliN of mostly Gram-negative species only harbors the FliN-homology domain, some bacteria like *B. subtilis* possess FliY comprising the FliN-homology domain and an additional CheC-phosphatase domain at their N-terminus (**Figure 3B**, (38)). One study also suggests a direct interaction between FliN and CheY thereby influencing the rotational switch of the flagellum (39). The presence of both FliY and FliN in some organisms such as *Helicobacter pylori* or *Campylobacter jejuni* contests its precise functions in flagellar assembly and regulation (reviewed in (6)). FliN interacts with FliH, a member of the cytoplasmic ATPase complex (FliH, FliI, FliJ) which is sorting substrates for export and their efficient entry into the FT3SS (41, 42). This FliN-FliH interaction mediates the localization of the ATPase complex (41).



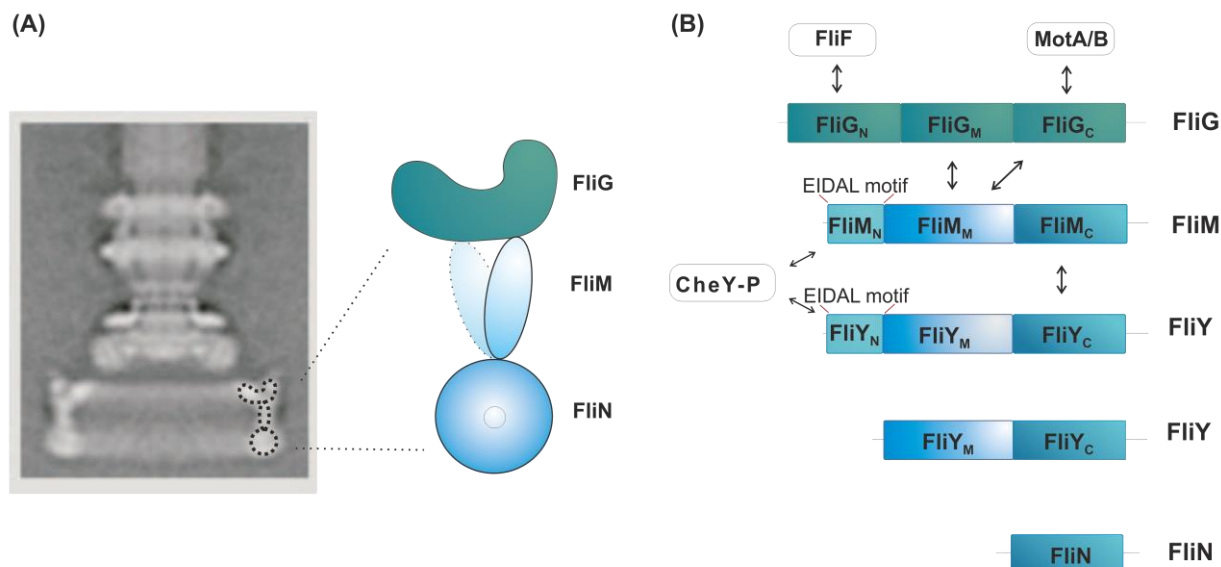
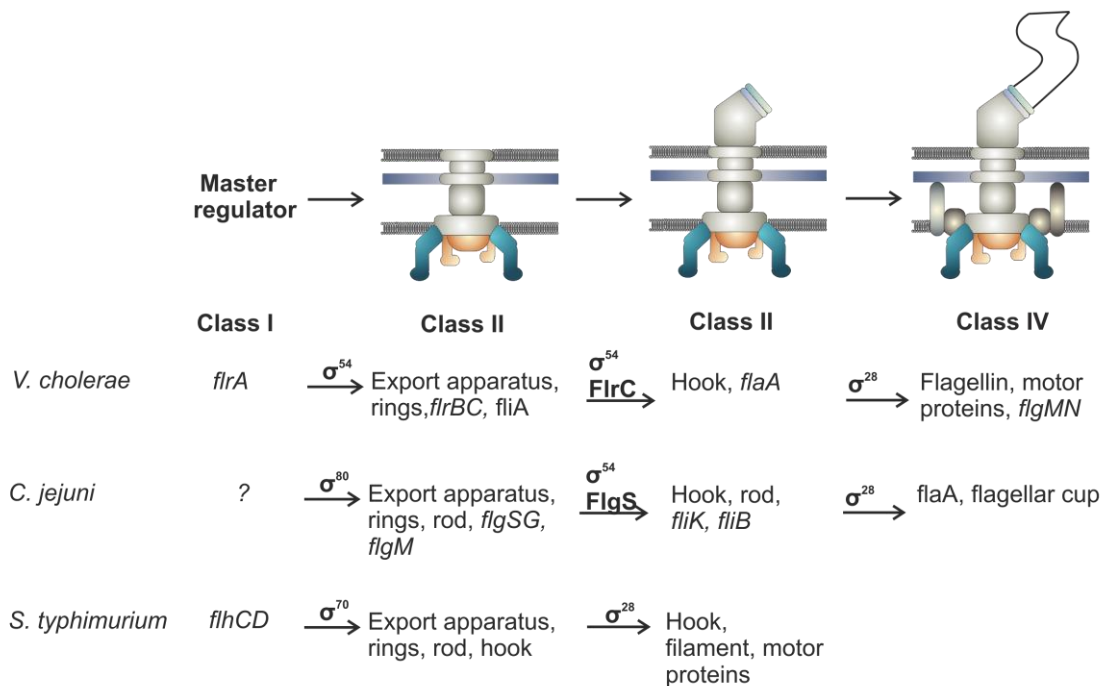


**Figure 3: The flagellar C-ring.** (A) The flagellar basal body of *Salmonella typhimurium* (43). The dashed lines indicate the C-ring components FliG, FliM and FliN. (B) Schematic representation of the domain architecture of FliG, FliM and FliN(Y). The arrows indicate direct interactions between the proteins. The figure was slightly adapted from ref. (24).

### 1.2.3 Flagella regulation

The expression of a flagellum is an energetically expensive process and involves more than 40 genes (44,45). Therefore, bacteria utilize hierarchical regulatory networks to control the ordered expression of the individual flagellar components to ensure correct flagella biogenesis. The transcriptional hierarchy has been extensively investigated in *E. coli* (reviewed in (22)), *S. typhimurium* (46), *Caulobacter crescentus* (47), *Vibrio parahaemolyticus* (48), *Vibrio cholerae* (49) and *C. jejuni* (reviewed in (50)) and revealed that the underlying regulatory mechanisms differ between these organisms (reviewed in (51)). Despite the differences between the regulatory programs used, these organisms share a conspicuous feature. In all cases, the flagellar genes can be classified based on their temporal expression and on their dependence on various nested transcriptional regulators (**Figure 4**) and reviewed in (16, 44–46). In the peritrichous flagellated *S. typhimurium*, three operon classes are described: class I genes encode the early flagellar proteins, class II genes for the middle flagellar proteins and the class III for the late flagellar proteins (53). Important components of the class I genes encode the master regulator FlhCD that together with the sigma factor  $\sigma^{70}$  controls the expression of the class II genes (44). The class II genes encode components for the basal body and the hook,  $\sigma^{28}$  (FliA) and the corresponding anti- $\sigma^{28}$  (FlgM) (54). FlgM inhibits  $\sigma^{28}$  up to the completion of the basal body at which FlgM can be






secreted from the cell via the  $\sigma^{28}$ . Subsequently,  $\sigma^{28}$  is then able to activate the transcription of the class III genes finalizing the flagellum and implementing the components of the chemotaxis system (55). The  $\sigma^{28}$ -FlgM interaction apparently serves as key checkpoint for the regulation of flagella biosynthesis. One of the most significant differences between the well-studied regulatory system of *Salmonella* species and that of other organisms (e.g.; *C. jejuni* and *V. cholerae*, **Figure 4**) is the use of alternative sigma factors. In the monoflagellate *V. cholerae*, the transcriptional hierarchy is divided in four classes of genes (49). Here, the class I genes encode the master regulator FlrA (FleQ) which in association with the alternative sigma factor  $\sigma^{54}$  regulates the transcription of class II genes. Class II consists of structural and regulatory components, including the two-component system (FlrBC) and the alternative  $\sigma^{28}$  (56). Class III genes are dependent on  $\sigma^{54}$  and FlrC for their activation. Upon the completion of the hook-basal body complex, FlgM is secreted from the cell and in turn  $\sigma^{28}$  can initiate the class IV genes (57). Again, expression and export of flagellin and motor proteins complete the flagellar assembly.



**Figure 4: Flagellar gene transcription hierarchies.** Three model systems for flagellar gene regulation found in *V. cholerae*, *C. jejuni* and *S. typhimurium*, respectively, are depicted. Gene transcription of flagellar genes can be divided into different stages (class I-IV). Sigma factors and regulatory proteins representing major checkpoints between the different stages are indicated above the arrows. The figure was adapted from ref. (58, 59).

### 1.3 Flagellation pattern

The core flagellar components and the basic principles of their transcriptional control mechanism during flagellar assembly are highly conserved among the motile bacteria. However, the flagella appear in a species-specific arrangement along the cell body in different number and location leading to different flagellation patterns characteristic for each species. The localization of the flagella at the cell body can either be spread over the entire length of the cell body or is limited to the cell pole. The number of flagella can range from one to more than 100 flagella per cell. Flagellation patterns of bacteria can be roughly divided into five major classes: peritrichous, medial, monotrichous, amphitrichous, and lophotrichous (**Figure 5**).

	Arrangement	Classification	Examples
(A)		Peritrichous	<i>Escherichia</i> <i>Salmonella</i> <i>Bacillus</i>
(B)		Medial	<i>Rhodobacter</i>
(C)		Monotrichous	<i>Vibrio</i> <i>Pseudomonas</i> <i>Caulobacter</i> <i>Shewanella</i>
(D)		Amphitrichous	<i>Campylobacter</i>
(E)		Lophotrichous	<i>Helicobacter</i>

**Figure 5: Bacterial flagellation patterns.** Schematic representations of flagellar patterns. A) Peritrichous: multiple flagella along the cell body. B) Medial: a single flagellum along the cell body. C) Monotrichous: one single flagellum at the pole. D) Amphitrichous: one single flagellum at both cell poles. E) Lophotrichous: more than one flagellum at one pole. The figure was slightly adapted from ref. (60).

Many bacterial clades shows peritrichous flagellation exhibiting many flagella distributed over the whole cell body including the cell pole (**Figure 5A**). Well-known representatives of this group are *E. coli*, *Salmonella enterica* and *B. subtilis* (14, 60, 61). *Rhodobacter sphaeroides* possesses only one flagellum at mid-cell and belongs to the group of medial-flagellated bacteria (**Figure 5B**, (62)). Polar flagellation where flagella are restricted to the cell pole(s) appears in different shapes (**Figure 5C-E**). Monotrichous-flagellated bacteria such as *V. cholera*, *P. aeruginosa* and *C. crescentus* carry one single flagellum at one cell pole (**Figure 5C**, (47, 48,

63)). *C. jejuni* exhibits one single flagellum at each cell pole and belongs to the group of amphitrichous-flagellated bacteria (**Figure 5D**, (64)). Lophotrichous flagellation is found in the human pathogen *H. pylori* and is characterized by bearing more than one flagellum at one cell pole (**Figure 5E**, (65)).

### 1.3.1 Dual flagellation systems

Highly viscous environments or surfaces reduce flagella-mediated motility. In this case, many peritrichous bacteria like *B. subtilis*, *E. coli*, *S. enterica* and *Proteus mirabilis* produce swarmer cells and increase the flagella number. In contrast, some polar flagellated bacteria are able to produce a second independent flagellar system. Bacteria able to form these so called dual flagella systems are *V. alginolyticus*, *V. parahaemolyticus*, *Shewanella putrefaciens*, *Azospirillum ssp.* and *Rhodospirillum ssp.* (reviewed in (66, 67), (68–70)). The primary and secondary flagella are encoded as separate gene cluster at different places on the genome (**Figure 6**, (48, 71)). Usually, the primary polar flagellum is present under all growth conditions. However, flagella of the secondary system are generated under specific conditions. *V. parahaemolyticus* induces the synthesis of several additional lateral flagella in viscous environments or on surfaces resulting in a polar-peritrichous flagellation pattern (66, 71). Another recently identified candidate harboring a dual flagella system is the Gram-negative marine bacterium *S. putrefaciens* (72). In contrast to *Vibrio ssp.*, *S. putrefaciens* exhibits only one or two additional lateral flagella which improve the navigation and swim behavior of *Shewanella* in a viscous milieu (**Figure 6A**, (72, 73)). A recent study illuminates the two gene clusters (cluster 1 and 2) encoding the primary and secondary flagellar system of *S. putrefaciens*, respectively (**Figure 6B**, (72)). Cluster1 contains genes encoding most structural units, all regulatory and assembly components for the polar flagellum and parts of the chemotaxis system (**Figure 6B**). Components of the secondary flagella are encoded in cluster 2 and contain all major structural subunits and components for flagellar assembly, some regulatory units and include the genes for the stator components (**Figure 6B**). However, cluster 2 lacks genes encoding components of the chemotaxis signaling pathway and distinct homologs of FlhF and FlhG necessary for the regulation flagella number and placement. The absence of components of the chemotaxis system fits to the observation that the secondary flagellar system does not respond to chemotactic signals (73).

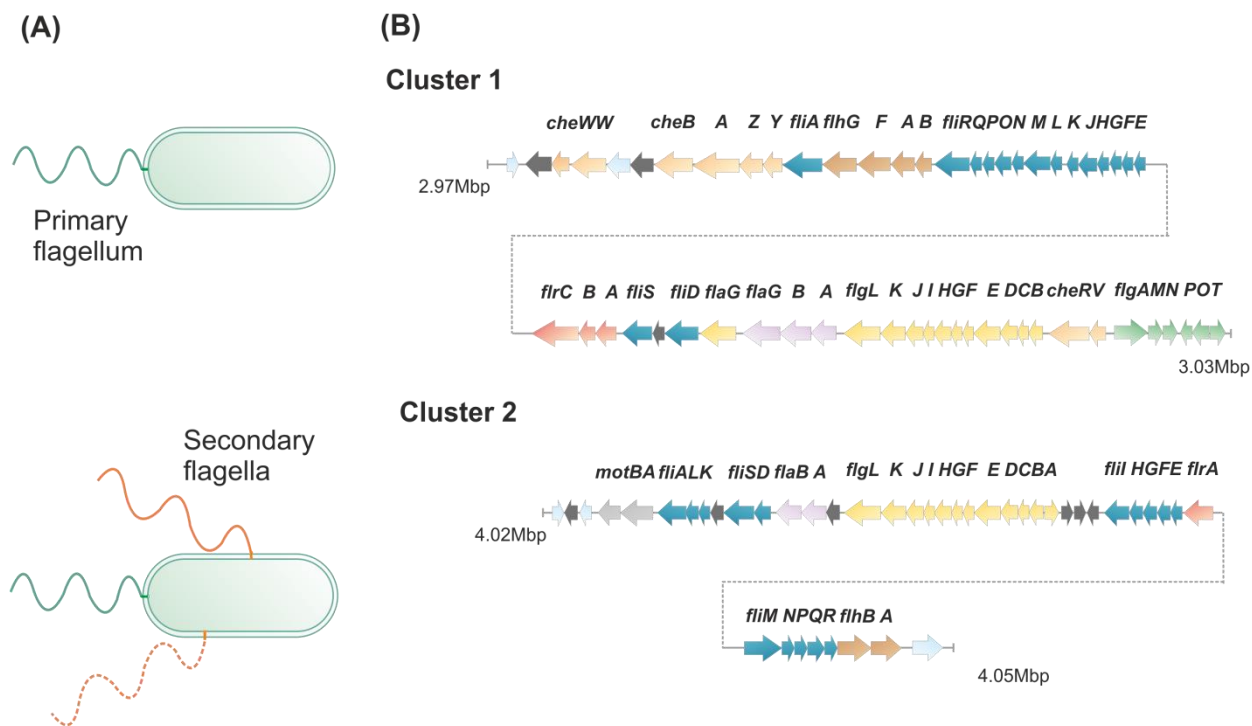


**Figure 6: Dual flagella system of *S. putrefaciens*.** (A) *S. putrefaciens* processes two independent flagellar systems, a single polar flagellum (primary flagellum, green) and one or two lateral flagella (secondary flagella, orange) only generated under specific growth conditions. (B) Both flagellar systems are encoded by different gene clusters in the genome of *S. putrefaciens*. Cluster 1 encodes for the primary, cluster 2 for the secondary flagellum. Color coding: *fli*-genes are dark blue, *flg*-genes are yellow, *flh*-genes are brown and *fla*-genes are light purple. The main regulators (*fliR*) are colored in red. Genes encoding for the chemotaxis genes are colored in light orange. The light blue colored genes have no names but their gene product has an annotated function. Genes colored in dark grey encode hypothetical proteins. The numbers indicate the position in the genome of *S. putrefaciens* CN-32. The figure was adapted from ref. (73).

## 1.4 Regulation of flagellation pattern

‘Flagellar research’ has primarily focused on the structure of the flagellum and how regulation ensures the sequential addition of subunits into the nascent flagellar structure. For a long time, the model organisms *E. coli*, *B. subtilis* and *S. enterica* were in the focus of intensive research. It was assumed that peritrichous flagellated bacteria like *E. coli* or *B. subtilis* generate a randomly distributed flagellation pattern. However, current studies in *E. coli* demonstrate that flagellar formation mainly avoids the cell pole and reveal an increased number of flagella in the old half of the cell during cell division (61). Similarly, *B. subtilis* contains 20 to 25 flagella that are not positioned randomly along the cell body. Instead, they are organized in a grid-like pattern around the mid-cell with minimal distances of approximately 0.4  $\mu\text{m}$  between each other (60). These

studies strongly suggest that the spatial and numerical arrangements of flagella underlie tight regulatory control regimes. The reproducible polar arrangement of one or more flagella after each cell division suggests an intrinsically regulation. The mechanisms by which bacteria recognize the cell pole or the control of spatial and numerical parameters of flagella biosynthesis are still poorly understood for most bacteria. In some polar-flagellated organisms, flagella localization is clearly mediated by ‘landmark’ proteins. However these landmark proteins are not restricted to flagellation localization but are also important for the correct localization of other processes such as chromosome segregation and cell division (74–76).

### 1.4.1 Landmark protein systems for localization of the flagella

One well-studied model organism for cell cycle regulation and polarity is *C. crescentus*. This Gram-negative  $\alpha$ -proteobacterium divides after each cell cycle into two morphologically and functionally different bacterial cells: a motile, DNA replication-quiescent swarmer cell and a sessile, DNA replication-competent, stalked cell (77–79). The swarmer cell possesses a cluster of type IV pili and a single polar flagellum at one pole. After a differentiation process that involves shedding of the flagellum, retraction of the pili and building of an adhesive stalk at the previously flagellated pole, the cell starts to elongate and constrict. During the cell cycle, *C. crescentus* forms a predivisional cell with a new assembled flagellum at one pole and a stalk at the other and divides into stalked cell which starts immediately with the next round of cell division and a new swarmer cell (77). The generation and progression of an asymmetric cell cycle requires an elaborate regulatory network of proteins, many of which localize to a specific pole of the cell. Several studies identified a number of components that are involved in this regulatory process. One of these proteins is TipN, a membrane coiled-coil protein that retracts at the previous cell division site and serves as a landmark protein to ensure the positioning of the flagellum during the cell cycle (74). Deletion of TipN leads to an increased number and dislocated flagella (74). TipN mediates the polar localization of TipF, a transmembrane protein with phosphodiesterase activity for cyclic di-guanosine monophosphate (c-di-GMP) which is important for the flagella assembly (80). TipF recruits a third flagella positioning factor PflI to the pole. When the flagellated predivisional cell constricts, TipN and TipF relocate to the cell division site and interact with the cytokinesis machinery. Upon completion of cell division, TipN and TipF are localized exclusively to the new cell pole. It is proposed that TipN/F act as a landmark protein system for subsequent targeting of flagellar components. Nevertheless, it is still unknown how TipN localizes during the cell cycle to the appropriate position and whether orthologues of TipN and/or TipF with a similar are present in other  $\alpha$ -proteobacteria.

A further landmark protein has recently been identified in *V. cholerae*, the multi-domain protein HubP which controls polar localization of the chromosome origin, the chemotactic machinery and the flagellum (81). Interestingly, all of these three structures rely on their corresponding ParA-like ATPases important for polar localization. ParA is required for the chromosome origin, ParC for chemotaxis proteins and FlhG for flagella components (81). HubP is a transmembrane protein, conserved among *Vibrio ssp.* and anchors the three ATPases to the pole. A deletion of

HubP disrupts the chemotactic system, the oriC is not targeted to the pole and cell populations shows increased number of flagella (81). A functional orthologue of VcHubP was found in *S. putrefaciens* suggesting that general features and mechanisms are conserved between HubP-like proteins of different species. Like VcHubP, SpHubP plays a role in proper chromosome segregation and recruitment of chemotaxis proteins (82). In contrast to VcHubP, SpHubP has no effect on the positioning of flagella but is crucial for normal flagella function (82).

## 1.5 Regulation of flagellation patterns by FlhF and FlhG

How bacteria regulate their flagella positioning is just at the beginning of being understood. Besides the landmark proteins (see above), the two proteins FlhF and FlhG (synonyms: YlxH, FleN, MinD2) are important for spatial and numerical control of flagellation. It is evident that FlhF and FlhG control most of the flagellation patterns found in bacteria (reviewed in (83, 84)). However, the underlying mechanisms allowing FlhF and FlhG to fulfill this important task are still cryptic.

### 1.5.1 FlhF and FlhG

FlhF belongs to the signal recognition particle (SRP)-MinD-BioD (SIMIBI) class of nucleotide-binding proteins and together with Ffh and FtsY constitutes the subfamily of SRP-GTPases (85,86). The SRP-protein Ffh and SRP-receptor protein FtsY together form universally conserved machinery that targets the ribosome nascent chain complex (RNCs) to the membrane. FlhF, Ffh and FtsY share significant sequence homology within their NG-domains consisting of a regulatory domain (N-domain) and the GTPase domain (G-domain) (**Figure 7A**). In the presence of GTP, Ffh and FtsY form a heterodimer that is necessary for the transfer of the RNC to the translocon (87, 88). In contrast, FlhF forms a GTP-dependent homodimer of so far unknown function. FlhF comprises a basic and natively unfolded domain (B-domain) N-terminal of its NG-domain. In contrast, FtsY harbors an acidic domain (A-domain) instead while Ffh possesses a C-terminal extension (**Figure 7A**).



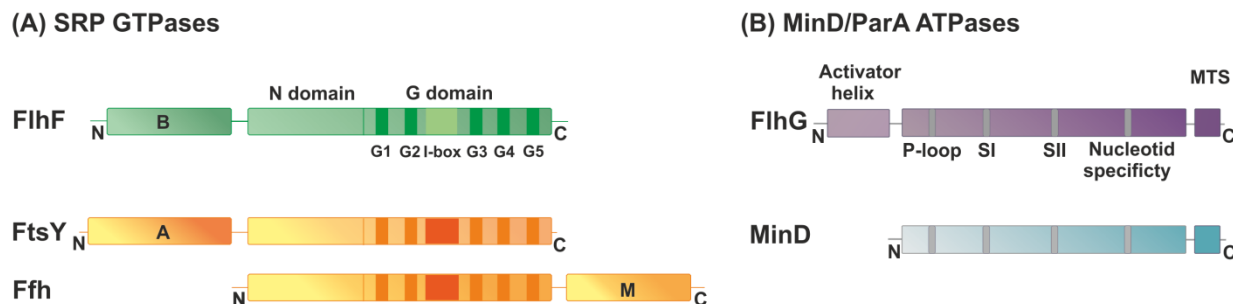


**Figure 7: Domain architecture of FlhF and FlhG.** (A) Domain structure of FlhF in comparison to the other proteins of the SRP-System, FtsY and Ffh. SRP-GTPase specific motifs, the insertion box (I-box) and conserved motifs for GTPase activity (G1-G5), are indicated. (B) Comparison of the domain structure of the ATPases FlhG and MinD. FlhG and MinD share specific motifs for ATPase activity, the P-loop (also Walker A), the switch regions I and II (SI and SII) essential for nucleotide recognition and a membrane targeting sequence (MTS). In addition, FlhG harbors a highly conserved motif DQAxLR (also named: activator helix) at its N-terminus, which stimulates the GTPase activity of FlhF.

FlhG is a ATPase, belongs to the SIMIBI class of NTPases and shows a high homology to the ATPase MinD (**Figure 7B**, (89)). MinD is part of the Min-system, which is required for the formation of cytokinetic Z-ring during cell division (90). MinD is able to form ATP-dependent homodimers that associate with the cytoplasmic membrane via its C-terminal amphipathic helix acting as membrane targeting sequence (MTS). The membrane associated MinD recruits MinC, which hinders polymerization of the Z-ring. Subsequently, the third member of the Min-System MinE disassembles the MinCD complex, whereby MinC and MinD dissociate from the membrane and diffuse to the opposite cell pole where polymerization starts again. This repetitive cycle (or oscillator) leads to a minimum of the MinC at mid-cell, where cell division occurs (reviewed in (91, 92)).

Like MinD, FlhG can form homodimers, which depend on ATP and phospholipids. The association with the membrane is mediated through the MTS (compare to MinD, (89)). In addition, FlhG harbors an N-terminal extension with a highly conserved ‘DQAxLR’ motif. The first molecular evidence that FlhG interacts directly with FlhF was performed in *B. subtilis* (93). Here it was shown that FlhG interacts via its N-terminus with the NG-domain of FlhF. The first 20 N-terminal amino acid residues (activator helix) of FlhG are necessary and sufficient for interaction stimulation of FlhF’s GTPase activity. (93). A crystal structure of FlhF-NG and the

activator helix of FlhG revealed that the conserved glutamine (Q8) side chain of FlhG inserts into the composite active site of the FlhF-NG homodimer and repositions the G2 arginine finger residue to stabilize the transition state geometry of the nucleotide substrate (93). GTPases often function as a molecular switch that changes between an inactive apo- or GDP-bound state and an active GTP-bound state. This 'GTPase switch' paradigm, in which a GTPase acts as a bimodal switch that is turned in a 'on' and 'off' state by external regulatory factors, serves in regulation of many fundamental cell processes. In this case, the GTPase FlhF together with FlhG forms a regulatory circuit, where FlhG triggers the transition of the active GTP-bound dimeric conformation of FlhF into a monomeric inactive conformation (**Figure 8**). Interestingly, some *Pseudomonas* and *Xanthomonas* species harbor an FlhG homologue which lacks the N-terminal 'DQAxLR' motif and it is unclear whether FlhG interacts with FlhF or stimulates its activity in these species (reviewed in (84) and (63)).

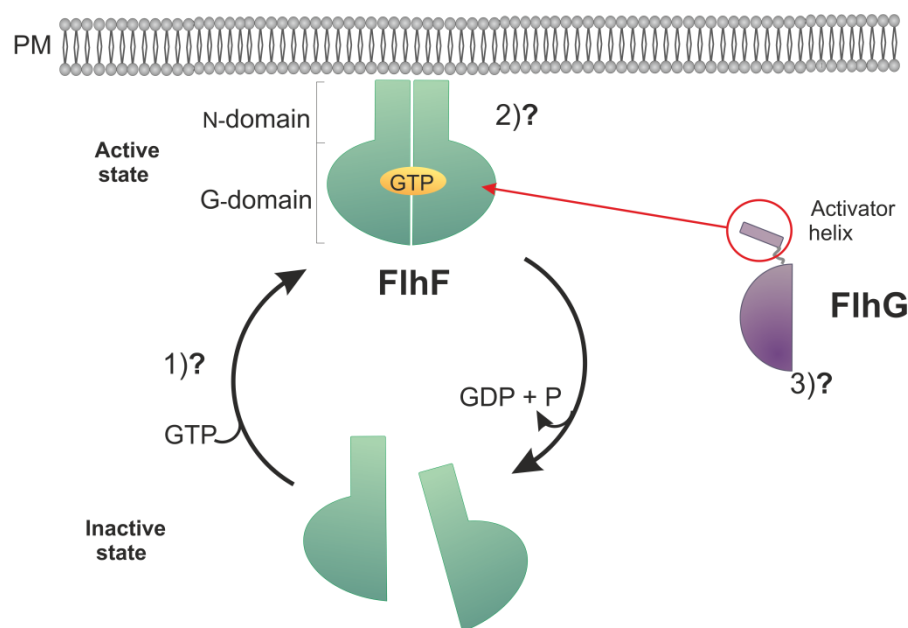


**Figure 8: Schematic model of the FlhF/FlhG cycle.** FlhF (green) is a molecular switch which changes between an active GTP-bound state (homodimer) and an inactive state (monomer). FlhG (purple) stimulates the GTPase activity of FlhF via its N-terminal activator helix. The FlhF homodimer localizes at the membrane that upon GTP-hydrolysis enters into its monomeric inactive state and dissociates from the membrane. This regulatory cycle of FlhF and FlhG raises some fundamental yet still unanswered questions. 1) What are the precise functions of the different states of FlhF? 2) How does FlhF associate with the membrane? 3) Does the monomeric or the dimeric state of FlhG stimulate FlhF?

## 1.5.2 Role of FlhF and FlhG in polar flagellated bacteria

The functional role of FlhF/FlhG has been mainly investigated in polar flagellated bacteria by cell biological and molecular genetic approaches.

### 1.5.2.1 Monotrichous flagellation

For a monotrichous flagellation in bacteria it is believed that the new flagellum is synthesized at the old cell pole of the daughter cell. In many polar-flagellated bacteria, fluorescent microscopy revealed a polar localization of FlhF mainly at the flagellated pole, even in the absence of other flagellar proteins (16). In *V. cholerae* it is supposed that FlhF is necessary for the recruitment of FlhF, which composes the inner membrane MS ring of the flagellum (16).

Although FlhF is highly conserved among bacteria and appears to be required for proper spatial arrangement of flagella at the poles in many polar flagellates, the mutation of FlhF revealed different effects on flagellation in some bacteria. While a deletion of FlhF in *Vibrio* species results in non-flagellated cells, knockout of FlhF in *P. aeruginosa* leads to a mislocated flagellum (94–96). In contrast, overproduction of FlhF in *Vibrio* and *Pseudomonas* species shows a hyper-flagellated phenotype (reviewed in (83, 84, 97)). Deletion of FlhG leads to hyper-flagellated cells in *Vibrio* or *Pseudomonas* that are severely impaired in motility (94, 98). Furthermore, it was shown that in *V. alginolyticus* the polar localization of FlhF depends on the presence of FlhG (99). In *V. alginolyticus* it was observed that FlhF localized both on the membrane and in the cytoplasm (**Figure 9A**). In contrast, deletion of FlhG shows an exclusive localization of FlhF at the cell pole, whereas an overproduction of FlhG results in an increased level of FlhF in the cytoplasm, indicating that FlhG releases FlhF from the pole (**Figure 9B, C**).

Furthermore, it has been demonstrated that FlhF and FlhG acts as transcriptional regulators for flagellar gene expression. The FlhG orthologue in *P. aeruginosa* is able to interact with FleQ (synonyms: FlrA, FlaK), a c-di-GMP-dependent master regulator, which activates the  $\sigma^{54}$ -transcription for further flagellar gene transcription (63, 100). It can be supposed that FlhG represses transcription of early class I genes by downregulation of FleQ, whereas FlhF acts as downstream activator of class III genes (63, 101, 102). Despite the varied consequences of deletion of FlhF/FlhG in different polar flagellated bacteria, these observations support the current model of action of FlhF and FlhG. In this, FlhG acts as negative regulator that controls

the flagella number, while FlhF controls the flagella assembly at the proper point and serves as a positive regulator in many bacterial species.

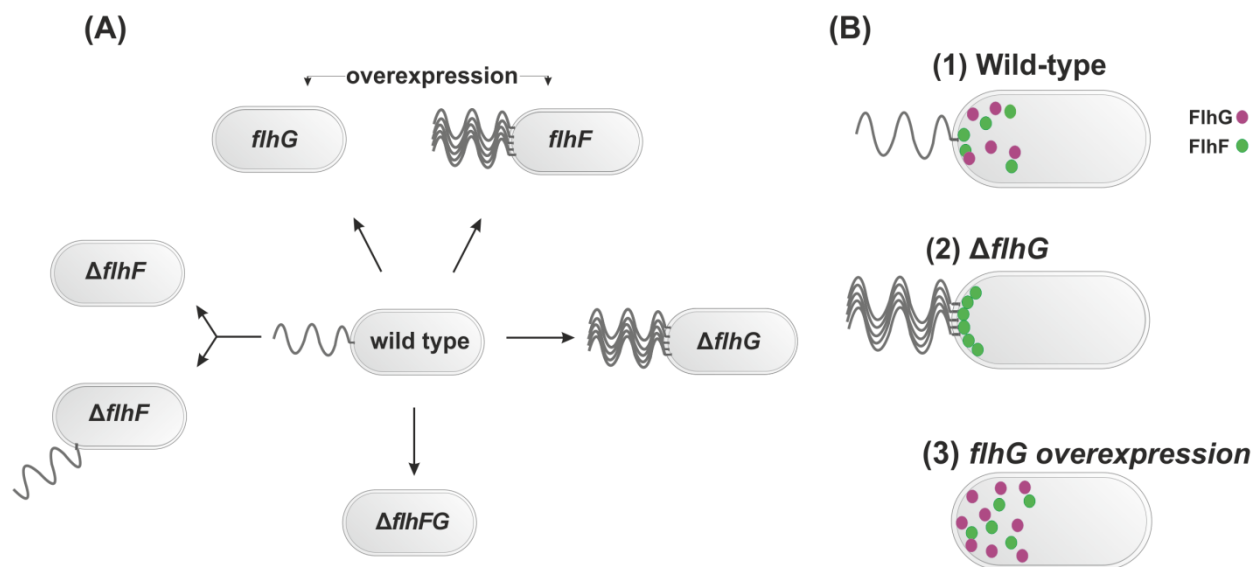


**Figure 9: Regulation of polar flagella number.** (A). Schematic model summarizing the effects of *flhFG* genes on polar flagellation. Deletion of *flhF* mainly results in non-flagellated cells or a mislocated flagellum. Both overexpression and deletion of *flhF* leads to hyper-flagellated cells. A strain overexpressing *flhG* or a  $\Delta flhFG$ -strain do not possess flagella. (B) Schematic model of flagella number regulation by FlhF and FlhG in *V. alginolyticus*. In this model, FlhF acts as a positive regulator, which initiates the flagella biosynthesis at the right place (pole). FlhG acts as a negative regulator and decreases the flagella number potentially by inactivation of FlhF through stimulation of its GTPase activity. (1) The interplay of FlhF and FlhG in the wild type strain is balanced and results in a single flagellum at the pole. (2) Deletion of *flhG* leads to accumulation of FlhF at the pole and hyper-flagellation. (3) When the concentration of FlhG is increased by overexpression, FlhF is constantly released from the membrane and FlhF cannot initiate the flagella biosynthesis. The images were adapted from ref. (94, 100).

### 1.5.2.2 Amphitrichous and lophotrichous flagellation

The interplay of FlhF and FlhG in amphitrichous and lophotrichous flagellated bacteria was mainly studied in the gastric pathogens *C. jejuni* and *H. pylori*. The flagellation pattern of *H. pylori* results in two to six flagella at one pole. Deletion of *flhG* leads to non-flagellated cells and an impaired motility (65). Like in other bacteria, deletion of *flhG* in *C. jejuni* results in hyper-flagellated cells while the outcome of *flhF* deletion are non-flagellated cells (64). Of note, deletion of *flhG* in *C. jejuni* also results in the appearance of minicells indicating that FlhG is not only involved in flagellar biogenesis but also in cell division (64).

### 1.5.3 Role of FlhF and FlhG in peritrichous flagellated bacteria

The physiological role of FlhG and FlhF was examined in *B. subtilis*, *Bacillus cereus* and *Geobacillus thermodenitrificans* which possess approximately 20-25 flagella along the cell axis (104). Deletion of *flhF* in *B. subtilis* does not impair the motility and the flagella number, however the symmetrical organized grid-like pattern of flagella seems disrupted (60). In contrast, deletion of *flhF* in *B. cereus* leads to a significantly reduced number of flagella (105). Unlike to the phenotypes observed in polar flagellated bacteria (see above), deletion of *flhG* in *B. subtilis* results in a reduced number and dislocated flagella. Here, high-resolution microscopy revealed that the flagellar basal bodies are aggregated which implies an involvement of FlhG in the correct positioning of the flagellar C-ring as part of the basal body (60). In agreement with this hypothesis, a direct interaction between FlhG and the C-ring component FliY could be shown in the thermophilic relative of *B. subtilis*, *G. thermodenitrificans* (89).

## 1.6 SRP-System

The core components of the SRP-System are conserved in all domains of life and are indispensable for the cellular membrane protein targeting machinery (106). In *E. coli*, the SRP-system consists of the SRP-protein Ffh and the SRP-RNA, together called the signal recognition particle (SRP) and the SRP-receptor (SR) FtsY (described in more detail under 1.6.1).

The previous model of the SRP-pathway begins when SRP interacts with the cytosolic RNCs that translate integral membrane proteins (IMP) and mediates the targeting of this complex to the membrane through its membrane associated SRP-receptor (**Figure 10A**). Finally, the RNC is transferred to the translocon upon which Ffh and FtsY disassemble. This model is mainly based on *in vitro* studies and does not explain how SRP finds the membrane with its receptor, how FtsY reaches the membrane or how SRP is capable to target this huge complex to the membrane (reviewed in (107)).

A current study gives another view on the SRP-pathway and suggests a different order of events where the SRP-receptor plays a central role. In this alternative model, FtsY and ribosomes are targeted to the membrane during translation of FtsY in an SRP-independent manner (**Figure 10B**). This alternative sequence is supported by *in vivo* studies revealing that the N-domain of FtsY is required for co-translational membrane attachment (108). Then, mRNAs encoding IMPs are targeted by an unknown mechanism to the membrane-bound ribosomes. Now SRP interacts with signal sequence as it emerges from the membrane bound ribosome and facilitates proper assembly of the RNC on the translocon (reviewed in (109)).

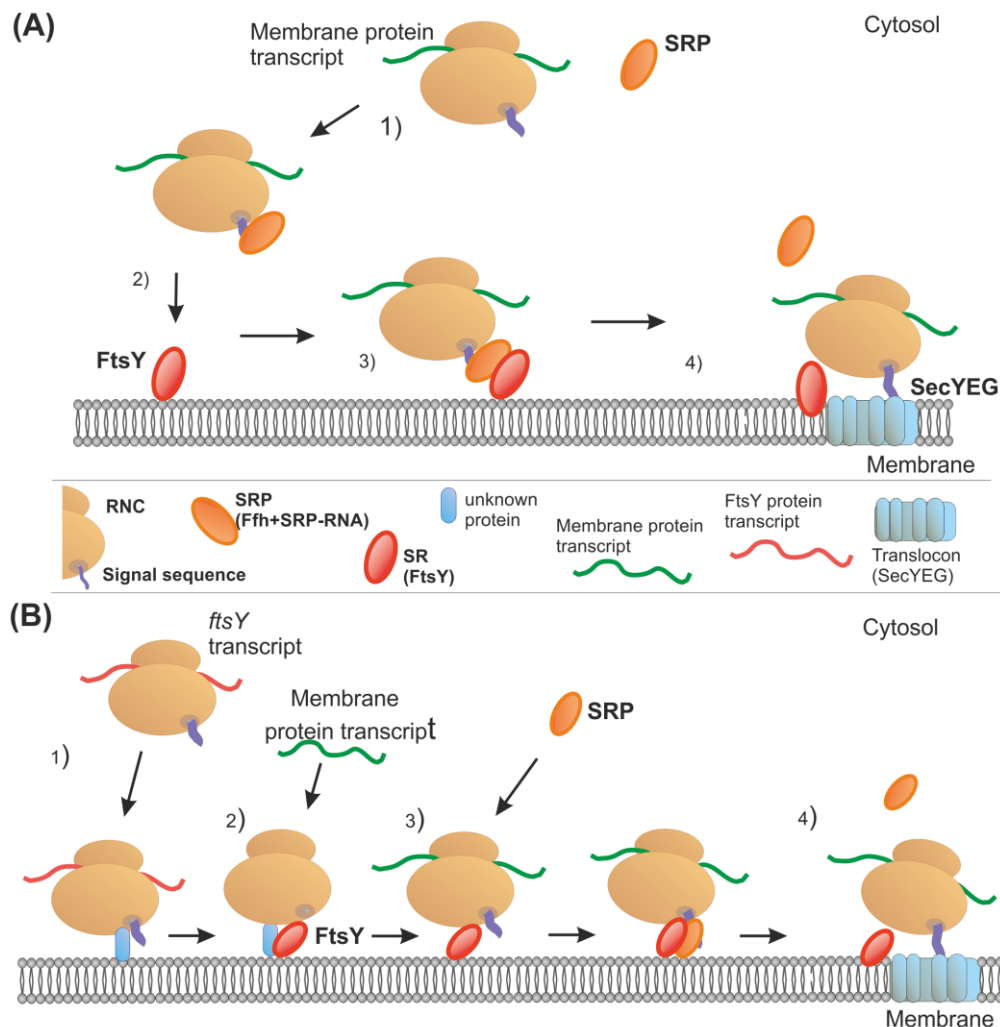


**Figure 10: Two models of the SRP-pathway.** (A) The SRP-mediated pathway starts with the recognition of the signal sequence which is emerging from the RNC in the cytosol (1). (2) The SRP-RNC complex is targeted to the SRP-receptor FtsY associated with the membrane. (3, 4) The RNC is transferred to the SecYEG translocon resulting in disassembly of SRP and FtsY. (B) In the SR-mediated pathway, FtsY targets to the membrane co-translationally mediated by its N-domain (1). After assembly of FtsY at the membrane or an unknown membrane bound protein, the ribosome remains membrane-bound. mRNA encoding an integral membrane protein (IMP) targets to the membrane-bound ribosome and forms a translation initiation complex (2). SRP recognizes the signal sequence of the nascent peptide chain emerging from the ribosome and binds FtsY and the ribosome (3). This SRP-FtsY-RNC targets to the next translocon through FtsY. The RNC transferred is to the translocon and FtsY-SRP dissociate from each other and the RNC-complex. This image was adapted from ref. (104, 105).

### 1.6.1. Rearrangement of the SRP-System during the targeting process

SRP are ribonucleoprotein particles (RNPs) that consist of the protein Ffh and the 4.5s RNA (also: SRP-RNA). Like FlhF, Ffh and FtsY are GTPases of the SIMIBI-class (see above). The

NG-domain of Ffh is followed by a C-terminal methionine-rich M-domain mainly guiding the interaction of Ffh with the tetraloop of the SRP-RNA (**Figure 10 (1)**, (110, 111)). The M-domain of Ffh together with the SRP-RNA recognizes and binds the signal sequence of the nascent peptide chain emerging from the ribosome nascent chain complex (RNC) (87). FtsY binds close to the tetraloop via its NG-domain and forms a GTP-dependent heterodimer with Ffh, being described as an early interaction complex (**Figure 10 (2)**, (112)). After the initial formation of the heterodimer, the NG-domains undergo a large-scale repositioning to the distal region of the SRP-RNA, whereas the M-domain of Ffh remains at the tetraloop region (**Figure 10 (3)**). The SecYEG translocon is now assumed to bind this rearranged complex via the A-domain of FtsY. Binding of SecYEG may induce the rotation of the SRP-RNA and result in stimulation of the GTPase activity of the SRP complex (**Figure 10 (4)**, (110)). Increased GTP-hydrolysis subsequently results in disassembly of the GTP-dependent Ffh-FtsY-heterodimer (**Figure 10 (5)**).

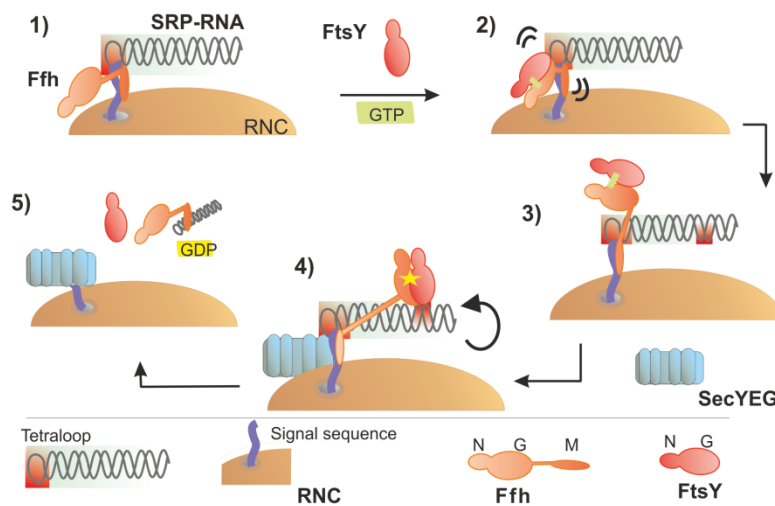


**Figure 11: The SRP cycle of SRP-mediated protein targeting.** (1) SRP consisting of Ffh and SRP-RNA recognizes the signal sequence of a nascent polypeptide chain emerging from the ribosome. (2) FtsY and Ffh interact in a GTP-dependent manner localizing close to the tetraloop of the SRP-RNA. (3) The heterodimer FtsY-Ffh undergoes a repositioning from the tetraloop to the distal end of the SRP-RNA. (4) The rotation of the SRP-RNA leads to a stimulation of the GTP-hydrolysis of the Ffh-FtsY complex and transfer the RNC to the translocon. (5) After GTP-hydrolysis, SRP-FtsY disassembles and from the RNC. The image was adapted from ref. (110).



## Aim of work

The bacterial flagellum is a remarkable nanomachine that allows bacteria to move in changing environmental conditions. Despite the well-characterized core flagellar components and basic principles for regulating flagellar gene expression, regulatory mechanisms for maintaining the flagellation pattern are far from being understood. The flagellation patterns are characteristic for each species and prerequisite for motility, but are also involved in biofilm formation and the pathogenicity of disease-causing flagellated bacteria.

Two proteins are described, which are involved in the numerical and spatial parameters of flagella biosynthesis in many flagellated bacteria, the nucleotide binding proteins FlhF and FlhG. How FlhF and FlhG interact with the flagellar system to assign the future flagellar assembly site and restrict flagella to a certain number are major questions in this field and part of this work. At first I want to understand on biochemical level, how FlhF and FlhG interacts with each other in the monotrichous *Shewanella putrefaciens* and the amphitrichous *Campylobacter jejuni*. In this case I wanted to uncover similarities and differences to the peritrichous *Bacillus subtilis*. Furthermore, I set out to identify interaction partners of FlhF and FlhG in the monotrichous *S. putrefaciens* and the peritrichous *B. subtilis* to gain insights into the mechanism underlying flagellation pattern control.

## 2. Results

### 2.1 The ATPase FlhG of *Shewanella putrefaciens* and *Campylobacter jejuni*

FlhG is a member of the SIMIBI class of nucleotide-binding proteins, which are often involved in partitioning and localizing other factors in prokaryotic cells (85). Previous biochemical studies performed mainly in peritrichous flagellated bacteria like *Bacillus subtilis* (*Bs*) or *Geobacillus thermodenitrificans* (*Gt*) have shown that FlhG is an ATPase and in addition an activator for the GTP-hydrolysis of FlhF (53, 54). The crystal structure of *Gt*FlhG confirmed a close structural homology to the MinD ATPase from *E. coli* (89). Amino acid sequence alignments of FlhG from different organisms reveal high conservation in the ATP-binding region, magnesium coordination site (switch II), core ATPase motifs (P-loop and switch II) the activator helix and the MTS (**Figure 12**).

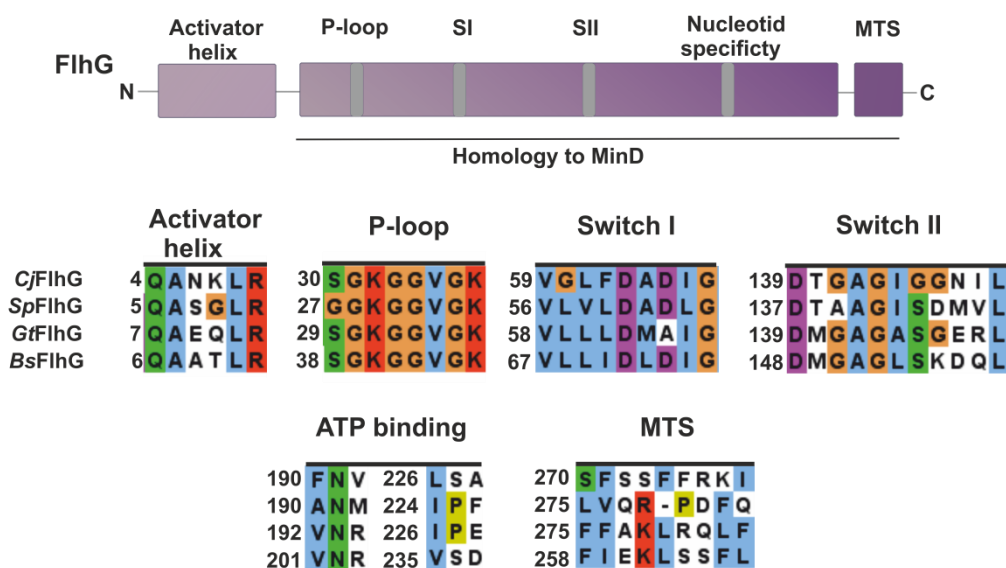


**Figure 12: Domain architecture und sequence alignments of FlhG.** Top: Domain structure of FlhG including the specific motifs for ATPase activity (P-loop, Switch I and II region, ATP-binding region), membrane targeting sequence (MTS) and the N-terminal 'DQAxLR' motif, which serves as an activator motif of the FlhF GTPase in *B. subtilis*. Bottom: Amino acid sequence alignments of FlhG homologs from *Campylobacter jejuni* (*Cj*), *Shewanella putrefaciens* (*Sp*), *Geobacillus thermodenitrificans* (*Gt*) and *Bacillus subtilis* (*Bs*) reveal high conservation in the core ATPase motifs, the activator helix and the MTS.

### 2.1.1. Purification of FlhG from *S. putrefaciens* and *C. jejuni*

FlhG from *S. putrefaciens* (*Sp*) and *C. jejuni* (*Cj*) were heterologously produced in *E. coli* BL21 (DE3). The plasmid-encoded sequence of both proteins contained a hexahistidine-tag at their N-termini allowing purification by a two-step protocol including Ni-NTA-affinity chromatography followed by size exclusion chromatography (SEC). A detailed protocol is described in the Materials and Methods section under 4.2.5. The purification of *Cj*FlhG yielded amounts was sufficient for further biochemical analysis assays and for crystallization (**Figure 13A**). The purification of overproduced *Sp*FlhG from *E. coli* BL21 (DE3) proved to be difficult since the purified protein showed high levels of precipitation at higher concentrations. Different buffer conditions did not improve the protein solubility. The amount of *Sp*FlhG did not allow the implementation of crystallographic experiments yet but was sufficient for biochemical analysis (**Figure 13B**). Protein concentration was determined by measuring the absorbance at 280 nm using a UV-spectrometer (NanoDrop Lite) and the theoretical extinction coefficient (web.expasy.org/protparam) that was predicted as  $11640 \text{ M}^{-1} \text{ cm}^{-1}$  and  $12950 \text{ M}^{-1} \text{ cm}^{-1}$  for *Sp*FlhG and *Cj*FlhG, respectively.

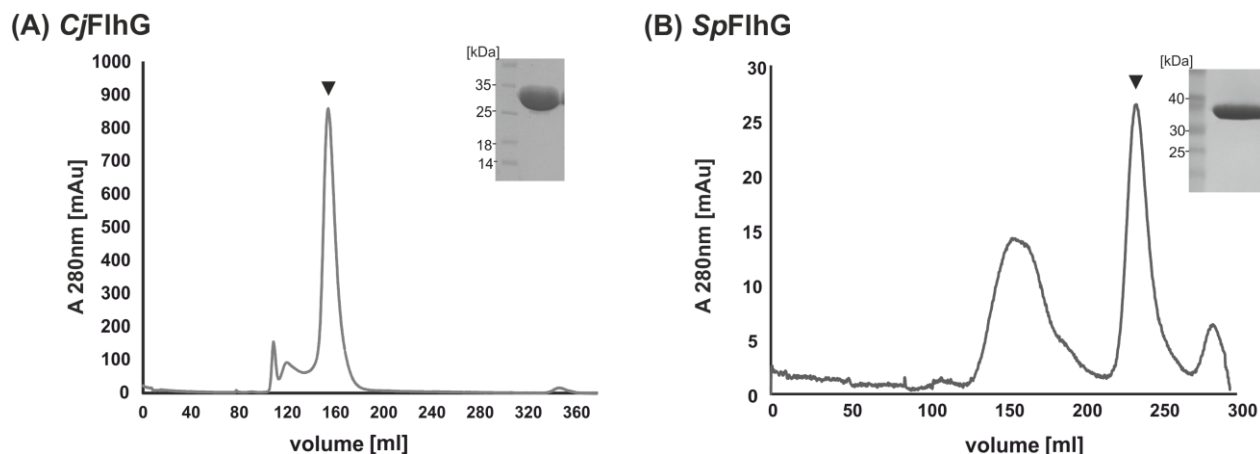


**Figure 13: Purification of *Cj*FlhG and *Sp*FlhG.** (A) Size exclusion chromatography profile of *Cj*FlhG and a corresponding Coomassie-stained SDS-PAGE of the main peak fraction marked with a triangle. (B) Size exclusion chromatography profile of *Sp*FlhG and a corresponding Coomassie-stained SDS-PAGE of the main peak fraction marked with a triangle.

## 2.1.2 Crystallization of *CjFlhG*

Purified *CjFlhG* was incubated with 10 mM ATP and concentrated to ~ 23 mg/ml. Crystallization was carried out by the sitting drop method in 96-well plates at room temperature, by mixing equal volumes of protein and precipitant solution (final drop volume 1  $\mu$ l). Initial hits were obtained after ~ 16 hours in the Joint Center for Structural Genomics (JCSG) core suite I condition E5 (0,2M ammoniumflouride and 20 % (w/v) Polyethylenglycol (PEG) 3350). High quality crystals were gained after one week and were flash frozen in liquid nitrogen in the presence of a cryo-protecting solution (mother-liquid supplemented with 20% (v/v) glycerol).

### 2.1.2.1 Structure determination and refinement of *CjFlhG*

Data collection was performed at the European Synchrotron Radiation Facility (ESRF) in Grenoble, France under cryogenic conditions (100 K) at the beamline ID23-1 to a diffraction limit of 2.8  $\text{\AA}$  resolution. Data were recorded with a DECTRIS PILATUS 6M detector. Data processing was carried out using iMosflm (113) and the CCP4-implemented program SCALA (114). The structure of ADP-FlhG was solved by molecular replacement (MR) with CCP4-integrated PHASER (115) using a monomer of the *GtFlhG* (pdb: 4RZ2) as search model at 2.8  $\text{\AA}$  resolution (**Table S1**). Structures were manually built in COOT (116) and refined using PHENIX refine (117). The structure was refined to an  $R_{\text{work}}/R_{\text{free}}$  of 21.4/23.8 %. The crystal structure of the *CjFlhG* monomer is unpublished.

### 2.1.2.2 Crystal structure of the monomeric *CjFlhG*

The crystal structure of *CjFlhG* comprises residues from 21-288 (**Figure 14A**). Absent in the structure are the first 20 amino acid residues, which contain the previously described activator helix and the residues 269 – 274. The same was observed in the crystal structure of *GtFlhG* most likely due to flexibility or degradation. The core of FlhG is composed of 7 parallel and one antiparallel  $\beta$ -sheet that are stacked in a helical shape and are surrounded by 9  $\alpha$ -helices. The overall shape of the monomeric *CjFlhG* shows the same fold and architecture as *GtFlhG* (**Figure 14C**). Both crystal structures can be superimposed with a root mean square deviation (r.m.s.d) 2.32  $\text{\AA}^2$  over 108 C $\alpha$ - atoms.

The structural comparison shows that both proteins share the same active site harboring the highly conserved motifs for ATP-hydrolysis (P-loop 30-37, Switch II motif 139-147) and magnesium binding (Switch I motif 59-67, **Figure 15A**). Notable differences between both FlhGs appear in the localisation of helix  $\alpha 3$  of *CjFlhG* (helix  $\alpha 4$  in *GtFlhG*) and the MTS-helix  $\alpha 9$  (helix  $\alpha 10$  in *GtFlhG*, **Figure 14C**). Helix  $\alpha 3$  of *CjFlhG* is slightly shifted away from the center of the molecule thereby widening the hydrophobic groove.

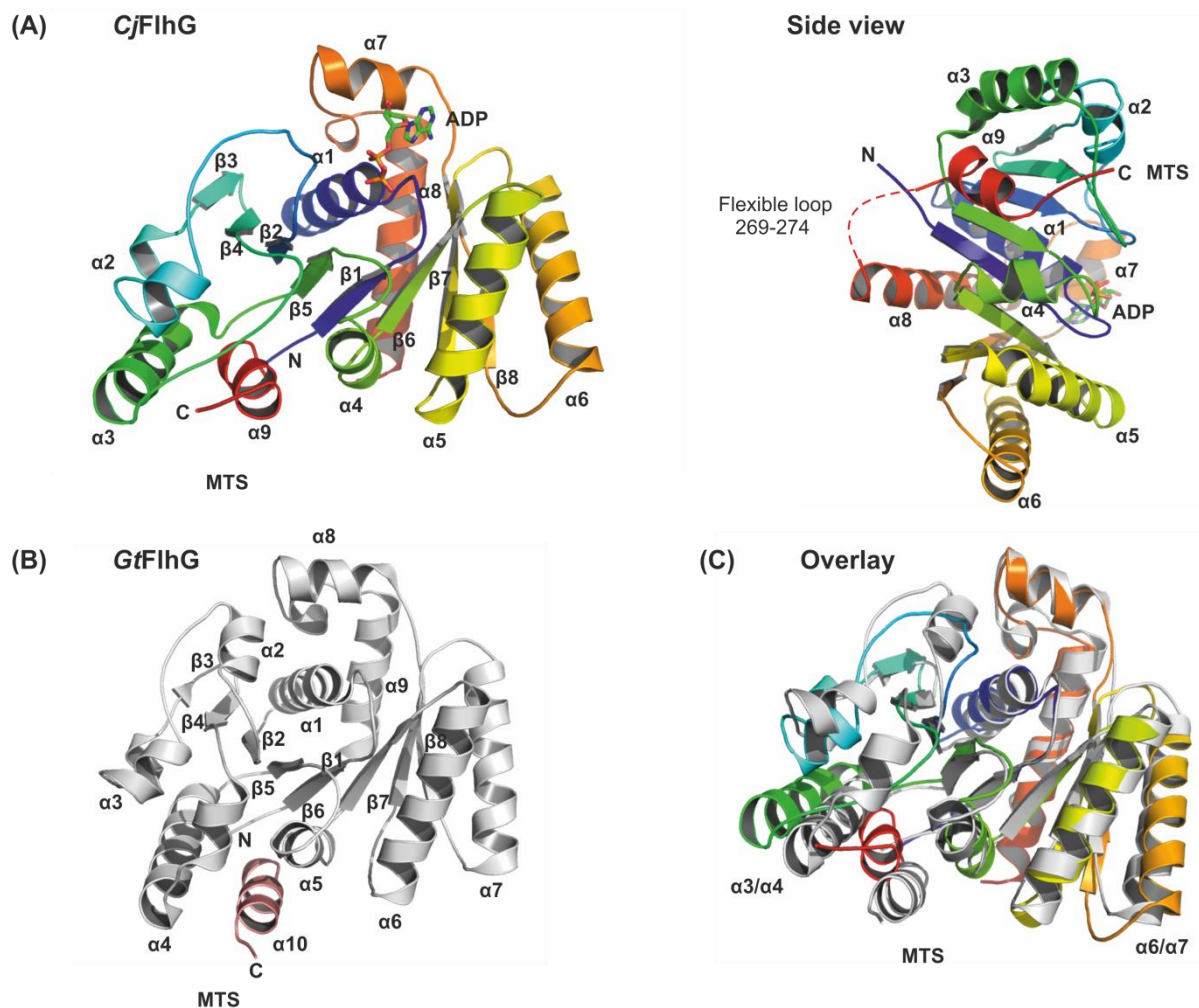


**Figure 14: Crystal structure of *CjFlhG*.** (A) Two views of the *CjFlhG* monomer, colored in rainbow. Alpha helices are labeled from  $\alpha 1$  to  $\alpha 10$ , and beta strands from  $\beta 1$  to  $\beta 8$ . The flexible loop which connects the core protein helix  $\alpha 9$  (membrane targeting sequence, MTS) and the N- and C termini is indicated. (B) Crystal structure of monomeric *GtFlhG* (pdb: 4RZ2). The protein core is colored in light grey and the helix  $\alpha 10$  (MTS) in light pink. (C) Overlay of monomeric *CjFlhG* (rainbow) and *GtFlhG* monomer (grey). Deviations of the localization of  $\alpha$ -helices are indicated.

### 2.1.2.3 Catalytic motifs and ADP coordination of monomeric *CjFlhG*

The crystal structure of monomeric *CjFlhG* contains all elements that are required for ATP-, magnesium- and nucleotide-binding (**Figure 15A**). Although the nucleotide ATP was added prior to crystallization, the crystal structure of *CjFlhG* reveals an ADP molecule bound to the protein. ADP is coordinated in a cavity at the prospective dimerization interface of FlhG, mainly formed by  $\alpha$ -helices ( $\alpha 2$ ,  $\alpha 5$ ,  $\alpha 7$  and  $\alpha 8$ ). The Walker A motif, also known as P-loop (phosphate-binding loop, ‘GKxxxGKT/S’), is conserved among ATPases and GTPases. The P-loop is composed of a loop region and an adjacent helical turn (**Figure 15A**). It contains two lysine residues (K32 and K37 in *CjFlhG*) crucial for nucleotide binding. In the crystal structure of *CjFlhG*-ADP, the side chain of K37 is located within a distance of 4.7 Å to the  $\beta$ -phosphate moiety of ADP (**Figure 15B**) establishing only weak interactions. The amino group of the adenine base of ADP is coordinated by asparagine 192 of the ATP-binding motif with a distance of 3.0 Å (**Figure 15B**). Further motifs of the active site are the switch I (‘DIxxxNI’) and the switch II motif (**Figure 15A**). The switch I motif coordinates a magnesium ion, the less conserved switch II motif assists in shaping of the active site of ATPases. It is apparent that ADP is only weakly coordinated in the crystal structure of *CjFlhG*-ADP (see above). This is in contrast with the crystal structure of *GtFlhG*-ADP (PDB: 4RZ3, (89)) which however was obtained using an *GtFlhG* variant (*i.e.*, D60A).

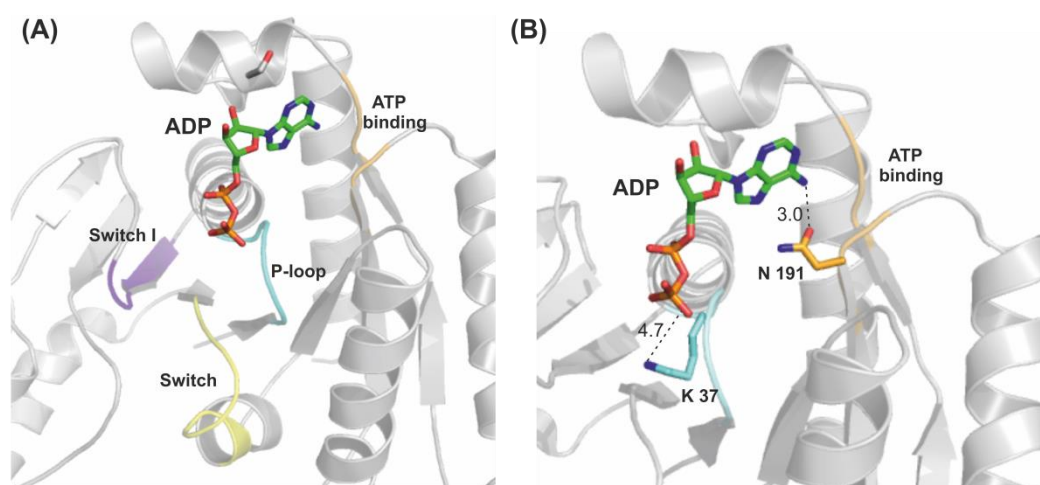


**Figure 15: ADP coordination and catalytic motifs** (A) Overview of *CjFlhG* with ADP bound in the active site. Important catalytic motifs are colored in cyan (P-loop), purple (Switch I), yellow (Switch II) and the orange (the ATP binding motif). (B) Coordination of ADP by *CjFlhG*. Catalytic motifs are colored as in A.

### 2.1.2.4 The C-terminal amphipathic helix of *CjFlhG*

Another feature of *CjFlhG* is the highly conserved C-terminal helix. Helix  $\alpha 9$  is protected into a hydrophobic cleft mainly formed by helices  $\alpha 3$  and  $\alpha 4$  (**Figure 16A**). This was also observed in the monomeric structure of *GtFlhG*, wherein the hydrophobic cleft is formed by helices  $\alpha 4$  and  $\alpha 5$  (**Figure 14C**). Helical wheel projection (rzlab.ucr.edu) of *CjFlhG* emphasizes an amphipathic propensity of the C-terminus of *CjFlhG*, which was also observed for the C-terminus of *GtFlhG* (**Figure 16B**). This suggests that the C-terminal helix serves as membrane targeting sequence (MTS) as previously observed for *GtFlhG* (89).

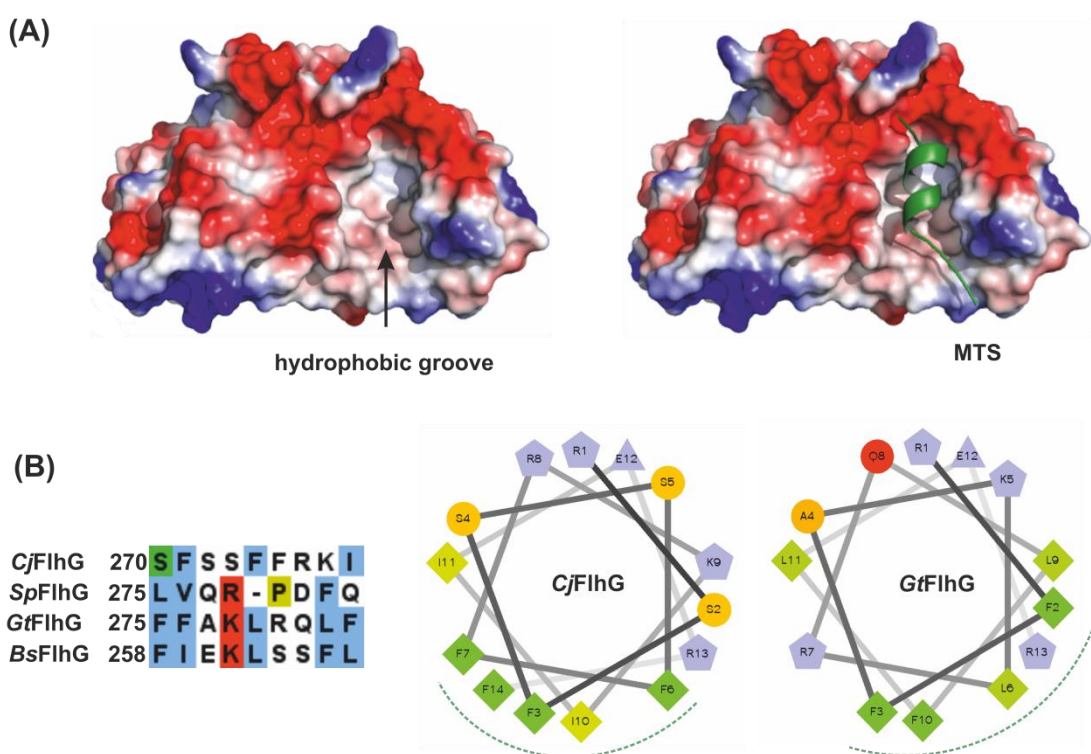


**Figure 16: MTS of *CjFlhG*:** (A) Electrostatic surface representation of *CjFlhG* shows the hydrophobic cleft in absence (left) and presence (right) of the MTS. Positive charges are indicated in blue, negative charges are indicated in red and the MTS in green. (B) Sequence alignments of the C-terminal helix of different FlhG proteins. Organisms are abbreviated: *C. jejuni* (*Cj*), *S. putrefaciens* (*Sp*), *G. thermodenitrificans* (*Gt*) and *B. subtilis* (*Bs*). Helical wheel projection of *CjFlhG* and *GtFlhG* show an amphipathic character and are indicated with green dashed lines.

### 2.1.3 ATPase activity of FlhG

To figure out whether FlhG from *S. putrefaciens* and *C. jejuni* were active ATPases, their putative ATPase activity was assayed by high-pressure liquid chromatography (HPLC).

Therefore, 50 to 100  $\mu\text{M}$  of purified protein were incubated with ATP for 60 min at 37 °C. Reactions were stopped by flash freezing with liquid nitrogen. The samples were thawed and immediately injected into an HPLC equipped with a C18 reversed-phase column. The eluent contained 40 mM  $\text{KH}_2\text{PO}_4$ , 40 mM  $\text{K}_2\text{HPO}_4$ , 10 mM tetrapentylammonium bromide (TPAB) and 15 % (v/v) acetonitrile. The inclusion of the cationic ion-pairing reagent TPAB allows for good retention and separation of the negatively charged analytes. The adenosine nucleotides were separated at a flow rate of 0.8 ml/min, detected at a wavelength of 260 nm and quantified via integration of the respective peak areas using Agilent ChemStation. For *CjFlhG*, different variants were included in this study, harboring distinct mutations in the corresponding conserved regions. These mutations comprise the activator motif (i.e.; Q4A), the P-loop (i.e.; K37A, ATP-binding) and the Switch I region (i.e.; D61A, ATP-hydrolysis).

The results show that both *SpFlhG* as well as *CjFlhG* exhibit ATPase activity. The ATPase activities of *SpFlhG* and *CjFlhG* were determined as  $5.2 \pm 0.06$  and  $18.2 \pm 0.2$  nmol ATP \* h<sup>-1</sup> \* nmol FlhG<sup>-1</sup>, respectively (**Figure 17**). The slightly lower activity of *SpFlhG* under the experimental conditions is in agreement with the difficulties during purification of the protein (see 2.1.1). The first 20 amino acids of *SpFlhG* (i.e.; the activator helix) fused to GST were assayed for ATPase activity and revealed similar degradation as a control reaction without enzyme (**Figure 17A**). The introduced variation in the activator helix at the N-terminus of *CjFlhG* (Q4A) did not alter its ATPase activity compared to the native protein (**Figure 17B**). This suggests that FlhG's activator helix does neither exhibit any enzymatic activity nor is influencing the ATPase activity. As expected, *CjFlhG* proteins with a variation in their motif for ATP-binding (K37A) or ATP-hydrolysis (D61A), showed almost no ATPase activity (**Figure 17B**). These data confirm that both proteins function as an ATPase compared to other FlhG homologs (89).



The biochemical evaluation of *CjFlhG*'s enzymatic activity was carried out in close collaboration with the lab of Dave Hendrixson (UT Southwestern, Dallas, Texas). Electron microscopic images of this lab from *C. jejuni* harboring the K37A or D61A variation in FlhG revealed a typical flagellation pattern in comparison to the wild type strain (118). In contrast to this exhibited a variation in the activator motif of *CjFlhG* a hyper flagellated phenotype. An explanation for this would be that *CjFlhG* is no longer able to bind FlhF via its activator helix, resulting in a loss-of function. This suggests that the ATPase activity of *CjFlhG* has no influence on the spatial and numerical flagellation pattern.

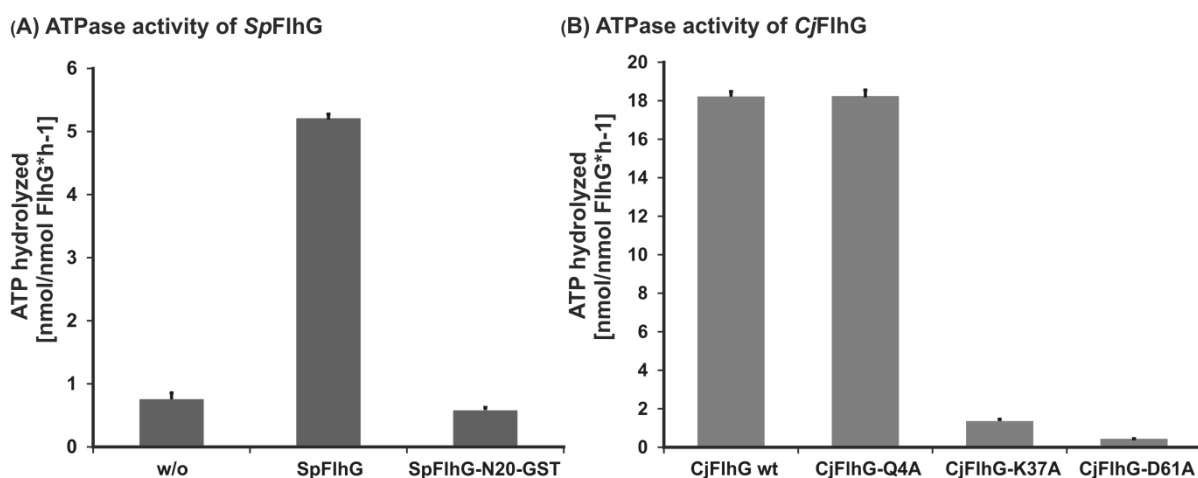


**Figure 17: ATPase activity of FlhG from *S. putrefaciens* and *C. jejuni*.** (A) ATP-hydrolysis in the absence of enzyme (w/o) and in presence of *SpFlhG* or a truncated variant of *SpFlhG* comprising only the first 23 amino acids fused to GST. (B) ATP-hydrolysis in the presence of *CjFlhF*, the catalytic deficient variants *CjFlhG* K37A and *CjFlhG*-D61A and *CjFlhG* being varied in the activator helix (Q4A). Data represent the mean  $\pm$  SD of three independent measurements.

To gain a deeper insight into the enzymatic properties of FlhG, a kinetic analysis of the ATPase activity of *CjFlhG* was performed. In brief, 100  $\mu$ M *CjFlhG* were incubated at 37°C in the presence of increasing amounts of ATP. Samples were taken at different time points (5/10/15/20/30 minutes) and treated as described above. The velocity of ATP hydrolysis for each ATP concentration was obtained by linear regression of quantified ADP at different time points. The slope of the regression curve, representing the velocity of ATP-hydrolysis was plotted against the concentration of ATP (**Figure 18**). The  $K_m$  and  $V_{max}$  values  $\pm$  SD of ATP-hydrolysis were obtained from a Michaelis-Menten fit of the v/S characteristic using the equation  $v = V_{max} * S / (K_m + S)$ . Kinetic data analysis was performed using GraphPad Prism version 6.04 for

Windows (GraphPad Software). Admittedly, a higher number of data points and implementation of higher ATP concentration (e.g.; 15 and 20 mM) will lead to a better fit. However, important conclusions can already be drawn from this preliminary data. The maximal velocity of ATP-hydrolysis by *CjFlhG* is almost reached at an ATP concentration of 10-15 mM. The intracellular concentration of ATP is estimated to be 10 mM for *E. coli* (119). When assuming a similar ATP pool for *C. jejuni*, *CjFlhG* would constantly be at its  $V_{max}$ . However, the  $V_{max}$  of  $8.9 \pm 0.5$   $\text{nmol} \cdot \text{min}^{-1} \cdot \text{mg}^{-1}$  FlhG is extremely low compared to other enzymes (120).

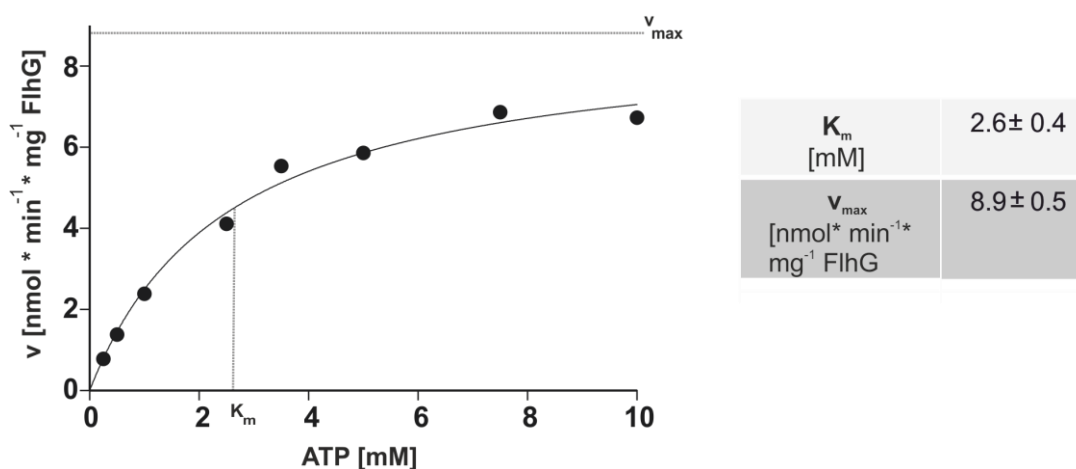


**Figure 18: v/S characteristic of ATP hydrolysis by *CjFlhG*.** v/S characteristic of ATP-hydrolysis by *CjFlhG*. Grey dashed lines indicate  $V_{max}$  and  $K_m$ . The exact values values  $\pm$  SD obtained from a Michaelis-Menten fit of the data are given in the table. The velocity is given in nanomoles per minute per milligram of *CjFlhG*.

## 2.2 Interaction partners of FlhG

The mechanism, how conserved homologs of FlhG can control different flagellation patterns in different species, is poorly understood. To gain a better understanding into this complex regulatory network, it seems necessary to identify the interaction partner(s) of FlhG. In *B. subtilis*, it was shown that FlhG interacts with the FlhF GTPase via its N-terminus and stimulates the GTPase activity of FlhF (93). Schuhmacher *et al.* could show that FlhG from *G. thermodenitrificans* is able to interact with components of the C-Ring (89). Since the previously known data are mainly covering mainly to peritrichous flagellated organisms, the question arises whether this is also true for FlhG homologs in polar flagellated organisms (e.g.; *S. putrefaciens*).

### 2.2.1 FlhG interacts with FlhF and stimulates its GTPase activity

To investigate a putative interaction between FlhG and FlhF, Glutathione-S-transferase (GST) fusion variants of FlhG from *S. putrefaciens* and *C. jejuni* were generated. These GST-FlhG variants and FlhF from both organisms were purified. Approximately 1 nmol GST-FlhG was immobilized on glutathione-sepharose beads, followed by incubation with 7 nmol FlhF in the absence or presence of 1 mM of guanosine nucleotides (GDP or GTP) and a non-hydrolyzable GTP analogue (GMP-PNP). After washing of the beads to remove unbound proteins, GST-FlhG, and in the case of an interaction also FlhF, are eluted from the column. The elution fractions of these GST pull-down assays were analyzed by Coomassie-stained SDS-PAGE.

The data shown, that FlhF and FlhG from both organisms interact in a nucleotide-dependent manner. In the case of FlhF/FlhG from *C. jejuni*, an interaction is already observed in the absence of nucleotides and in presence of GDP. Nevertheless, in presence of GTP and GMP-PNP the interaction seems increased (**Figure 19A**). It might be possible that the preparation of either of the proteins contained residual amounts of GTP explaining the interaction observed in the absence of nucleotides. In *S. putrefaciens* were used a *Sp*FlhG variant, which harboring only the first 20 N-terminal amino acids of FlhG ('activator helix of FlhG', compare to 1.5) fused to GST was employed. While no interaction between the proteins is observed in the absence guanosine nucleotide and only weak interaction in presence of GDP or GMP-PNP, the interaction is strongest in the presence of GTP (**Figure 19B**). Although no plausible explanation can be provided for the only weak interaction in presence of GMP-PNP compared to GTP, it is evident

from the assay experiments that FlhF and FlhG from both organisms interact in a nucleotide-dependent manner.

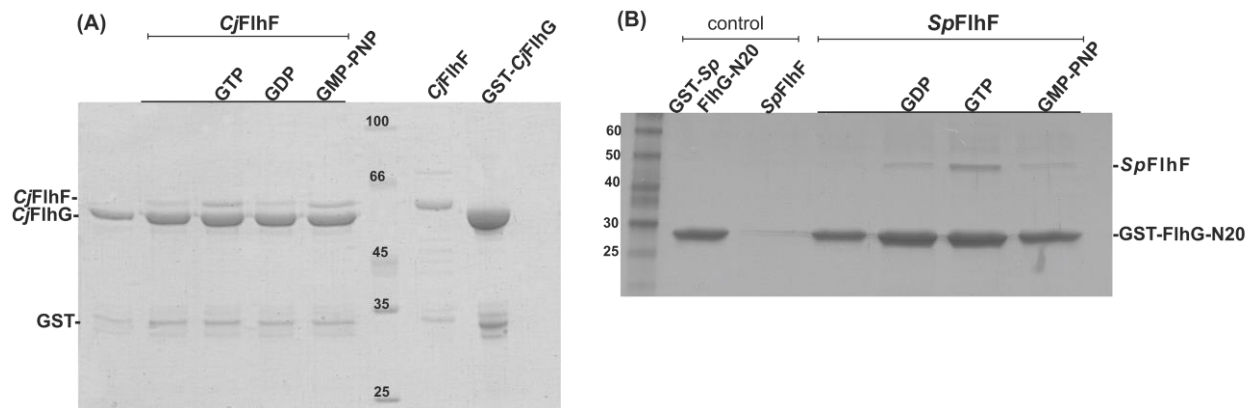


**Figure 19: Interaction of FlhF and FlhG in *Cj. jejuni* and *Sp. putrefaciens*.** (A) The Coomassie-stained SDS-PAGE shows a pull down assay with GST-*Cj*FlhG and *Cj*FlhF in presence of nucleotides (GTP, GDP, GMP-PNP). (B) Coomassie-stained SDS-PAGE of an interaction assay, which shows GST-tagged activator helix of *Sp*FlhG (GST-*Sp*FlhG) in presence of *Sp*FlhF and nucleotides (GTP, GDP, GMP-PNP).

To assess whether FlhF from *S. putrefaciens* and *C. jejuni* are active GTPases whose activity is affected by FlhG as inferred from previous studies in *B. subtilis* (93), the GTPase activity of FlhF was quantified by HPLC. In this case mutations were generated within *Cj*FlhF and *Sp*FlhF. Therefore, were made GTP hydrolysis deficient variants in *S. putrefaciens* FlhF (R285A) and *C. jejuni* FlhF (R324A, (118)). To probe the GTPase-stimulating properties of FlhG homologs, either the first 20 N-terminal amino acids of FlhG fused to GST (*S. putrefaciens*) or a FlhG variant harboring the point mutation Q4A within the activator helix (*C. jejuni*), were used.

FlhF and FlhG and its variants were incubated in presence of 5 mM GTP for 1 h at 37 °C. Reactions were stopped by flash-freezing in liquid nitrogen and subsequently subjected to isocratic reversed-phase HPLC using a C18 column. The eluent contained 40 mM KH<sub>2</sub>PO<sub>4</sub>, 40 mM K<sub>2</sub>HPO<sub>4</sub>, 10 mM TPAB and 15 % (v/v) acetonitrile. The nucleotides were detected at a wavelength of 253 nm. Nucleotide levels were quantified by integration of the peak areas using Agilent ChemStation.

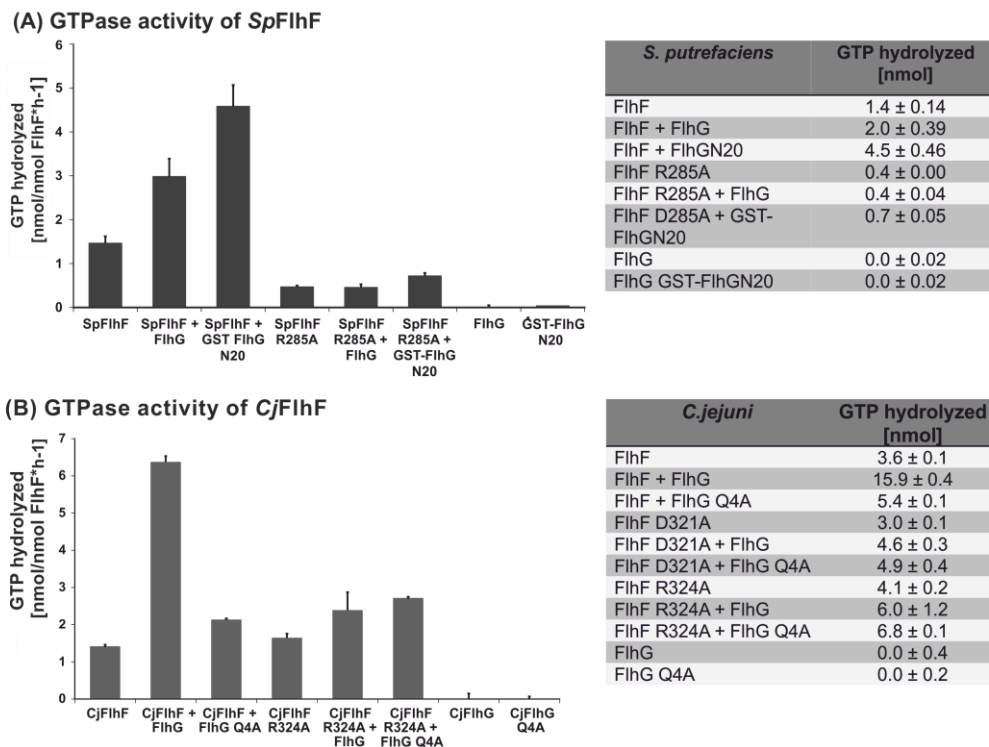


**Figure 20: GTPase activity of FlhF.** (A) The GTPase activity of *Sp*FlhF is stimulated by *Sp*FlhG or its N-terminal region (*Sp*FlhG-N20). This stimulation was decreased in the catalytically deficient *Sp*FlhF-R285A variant. Data represent the mean ± SD of three independent measurements. The table summarizes the catalytic activities. (B) Stimulation of GTPase activity of *Cj*FlhF by *Cj*FlhG. The *Cj*FlhG variant Q4A is unable to stimulate *Cj*FlhF. Data represent the mean ± SD of three independent measurements. The table summarizes the catalytic activities.

The data show that FlhF from *S. putrefaciens* alone has only a minor GTPase activity (**Figure 20A**). In the presence of the full length *Sp*FlhG or its N-terminal region, the GTPase activity increases 2-3-fold (**Figure 20A**). This stimulation was abolished in a GTP-hydrolysis deficient *Sp*FlhF variant (FlhF-R285A). Similar observations are made for the FlhF/FlhG proteins from *C. jejuni*. The GTPase activity of *Cj*FlhF increases ~ 5-fold in the presence of *Cj*FlhG (**Figure 20B**). The stimulation of FlhF by FlhG is reduced in the GTP-hydrolysis deficient variant (*Cj*FlhF-R324A). Variation in the activator helix of *Cj*FlhG (Q4A), also leads to a decreased stimulation of *Cj*FlhF. In both data sets, determination of the GTPase activity of FlhG served as control for the quality of the protein preparations.

These data demonstrate that FlhG from both *S. putrefaciens* and *C. jejuni* stimulates the GTPase activity of FlhF. The first 20 amino acids of FlhG, which include the activator ('QAxRL') motif, are necessary for this stimulation. This is clarified by the fact, that the first 20 amino acids of *Sp*FlhG are sufficient to stimulate *Sp*FlhF, while a variation in the activator motif of FlhG led to

reduced stimulation (**Figure 20A, B**). These results demonstrate on a molecular level that the current model of FlhG and FlhF cycle (**Figure 8**), which is so far based only of the peritrichous flagellated model organism *Bacillus*, can also be transferred to the polar flagellated organisms *S. putrefaciens* and *C. jejuni*.

### **2.2.2 C-ring components of the polar and lateral Flagella system in *Shewanella putrefaciens***

At first, I investigated whether the C-ring components FliM and FliN from the polar and lateral flagellum of *S. putrefaciens* form a stable complex. By convention, the proteins from the polar and lateral flagellum will be numbered with 1 and 2, respectively. The interaction between FliM and FliN was probed by Ni-NTA affinity chromatography followed by size-exclusion chromatography (SEC). For this, FliM contained a C-terminal hexahistidine-tag while FliN was not tagged. Both the polar and the lateral C-ring components form a stable complex after SEC (**Figure 21A, B**). The next question was, are the C-ring components of the lateral and polar flagellum interchangeable. Using Ni-NTA affinity pulldown assays, all four possible C-Ring combinations (FliM<sub>1</sub>/FliN<sub>1</sub>, FliM<sub>1</sub>/FliN<sub>2</sub>, FliM<sub>2</sub>/FliN<sub>1</sub> and FliM<sub>2</sub>/FliN<sub>2</sub>) were tested (**Figure 21C**). The interaction between FliM<sub>1</sub>N<sub>1</sub> and FliM<sub>2</sub>N<sub>2</sub> is evident while no interaction can be observed for FliM<sub>1</sub>/FliN<sub>2</sub> and FliM<sub>2</sub>/FliN<sub>1</sub>. This demonstrates that FliM and FliN proteins belonging to the polar and lateral flagellum interact specifically only with their cognate partner and are not interchangeable.

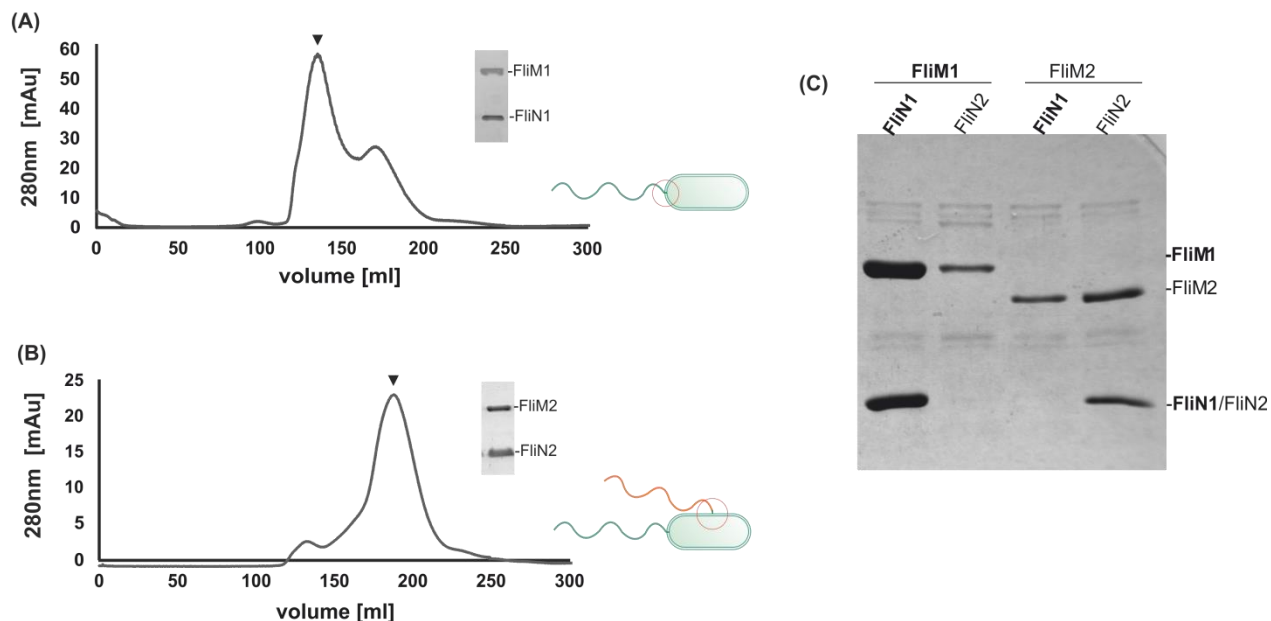


**Figure 21: Interaction of *SpFliM* and *SpFliN* from the lateral and polar flagellar C-ring.** Size-exclusion chromatograms of the *SpFliM*<sub>1</sub>/*FliN*<sub>1</sub> complex of the polar flagellar system (A) and the *SpFliM*/*FliN*<sub>2</sub> complex of the lateral flagella system (B). The main peak fractions of the *FliM*/*FliN* complexes are marked in the graphs with a triangle and shown on Coomassie-stained SDS-PAGE in the insets. (C) Coomassie-stained SDS-PAGE of a pull-down assay of different combinations of *FliM* and *FliN* from both flagellar systems (image kindly provided by J. Schuhmacher).

### 2.2.3 FlhG interacts with a component of the polar C-ring of *Shewanella putrefaciens*

In the next step, a putative interaction between *SpFlhG* and the C-ring components *FliM*<sub>1</sub>/*FliN*<sub>1</sub> and *FliM*<sub>2</sub>/*FliN*<sub>2</sub> was examined. This was again carried out with Ni-NTA affinity pull downs, where *SpFlhG* was tagged with an N-terminal (His)<sub>6</sub>-tag and *FliM*<sub>1</sub>/*FliM*<sub>2</sub> as well as *FliN*<sub>1</sub>/*FliN*<sub>2</sub> were untagged. This interaction studies revealed that only the polar C-ring complex of *SpFliM*<sub>1</sub>/*FliN*<sub>1</sub> is able to bind *SpFlhG* (Figure 22B). Of note, the interaction with individual components *FliN* or *FliM* does not seem to be stable. One explanation for this observation is that the formation of the *FliM*<sub>1</sub> and *FliN*<sub>1</sub> complex improves the solubility of *FliM*. In agreement with this, attempts of purifying hexahistidine-tagged *FliM*<sub>1</sub> by Ni-NTA chromatography and SEC proved to be difficult due to protein instability. However, it might also be possible that the conformation of *FliM*<sub>1</sub> differs between the *FliM*<sub>1</sub>/*FliN*<sub>1</sub> complex and *FliM*<sub>1</sub> alone which would give rise to fascinating implications of the biological context of this interaction.

The lateral C-ring components showed no interaction with FlhG, either alone or in complex (**Figure 22B**). Additionally was the ternary complex *Sp*FlhG/FliM<sub>1</sub>/FliN<sub>1</sub> purified without any precipitation problems by SEC (**Figure 22A**). Despite the stable complex, remained crystallization tries without success. The fact that *Sp*FlhG interacts exclusively with the polar C-ring complex (FliM<sub>1</sub>/FliN<sub>1</sub>), is a molecular explanation why *Sp*FlhG only affects the polar pattern in *in vivo* studies in *S. putrefaciens* (Thormann, unpublished data).

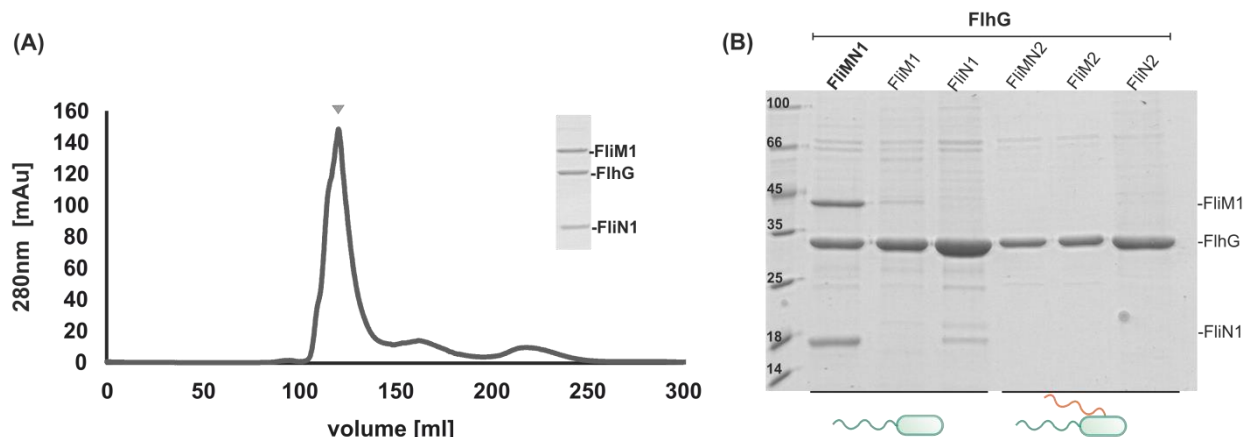


**Figure 22: Interaction of *Sp*FlhG with the FliM/FliN1 complex.** (A) Size-exclusion chromatography reveals a ternary complex of FlhG, FliM and FliN which is indicated with a triangle and shown as Coomassie-stained SDS-PAGE in the inset. (B) The Coomassie-stained SDS-PAGE shows interaction studies with (His)<sub>6</sub>-tagged *Sp*FlhG and untagged FliM<sub>1/2</sub> and FliN<sub>1/2</sub> alone or in complex.

## 2.2.4 Formation of the FlhG-FliM<sub>1</sub>/FliN<sub>1</sub> complex requires the ‘EIDALL’ motif

To figure out where is the interface between FlhG and the polar C-ring complex, helps a closer look at the domain architecture of different C-ring components in *S. putrefaciens*. This shows that FliM<sub>1</sub> comprises some typical known features, like an N-terminal ‘EIDAL’ motif, a middle domain containing FliG binding motifs and a C-terminally FliN homology domain. An alignment of polar FliM<sub>1</sub> and lateral FliM<sub>2</sub> revealed that FliM<sub>1</sub> harbors an additional domain at its N-terminus (**Figure 23A**). The N-termini of FliM<sub>1</sub> and FliM<sub>2</sub> were closer inspected by comparing the amino acid sequences of FliM<sub>1</sub> from *S. putrefaciens* (*Sp*), *V. cholerae* (*Vc*), *G. thermodenitrificans* (*Gt*) and *C. jejuni* (*Cj*) with FliM<sub>2</sub> from *S. putrefaciens* and reveal a conserved motif (‘EIDAL’) within FliM<sub>1</sub> homologs.



For FliN<sub>1</sub> and FliN<sub>2</sub> are no major differences determine. Based on the fact that FliM<sub>2</sub> does not shares the ‘EIDAL’ motif and the knowledge that *B. subtilis* FlhG interacts with FliY via its ‘EIDAL’ motif can be assumed that the interaction between *Sp*FlhG and the FliM<sub>1</sub>/FliN<sub>1</sub>-complex is mediated via the ‘EIDAL’ motif. Therefore a new variation of the polar FliM<sub>1</sub> was generated, which lacks the first 27 amino acids residues inclusive the ‘EIDAL’ motif. A pull-down assay employing hexahistidine-tagged *Sp*FlhG together with non-tagged FliM<sub>1</sub> or FliM<sub>1</sub>ΔN27 confirms that the N-terminus of FliM<sub>1</sub> containing the ‘EIDAL’ motif is necessary for a sufficient interaction with *Sp*FlhG (**Figure 23B**).

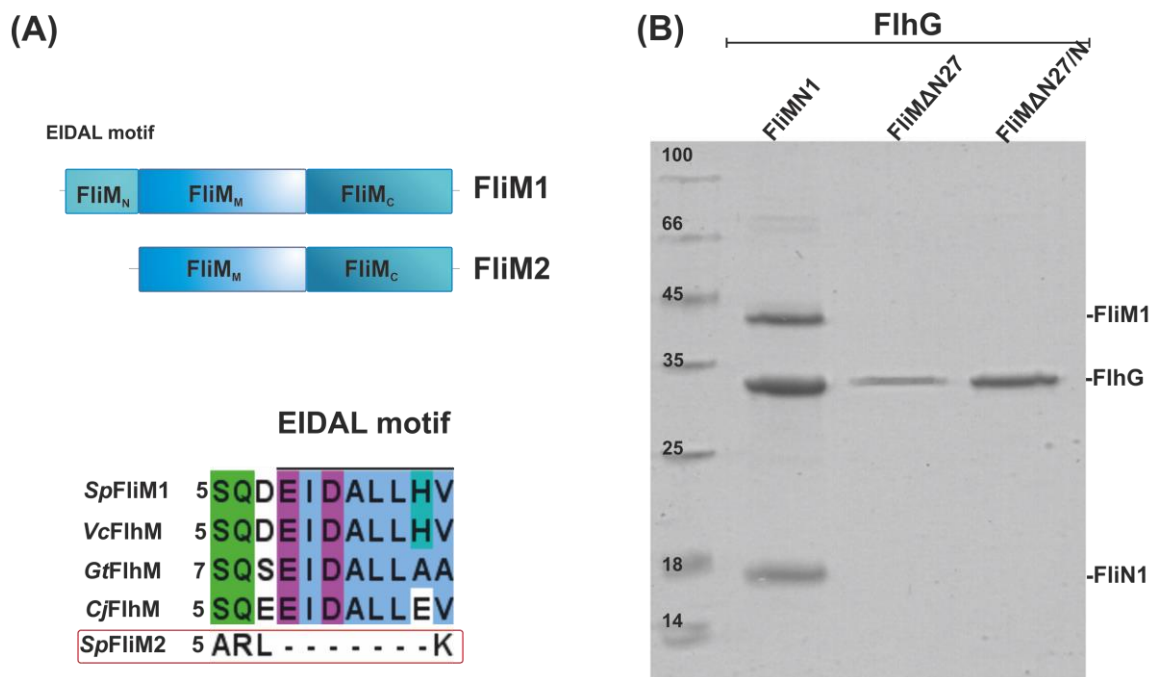


**Figure 23: Interactions between FlhG and FliM<sub>1</sub>/FliN<sub>1</sub> is mediated by the ‘EIDAL’ motif.** (A) Schematic domain architecture of FliM<sub>1</sub> and FliM<sub>2</sub> (*top*) and sequence alignments of the N-termini of FliM of different bacteria (*bottom*). (B) The N-terminus of FliM<sub>1</sub> containing ‘EIDAL’ is crucial for a stable interaction between *Sp*FlhG and the FliM<sub>1</sub>/FliN<sub>1</sub> complex.

### 2.2.5 FlhG and C-ring components of *C. jejuni*

The pathogen *Campylobacter jejuni* exhibits an interesting flagellation pattern in a way that this bacterium shows one flagellum at each of its cell poles (amphitrichous). Interestingly, the genome of *C. jejuni* contains homologues of FliN and FliY albeit the corresponding genes being located at different genomic loci (**Figure 24**).

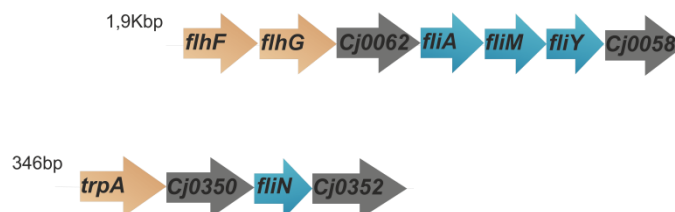


**Figure 24: Localisation of *fliM*, *fliY* and *fliN* genes in *Campylobacter jejuni*.**

To figure out in which constellation the C-ring components are interact with each other and whether FlhG can also interact with C-ring components of *C. jejuni*, further interaction assays were performed. The handling of *CjFliM* proved to be difficult because of a weak expression that could not be improved by co-expression with its potential counterparts FliY or FliN. Nevertheless, initial GST-affinity pull-down assay experiments showed an interaction between *CjFliH*G and *CjFliM* but not with *CjFliN* (**Figure 25A**). *CjFliH*G including an N-terminal GST-tag and *CjFliM* harbors for stabilization an N-terminal MBP-tag (Maltose binding protein). An interaction between *CjFliM* and *CjFliY* or *CjFliN* could not be observed, which is probably due to the weak expression of *CjFliM* or the MBP-tag disturbing the integrity/binding ability of *CjFliM*. In contrast, it could be shown through Ni-NTA affinity chromatography and SEC, that a (His)<sub>6</sub>-tagged *CjFliN* and untagged *CjFliY* form a stable complex (**Figure 25B**). The question how the C-ring of *C. jejuni* is constructed and how FlhG is involved in this process could not solved in this case and requires further research. These experiments provide the first molecular evidence that FlhG interacts with FliM from *C. jejuni* and raises the possibility that the C-ring of *C. jejuni* might consist of three components (FliM, FliY and FliN) instead of two (FliM and FliN) as true for many other bacterial species (24, 27).

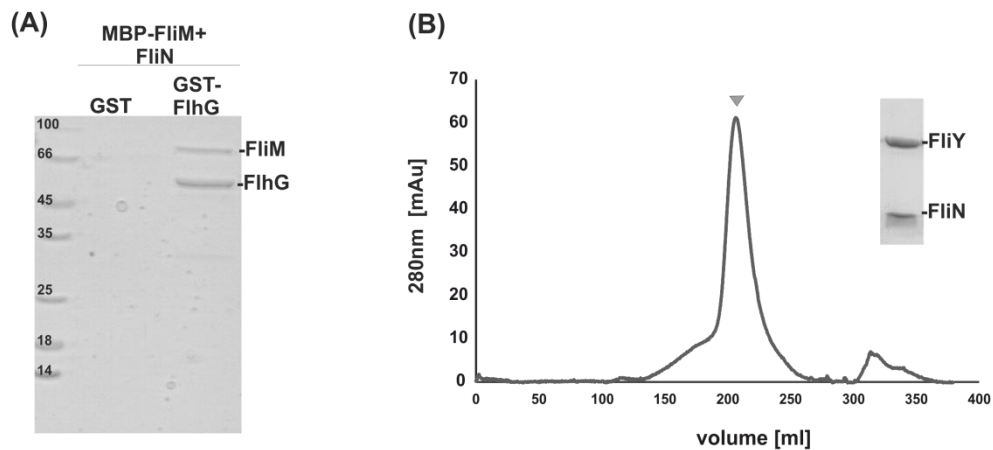


**Figure 25: Interaction of FlhG, FliM, FliY and FliN from *C. jejuni*.** (A) Coomassie-stained SDS-PAGE of a GST-affinity pull-down assays using *Cj*FlhG carrying a GST-tag and *Cj*FliM, *Cj*FliN and GST beads as negative control. (B) The size exclusion chromatography of the *Cj*FliY/FliN in complex. A Coomassie-stained SDS-PAGE of the main peak fractions marked with the triangle is shown in the inset.

## 2.3 Crystallization of *Sp*FliN<sub>1</sub> from *S. putrefaciens*

For a deeper insight into their interaction interface, FliM<sub>1</sub>/FliN<sub>1</sub> and FliM<sub>2</sub>/FliN<sub>2</sub>, which are system-specific and only interact with their cognate C-ring partners, were attempted to crystallize. Neither FliM<sub>1</sub> alone or in complex with FliN<sub>1</sub> or FliM<sub>2</sub> alone or in complex with FliN<sub>2</sub> afforded determination of the crystal structure of FliM. Only FliN<sub>1</sub> could be crystallized.

Purified *Sp*FliN<sub>1</sub> was concentrated to ~ 21 mg/ml. The crystallization was carried out by the sitting drop method in 96 well-plates at room temperature. Initial hits were obtained after one week in the Joint Center for Structural Genomics (JCSG) core suite II condition B2 (0.2 M Lithium sulfate, 0.1M Tris pH 8.5, 40% (w/v) PEG-400). High quality crystals were gained three days and were flash frozen in liquid nitrogen in the presence of a cryo-protecting solution (mother-liquid supplemented with 20% (v/v) glycerol).

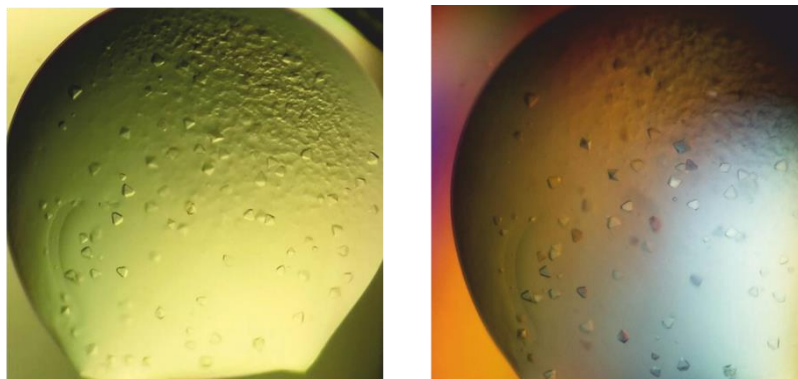


**Figure 26: Crystallization of FliN.** Bi-pyramidal crystals obtained after one week in core suite II B2 (0.2 M Lithium sulfate, 0.1 M Tris pH 8.5, 40% (w/v) PEG400).

### 2.3.1 Structure determination and refinement of *Sp*FliN<sub>1</sub>

Data collection was performed at the ESRF in Grenoble, France under cryogenic conditions (100 K) at the beamline ID 23-2 to a diffraction limit of 2.0 Å resolution. Data were recorded with a DECTRIS PILATUS 6M detector. Data processing was carried out using iMosflm (113) and the CCP4-implemented program SCALA (114). The structure of *Sp*FliN<sub>1</sub> was solved by molecular replacement (MR) with CCP4-integrated PHASER (115) using the *Thermotoga maritima* (*Tm*) FliN dimer (pdb:1O6A) as search model at 1.85 Å resolution (Table S1). Structures were

manually built in COOT (116) and refined using PHENIX (117) refine. The structure was refined to a  $R_{\text{work}}/R_{\text{free}}$  of 21.8/26 %.

### 2.3.1 Crystal structure of FliN<sub>1</sub>

The crystal structure of *Sp*FliN was determined at 2.0 Å resolution (Table S1) and the structure was complete except for the first 39 amino acids and the last eight residues due to either flexibility or degradations. The structure revealed a dimer of *Sp*FliN whereby the overall shape of the dimer is reminiscent of a saddle (**Figure 27A**). Each chain contains 2  $\alpha$ -helices and 5  $\beta$ -sheets. The  $\beta$ 1-sheets of each chain build a two  $\beta$ -barrel and keep the two subunits together. Further interactions between the subunits of the dimer are established between  $\beta$ 2 of one chain with  $\beta$ 5 of the other chain. The helix  $\alpha$ 1 is directed away from the main body of the molecule. The FliN homodimer shows significant structural similarity to the FliN-homology domain of *T. maritima* with a root mean square deviation (r.m.s.d) of 1.31 Å<sup>2</sup> over 38 C $\alpha$ - atoms. Compare to *Tm*FliN, the  $\alpha$ 3 helix is not present in the *Sp*FliN structure.

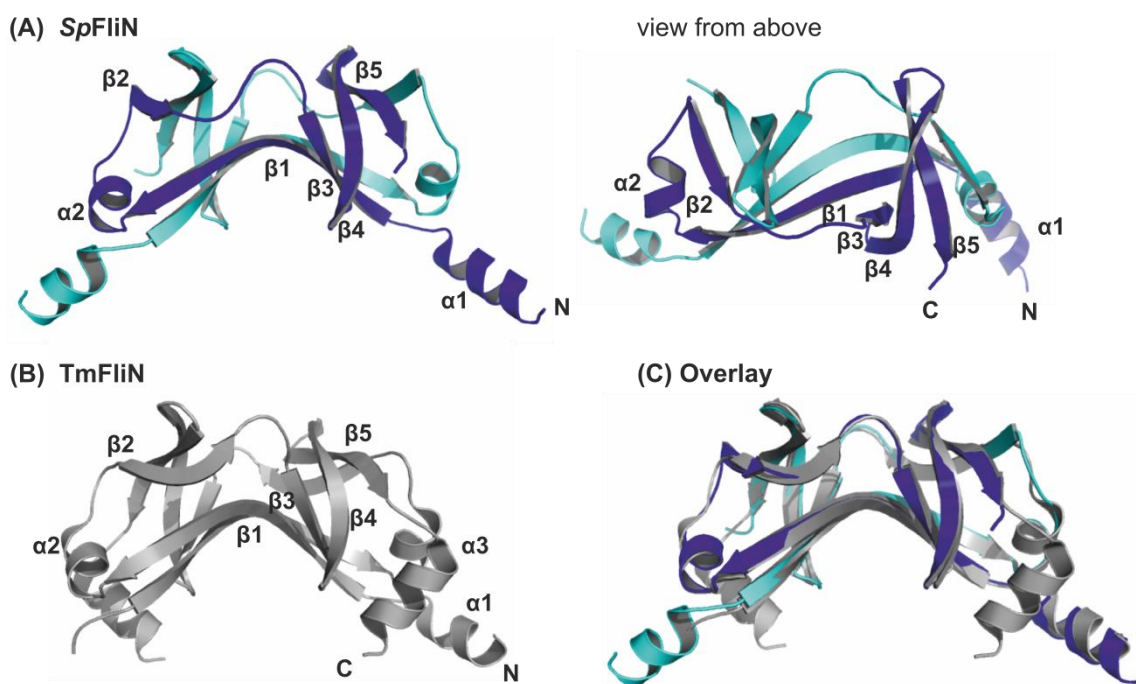


**Figure 27: Crystal structure of *Sp*FliN.** (A) Two views of the *Sp*FliN dimer with one chain in blue and the other chain in cyan. The crystal structure of the *Tm*FliN dimer (pdb: 1O6A) and the (C) overlay of *Sp*FliN monomer (blue, cyan) and *Tm*FliN monomer (grey).

## 2.5 Characterization of FlhF

FlhF is a SRP-GTPase and builds together with the signal recognition particle Ffh and the signal recognition receptor FtsY the subfamily of SRP-GTPases of the SIMIBI class of nucleotide binding proteins. FlhF is conserved among many bacterial species and is essential for the correct establishment of flagella (reviewed in (83, 84)). A closer look to the domain architecture of FlhF shows that FlhF can be divided into three domains, the NG-domain and B-domain. The N- and G-domain share a significant sequence homology with Ffh and FtsY within their NG-domains and are important for the GTPase activity (**Figure 28**). All FlhF proteins contain a natively unfolded and overall basically charged extension at its N-terminus (B-domain), which differs in size and conservation among the species. The first and only crystal structure of FlhF to date comes from *B. subtilis* (86). This crystal structure contains only the NG-domain and shows a GTP-dependent homodimer. However, the functional role of the FlhF GTPase homodimer for formation of the flagellation pattern is unclear. It is also unknown, how FlhF is able to localize to the membrane or to the appropriate cell pole. Besides FlhG (compare to **2.1** and **2.2**), no other interaction partner on a molecular level of FlhF could be identified. Given the complexity of spatial and numerical regulation of flagellation patterns it is hard to imagine that these regulatory mechanisms should be solely governed by FlhF, FlhG and the FlhFG-complex. The identification of additional interaction partners for either of the proteins will surely aid our understanding of the development of flagellation patterns in bacteria as a whole.

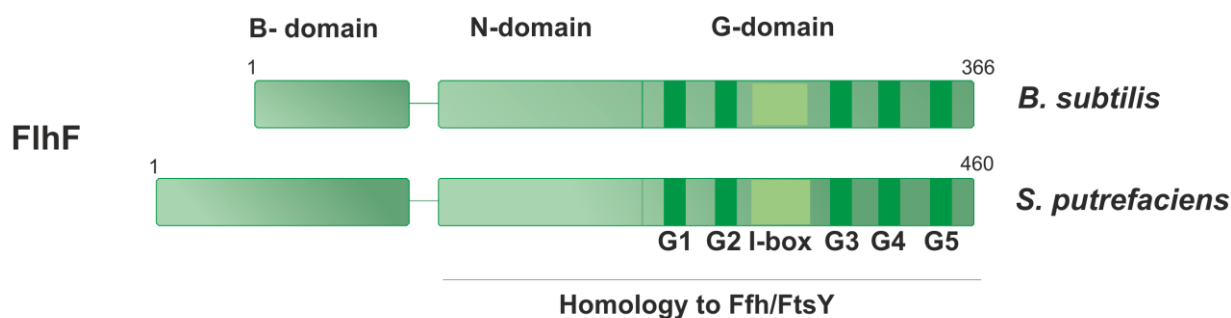


**Figure 28: Domain organization of FlhF.** Domain organization with G-elements of FlhF. Domain architecture of FlhF from *S. putrefaciens* and *B. subtilis*. The NG-domain of FlhF homologs shares high sequence homology with the NG-domains of Ffh and FtsY. Specific motifs for GTPase activity (G1-G5) are indicated.

### 2.5.1 Purification of FlhF from *S. putrefaciens*

To figure out, whether FlhF from *S. putrefaciens* compared to FlhF from *B. subtilis* possesses GTPase activity and can be stimulated by *Sp* FlhG, it was necessary to purify *Sp*FlhF. First a truncated variant of FlhF from *S. putrefaciens* harboring only the NG-domain (i.e.; FlhF  $\Delta$ N152) was cloned containing an N-terminal hexahistidine-tag. After protein production in *E. coli* BL21 (DE3) and protein purification by Ni-NTA affinity chromatography, the protein shows heavy precipitation. Different buffer conditions or the supplementation of various guanosine nucleotides did not improve the protein solubility. Since the truncated variant of FlhF was not soluble as true for the homolog from *B. subtilis* (93), full-length FlhF should show improvement. But even the purification of full-length FlhF yielded in a low amount of soluble protein accompanied by precipitation. However the concentration of soluble FlhF was sufficient for biochemical analysis as it was previously described in section 2.2.1 (**Figure 20**).

### 2.5.2 The N-terminal region of FlhF from *S. putrefaciens*

Even if the purification of FlhF and its variant FlhF-NG proved to be difficult, interesting observations could be made. FlhF-NG could be purified in good quantity and purify by Ni-NTA affinity chromatography (**Figure 29A**). In contrast, purification and SDS-PAGE analysis of full-length FlhF reveals many contaminating proteins of a size below 40 kDa (**Figure 29B**). Mass spectrometry analysis of the contamination signals revealed a prominent amount of ribosomal proteins (Table S2). This suggests that full-length FlhF interacts with ribosomes (see also **2.5.4**). Moreover, the B-domain of FlhF can be defined as the part of FlhF that mediates the interaction as FlhF-NG does not interact with ribosomal proteins while full-length FlhF does (**Figures 29A and B**). The B-domain of FlhF is natively unfolded and differs in length between FlhF homologs from different species. However, close inspection of the amino acid sequence of the B-domain of FlhF from different bacterial species reveals high conservation within the N-terminal region of FlhF (**Figure 29D**).

To test the hypothesis that the N-terminus of FlhF is mediating the interaction with ribosomal proteins, an FlhF variant lacking the first ten amino acids (FlhF $\Delta$ N10) was constructed and purified by Ni-NTA affinity chromatography. The amount of ribosomal proteins co-purified with FlhF $\Delta$ N10 is drastically decreased compared to full-length FlhF (**Figure 29C**). FlhF $\Delta$ N10 is a

promising protein construct from which the dissection of FlhF's regulatory and enzymatic network by biochemical and genetic methodology can be further approached.

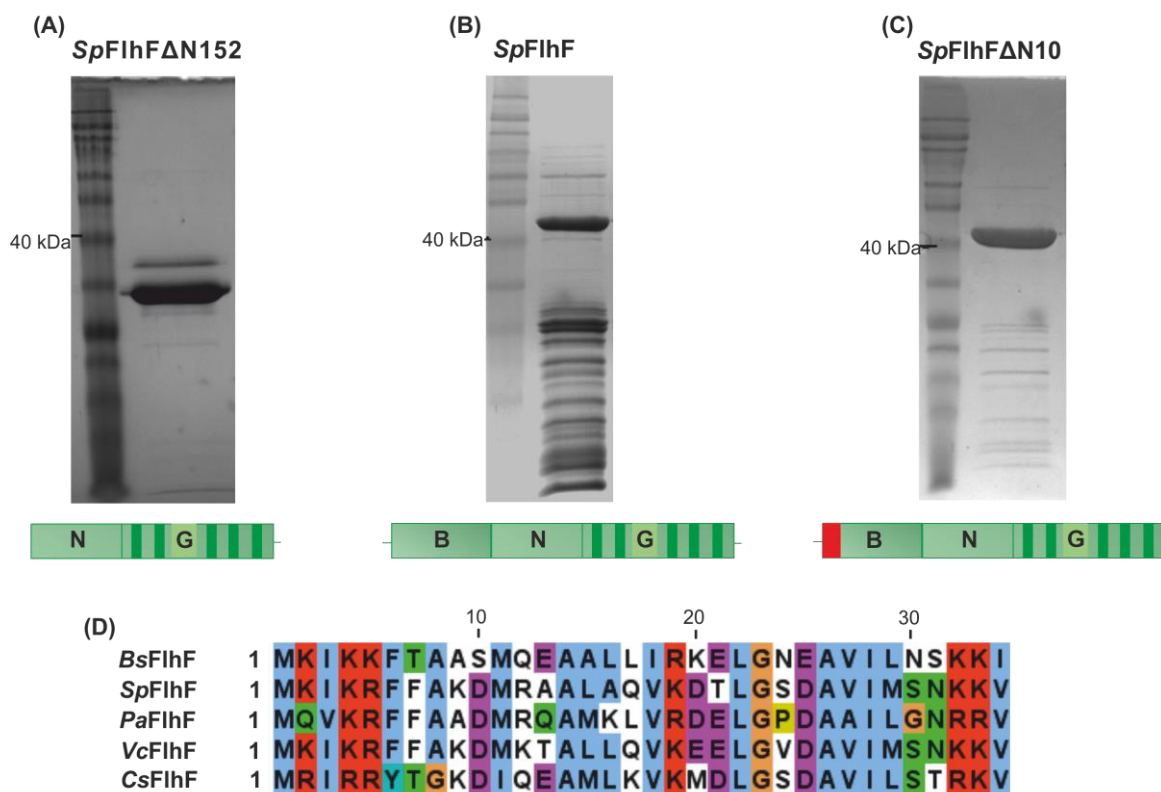


**Figure 29: Purification of FlhF variants.** Coomassie-stained SDS-PAGE after Ni-NTA chromatography of (A) FlhFΔN152, (B) full-length FlhF and (C) FlhFΔN10. (D) Amino acid sequence alignments of the N-terminus of FlhF from different organisms: *B. subtilis* (*Bs*), *S. putrefaciens* (*Sp*), *V. cholera* (*Vc*), *P. aeruginosa* (*Pa*), *Clostridium stercorarium* (*Cs*).

In conformance with the biochemical evaluation of FlhFΔN10 (see above), motility assays of *S. putrefaciens* on soft agar plates demonstrate that *flhF*ΔN10 cells exhibit a significantly reduced swimming behavior comparable to a *ΔflhF* mutant (**Figure 30B**). This was done in laboratory of Prof. Dr. Kai Thormann. Further *in vivo* studies on *S. putrefaciens* revealed, deletion of the first ten amino acids effects also the polar localization of FlhF. FlhF which lacks the N-terminal region is no longer able to localize at the pole (Thormann, unpublished data). These observations suggests that the N-terminus of FlhF contains a functional important motif that could be serve as a potential interaction platform and either by this or some other unknown mechanism influence the localization of the flagellum to the cell pole.



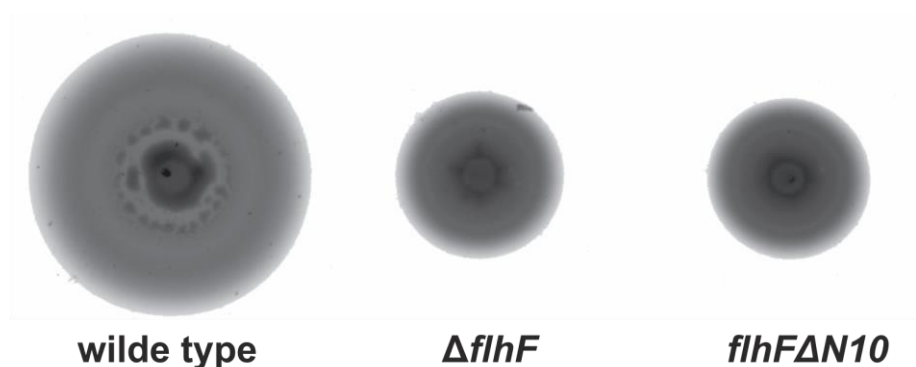


**Figure 30: Influence of *flhFΔN10* on the motility of *S. putrefaciens*.** Motility behavior of  $\Delta flhF$  and *flhFΔN10* mutants compare to the wild type (Data were kindly provided by the Kai Thormann).

### 2.5.3 The N-terminus of FlhF interacts with ribosomes

Based on the observation that the N-terminus of FlhF might serve as an interaction platform for ribosomal proteins, a truncated variant of FlhF comprising only its first 32 amino acids fused to an N-terminal GST-tag (i.e.; GST-FlhF-N32) was generated and purified. GST-FlhF-N32 was then incubated with freshly prepared cell lysate from *S. putrefaciens* and the protein content was visualized by Coomassie-stained SDS-PAGE. Signals corresponding to putative interaction partners were analyzed by mass spectrometry (**Figure 31A**). The GST-*Sp*FlhG and GST-*Bs*YpsB served in this GST-pulldown as negative controls. The proteins co-purified with GST-*Sp*FlhF-N32 were subjected to mass spectrometric analysis following tryptic digestion and again revealed more than ten ribosomal proteins from both the small and large ribosomal subunit (**Figure 31B**, also compare to **2.5.2** and **Figure 29**). The large number of ribosomal proteins co-purified by the N-terminal part of *Sp*FlhF in two independent experiments strongly suggests that FlhF interacts with the ribosome as a whole rather than with single components.

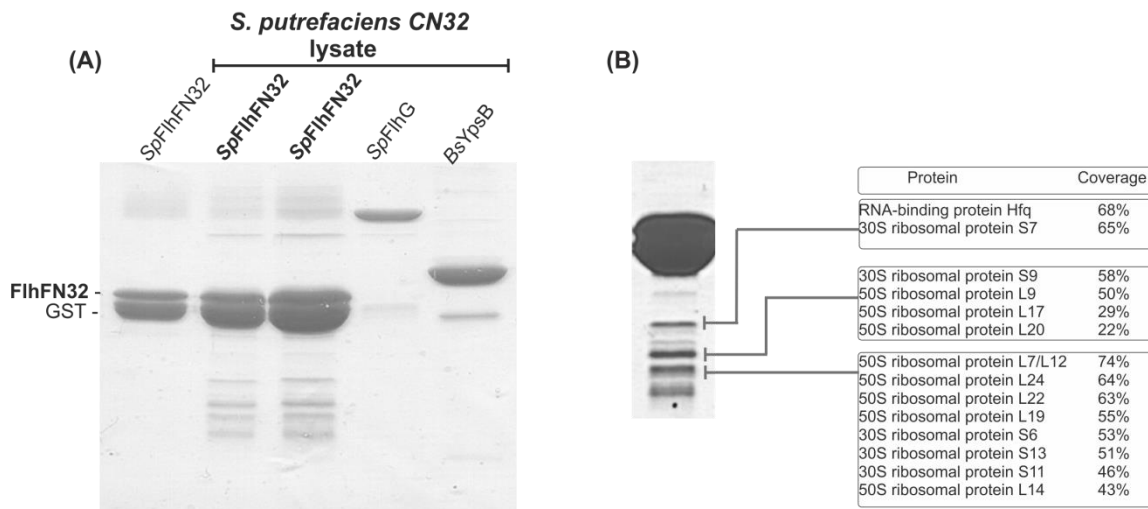


**Figure 31. Interaction of FlhF-N32 with ribosomal proteins.** (A) Shows Coomassie-stained SDS-PAGE of a pull-down assay with GST-*SpFlhF-N32* with different concentrations (1nmol, 5nmol) and freshly prepared cell lysate from *S. putrefaciens*. *SpFlhG* and *BsYpsB* served as negative controls. (B) Summary of proteins identified from the pull-down assay in A by mass spectrometry following tryptic digestion.

## 2.5.4 FlhF associates with ribosomes

To verify the hypothesis that FlhF associates with ribosomes, ribosomes were purified from *S. putrefaciens CN-32* according to a well-established protocol of Bommer and co-workers (121). One liter cell culture of *S. putrefaciens CN-32* was grown in LB-medium at 37 °C and vigorous shaking until mid-logarithmic phase. The first part of ribosome purification contains cell lysis and remove of the cell debris, which require different centrifugation steps with special buffers (detailed in 4.5.1). The Aliquot of potential ribosomes are layered onto a 10%-40% (w/v) sucrose gradient. The sucrose density gradient is then centrifuged in a swinging-bucket rotor for 12 h at 4 °C and 80,000 x g separating polysomes and 70S ribosomes from the 30S and 50S subunit (**Figure 32A**). After ultra-centrifugation the gradient was collected by hand from the top to the bottom in 16 fractions. The samples were analyzed by SDS-PAGE and Western blotting using anti-FlhF antibodies. The SDS-PAGE shows the ribosome profile, but it seems that only the 30S subunit and the 50S subunit are separated (Fractions 1-8, **Figure 32B**). The 70S subunit and polysomes would have been expected in fractions 9-16. However, Western blot analysis with anti-FlhF reveals protein presence in the fractions 4-7 correlating to the fractions containing 50S ribosomal subunits (**Figure 32B**).

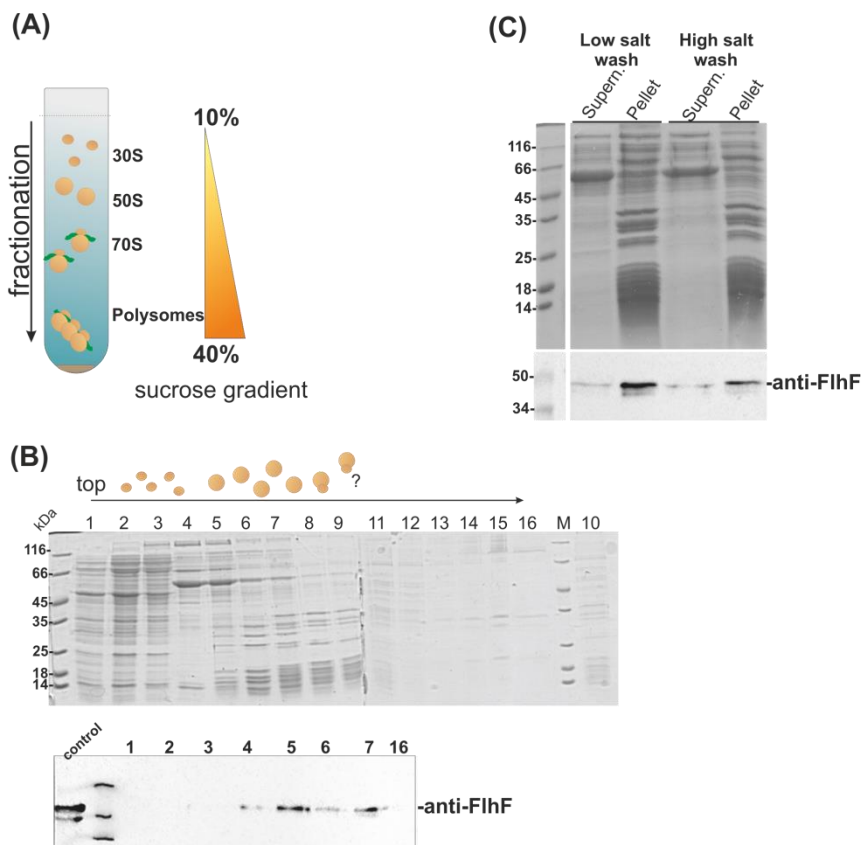


**Figure 32: FlhF associates with ribosomes in *S. putrefaciens*.** (A) Schematic model of ribosome purification by sucrose density-gradient centrifugation. (B) Collected fractions of the sucrose density gradient were analyzed by Coomassie-stained SDS-PAGE and western blotting with anti-FlhF antibodies. (C) Ribosome purification under high and low salt conditions, were analyzed by Coomassie-stained SDS-PAGE and western blotting with anti-FlhF antibodies

In order to investigate ribosome binding of FlhF protein, salt wash experiment was performed. Therefore, the ribosomes from one liter cell culture of *S. putrefaciens* CN-32 were isolated as described before. The ribosomal pellet was resuspended in 2 ml of ribosome lysis buffer (20 mM HEPES-K pH 7.5, 60 mM K-acetate, 5 mM MgCl<sub>2</sub>, 5 mM DTT and 1 mM PMSF) and laid over a cushion of 25 % (m/v) sucrose in lysis buffer supplied with either 100 mM K-acetate for low salt wash or 800 mM for high salt wash, respectively. The samples were centrifuged at 247,000 x g for 2 h at 4 °C and divided into supernatant and pellet fraction. The supernatant was precipitated with 50% TCA, and solubilize in a volume of 200 µl. Samples were taken at all relevant purification steps and analyzed by SDS-PAGE and Western blotting using anti-FlhF antibodies. The Western blot analysis showed that FlhF is found in the pellet fraction under both, high and low salt conditions (**Figure 32C**). That lead to the conclusion that FlhF associates with ribosomes, in a salt independent manner. This suggests that interaction between FlhF and

ribosomes are stable. At this point, it cannot be define, if that binding occurs via either direct or indirect interaction with the ribosome.

### 2.5.5 The N-terminal region of FlhF interacts with SRP-RNA

It is proposed that FlhF is involved in the localization of the first flagellar components to the membrane (16). Moreover FlhF is a homolog of the SRP components Ffh and FtsY. Therefore, the question arises whether FlhF is able to interact with components of the SRP-System.

As described above, the N-terminus of FlhF is highly conserved among the species and the N-terminal first ten amino acids are required for ribosome interaction (**Figure 29**). Moreover, GST-FlhF-N32 is able to bind ribosomes (**Figure 31**). We therefore speculated that this N-terminal fraction of FlhF could be involved in a putative interaction of FlhF with Ffh, FtsY or SRP-RNA. Notably, GST-FlhF-N32 interacts with the SRP-RNA (**Figure 33**). However, GST-FlhF-N32 is not able to interact with Ffh or FtsY. Furthermore, initial lysate pull-down assays with full-length FlhF and FtsY, Ffh or FtsY/Ffh in a nucleotide dependent manner, could not be observed any direct interactions (data not shown).

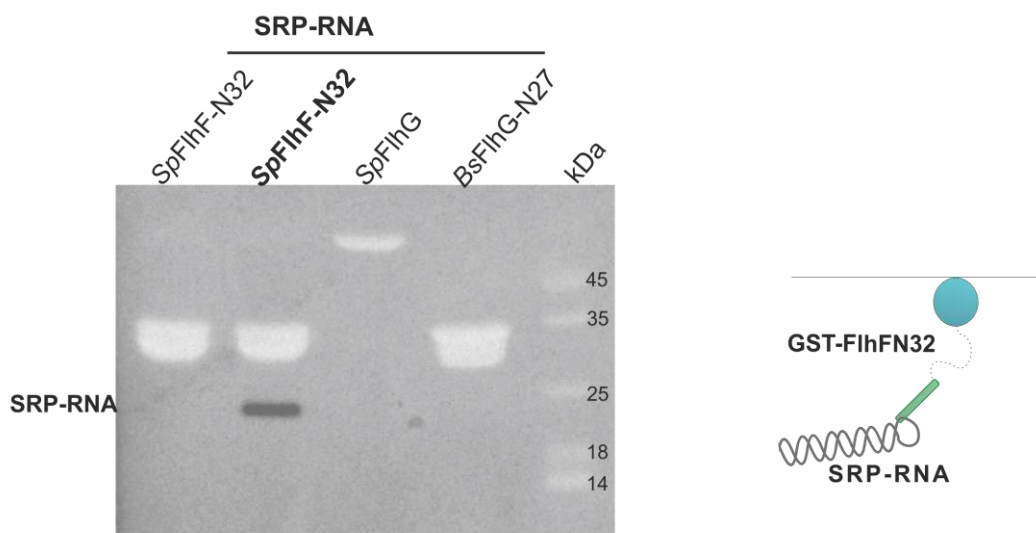


**Figure 33: the N-terminal 32 residues of FlhF interact with the SRP-RNA.** Coomassie and ethidium bromide-stained SDS-PAGE of a pull-down assay where GST-*SpFlhF-N32* was incubated with SRP-RNA. GST- *SpFlhG* and GST-*BsFlhG-N27* served as negative controls.

### 2.5.5.1 Ffh and FtsY modulate the interaction of FlhF-N32 with SRP-RNA

Next, we asked whether the presence of Ffh, FtsY or nucleotides could impact the interaction of GST-FlhF-N32 with the SRP-RNA. Addition of full-length Ffh and FtsY or both abolished the interaction of FlhF-N32 with the SRP-RNA (**Figure 34A, B**). In contrast, the NG-domain of Ffh (Ffh-NG) lacking the SRP-RNA binding M-domain, is not sufficient to remove the interaction between FlhF-N32 and SRP-RNA (**Figure 34A**). Interestingly, addition of nucleotides like the non-hydrolysable GTP analogue GMP-PNP restores the interaction of FlhF-N32 and SRP-RNA in presence of Ffh and FtsY (**Figure 34A**). A similar effect was observed with GTP but with a distinct lower signal of SRP-RNA bound to GST-FlhF-N32.

As described in section 1.6; the NG-domain of FtsY and the M-domain of Ffh bind to a region proximal to the tetraloop of the SRP-RNA. The GTP-dependent heterodimer of Ffh and FtsY, however, binds to the distal end of the SRP-RNA. Therefore, these experiments suggest that FlhF binding to the SRP-RNA is not possible when the tetraloop region is blocked by Ffh or FtsY. This suggests that the N-terminal region of FlhF binds in close proximity to the tetraloop of the SRP-RNA. This conclusion is further supported by the observation that an FlhF/SRP-RNA interaction in the presence of Ffh and FtsY is only possible when the latter ones are bound to the distal end of the SRP-RNA. According to the current model, it would be expected that the fixed heterodimeric state of Ffh and FtsY binds close to the distal end of the RNA, but in these pull-down assays it was never seen a FtsY or Ffh signal (**Figure 34A, B**). In this case it seems that the Ffh/FtsY complex did not bind the SRP-RNA or the FlhF-N32/SRP-RNA complex.

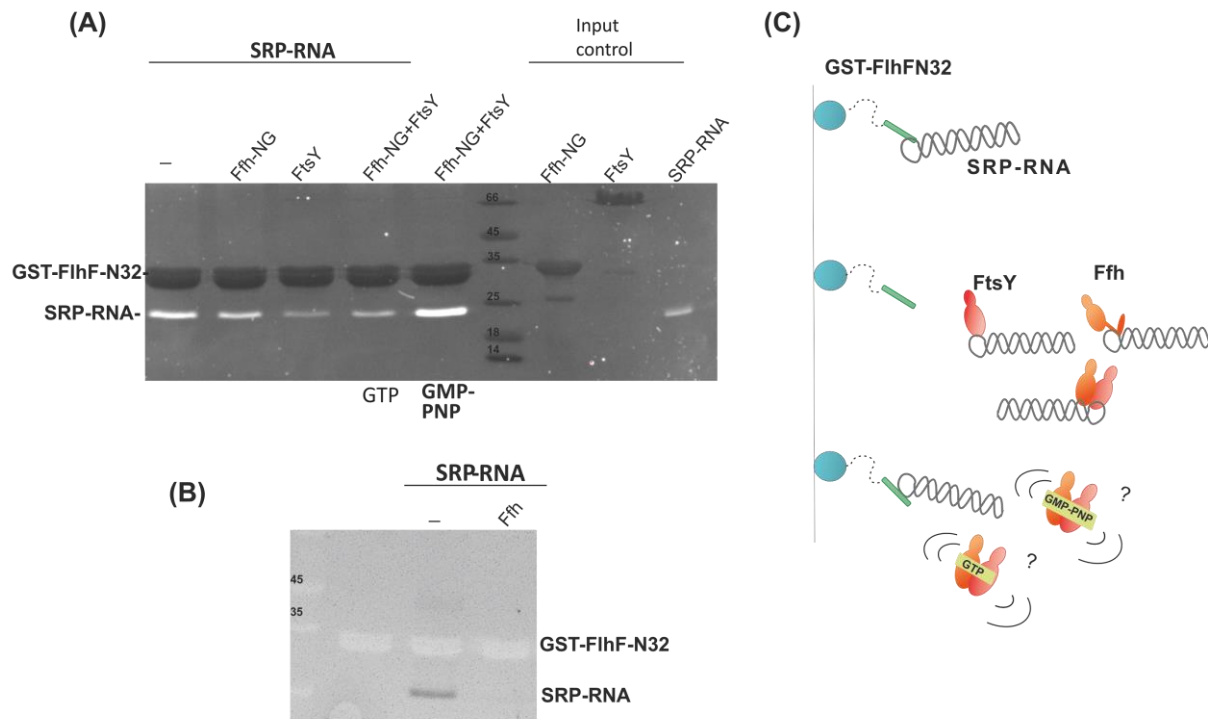


**Figure 34: The N-terminal residues of FlhF bind SRP-RNA.** (A) and (B) Coomassie- and ethidium bromide-stained SDS-PAGE of pull-down assays with GST-*Sp*FlhF-N32, Ffh and FtsY incubated with SRP-RNA and with nucleotides (not indicated means without addition of nucleotides, GTP, GMP-PNP) (C) Summarized model of interaction from (A) and (B).

### 2.5.6 Interaction of FlhF with C-ring components in *B. subtilis*

Initial lysate pulldown assays suggested to us that the B-domain of FlhF could interact with the C-ring proteins FliM/FliN and FliM/FliY in *S. putrefaciens* and *B. subtilis*, respectively (data not shown). To consolidate this observation, we first tested the direct interaction of the B-domain of FlhF from *B. subtilis* with the *G. thermodenitrificans* C-ring proteins FliY and FliN/FliY (**Figure 35A**). The *in vitro* pull-down assays demonstrated that full-length FlhF and its B-domain are able to bind FliY and the FliM/FliY complex (**Figure 35A**). The NG-domain of FlhF (*Bs*FlhF-NG) was not sufficient to bind FliY and FliM/FliY. Therefore, we conclude that the B-domain of FlhF interacts with the FliM/FliY complex via the FliY protein (**Figure 35A**). To identify a the FliY binding site within the B-domain of FlhF, different truncated variants of *Bs*FlhF B-domain were generated progressively lacking 20 amino acids from the N-terminus: *Bs*FlhF-B 21-111, *Bs*FlhF-B 41-111, *Bs*FlhF-B 81-111. These pull-down assays showed that the first 40 amino acids of the B-domain were required for the interaction with FliY and the FliM/FliY complex (**Figure 35B, C**). *Vice versa*, the first 47 amino acids of FlhF were sufficient to interact with FliY (**Figure**

35C). To further delineate the binding site, a construct containing residues 20 to 47 was generated. This FlhF-B 21-47 variant was still able to interact with FliY (Figure 35B, C). We therefore conclude that the FliY binding motif is located within residues 21 to 47 of the B-domain of FlhF (Figure 35D).

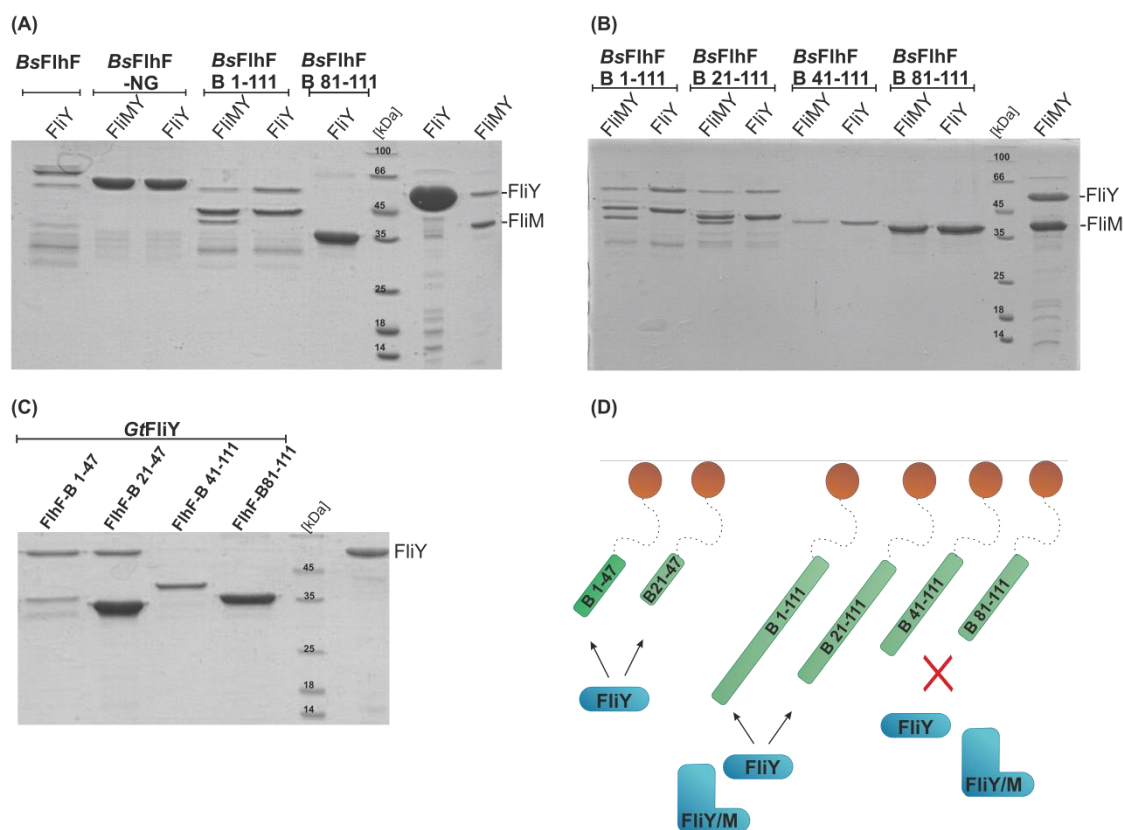


**Figure 35: The B-domain of FlhF interacts with FliY and FliM/FliY.** (A) Coomassie-stained SDS-PAGE of interaction assays using different GST-FlhF variants and FliY or FliM/FliY. (B, C) Coomassie-stained SDS-PAGE of a pull-down assays employing different GST-tagged FlhF B-domain variants, FliY and FliM/FliY (D). Interaction scheme concluded from the pulldown experiments displayed in (B) and (C). The upper part represents the immobilized GST-tag (orange) of the FlhF B-domain and its variants (green). The lower part shows the putative interaction partners (blue) assayed in this experiment.

### 2.5.6.1 The B-domain of *B. subtilis* FlhF interacts with the FliN-homology domain of the C-ring protein FliY

In the previous pull-down experiments a direct interaction between the B-domain of FlhF from *B. subtilis* and the C-ring protein FliY from *G. thermodenitrificans* could be established. In the next step I tested whether the B-domain of *BsFlhF* could also interact with C-ring components from *S. putrefaciens*. FliN from *S. putrefaciens* interacts with the B-domain of *B. subtilis* FlhF (Figure 36A). GST affinity pulldown assays employing the different *B. subtilis* B-domain variants introduced in the previous chapter showed that *S. putrefaciens* FliN interacts with the same

fraction (i.e.; amino acids 21 – 40) of the B-domain as its *B. subtilis* counterpart FliY (compare to previous chapter). Because *S. putrefaciens* FliN and *B. subtilis* FliY only share the FliN-homology domain (**Figure 36C**), we conclude that the B-domain of *B. subtilis* FlhF interacts with the FliN-homology domain of the C-ring protein FliY.

To investigate whether *S. putrefaciens* FliN or *B. subtilis* FliY would also interact with the B-domain of *S. putrefaciens* FlhF, we performed a GST pull-down assay employing different variants of the B-domain of *S. putrefaciens* FlhF (**Figure 36B**). *S. putrefaciens* FliN as well as *B. subtilis* FliY interacted with the B-domain of *S. putrefaciens* FlhF (**Figure 36B**). As observed before, the first 40 amino acids of the *S. putrefaciens* FlhF were necessary and sufficient for these interactions. In strong contrast to *B. subtilis* FlhF, the first 10 amino acids were required for this interaction (**Figure 36B**). Therefore, we conclude that although the overall interaction of the B-domain with FliN and FliY is conserved, subtle differences seem to exist at the molecular level of these interactions. Whether these are of relevance for productive flagellation pattern formation remains to be investigated.

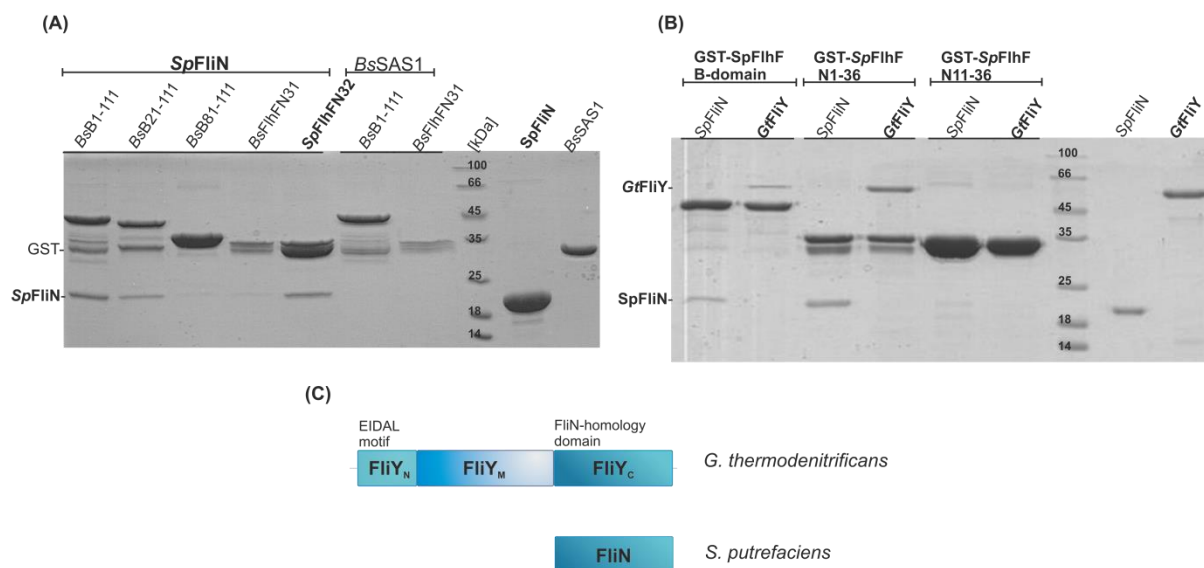


**Figure 36: Compatibility of flagellar components from different organisms.** (A) Coomassie-stained SDS-PAGE of interaction studies employing GST-*BsFlhF* B-domain and its variants and *SpFliN*. GST-*SpFliFN32* together with *SpFliN* serves as positive control and *BsB1-111/BsFlhF-N31* together with *BsSAS1* as negative control. (B) Pull-down assay with GST-*SpFlhF* B-domain and truncated variants of the B-domain together with *GtFliY* and *SpFliN*. (C) Domain architectures of FliY and FliN. ‘N’, ‘M’ and ‘C’ refer to N-terminal, middle and C-terminal domain, respectively.



## 3. Discussion

### 3.1 The nucleotide-binding proteins FlhF and FlhG

FlhF and FlhG are nucleotide-binding proteins and play essential roles for the determination of the correct flagella localization and number of flagella in many different bacteria. While deletion of *flhF* in peritrichously flagellated bacteria (i.e; *B. subtilis*, (60)) results in accumulated basal bodies towards the poles, the deletion of *flhF* in polar flagellated bacteria mainly results in non-flagellated cells or misplaced flagella (reviewed in (89, 93)). Deletion of *flhG* in *B. subtilis* leads to a tuft-like pattern (60). In contrast, polar-flagellated bacteria lacking *flhG*, show a hyper-flagellated phenotype (103). These data clearly demonstrate that FlhF and FlhG are essential for formation of different flagella patterns.

However, the molecular mechanism by which FlhF and FlhG orchestrate these different flagellation only poor understood.

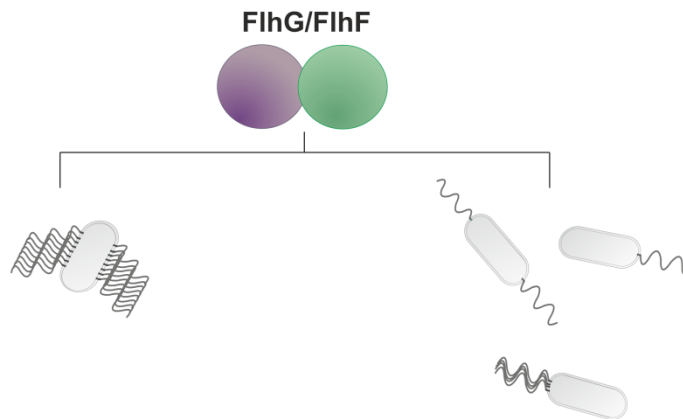


**Figure 37: Schematic overview of the flagellation patterns determined by FlhG (purple) and FlhF (green).**

Nucleotide-binding proteins (i.e.; GTPases and ATPases) often function as molecular switches that regulate biological processes following the ‘GTPase switch’ paradigm. Nucleotide-binding proteins can exist and switch between two discrete states that are defined by the bound nucleotide: i. the ‘GTP/ATP’ and ii. ‘GDP/ADP’-bound state. Following the switch paradigm,

the ‘GTP/ATP’-state is considered to be the ‘ON’-state in which the protein can bind to effector molecules, while in the ‘GDP/ADP’ state this is not the case (‘OFF’-state). Switching between the ‘ON’ and ‘OFF’-states usually requires the presence of nucleotide exchange factors (GEFs) or GTPase/ATPase activating proteins (GAPs and AAPs, respectively) (89).

Both FlhF and FlhG can be viewed as nucleotide-dependent molecular switches. For FlhG, it was recently observed that the monomer is located in the cytoplasm and represents the inactive state. The ATP-dependent homodimer of FlhG is restricted to the membrane through its MTS and represents the active state (89). So far, neither for FlhG nor for other dimeric ATPases, an additional protein for exchanging nucleotides has been identified.

FlhF forms GTP-dependent homodimers that are considered as the ‘ON’-state. GTP-bound, dimeric FlhF is associated to the membrane, while the GTP or free, monomeric FlhF locates in the cytoplasm (93,103). For *B. subtilis*, it was shown that FlhG interacts with the GTP-bound FlhF homodimer through its highly conserved N-terminal activator helix and stimulates the GTPase activity of FlhF. In this study, I was able to demonstrate that the GTP-dependent interaction of FlhG and FlhF is highly conserved and exists also in the polar-flagellated *S. putrefaciens* and the amphitrichously flagellated *C. jejuni*. The N-terminal activator helix of FlhG, which comprises the conserved ‘DQRXXL’ motif, is necessary and sufficient for this stimulation.

Therefore, it seems that the function of FlhG as a negative regulator seems highly conserved among the flagellated bacteria (**Figure 9B**). By now it seems that FlhF and FlhG form a regulatory network and form a regulatory circuit with two connected molecular switches to control number and placement of the flagella. However, it is not clear, whether activation of FlhF requires an FlhG homodimer and therefore may take place at the plasma membrane. So far, no further components have been identified, which may influence the nucleotide exchange of FlhF and FlhG as well as an activator for FlhG. Although the consequence of the GTPase stimulation of FlhF by FlhG in peritrichous flagellated bacteria is still unknown, it seems the mechanism is highly conserved between the different organisms.

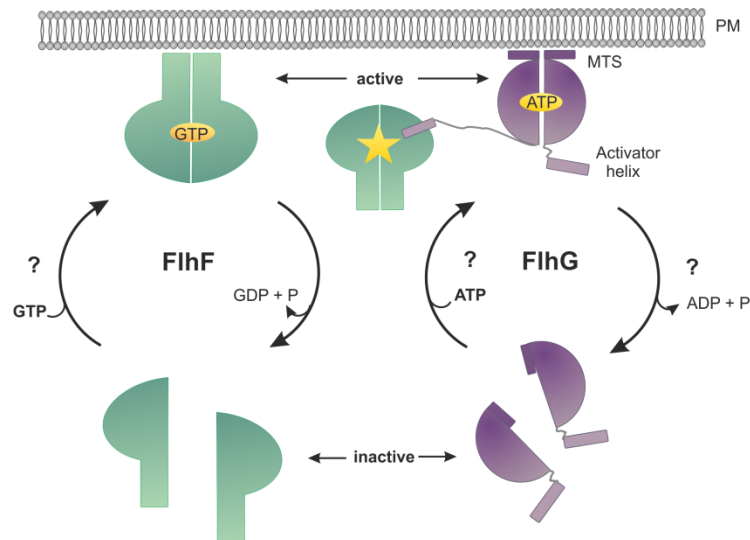


**Figure 38: Figure 39: Regulatory cycle of FlhF and FlhG.** The SRP GTPase FlhF (green) forms a GTP-dependent homodimer and represents the active state. After stimulation of FlhF through the activator helix of FlhG (purple), the homodimer might disassemble and enters the monomeric inactive state. FlhG forms an ATP-dependent homodimer and associates with the membrane via its membrane targeting sequence (MTS, active state). After ATP-hydrolysis, FlhG falls apart and localizes in the cytoplasm (inactive state). The model was slightly adapted from ref. (83).

### 3.2 FlhG supports C-ring assembly

The first crystal structure of FlhG was solved from the peritrichously flagellated *G. thermodenitrificans* and reveals a strong structural homology to the MinD ATPase, which is involved in the assembly of the cytokinetic Z-ring during cell division of rod-shaped bacteria (89). FlhG shares the hallmarks of MinD such as the overall fold, active site architecture, and ATPase activity (89). Like MinD, FlhG builds an ATP-dependent homodimer that interacts with a membrane through its conserved MTS. Therefore, FlhG cycles between a monomeric and dimeric state. Furthermore, it was recently shown that FlhG from *G. thermodenitrificans* interacts with the C-ring component complex FliM/FliY in a nucleotide-independent manner. Moreover, *in vitro* studies revealed that FlhG promotes the assembly of FliM/FliY together with the C-ring protein FliG. This FlhG driven assembly into the FliM/FliY/FliG complex is enhanced by ATP and lipids (89). Furthermore, FlhG remains bound to the FliM/FliY/FliG complex *in vitro* suggesting that an additional factor is required for promoting the release of FlhG into the cytoplasm (**Figure 38**).

Moreover, it was demonstrated that FlhG from the monotrichously flagellated *S. putrefaciens* is able to interact with the C-ring components FliM/FliN (Chapter 2.2.3). In contrast to FlhG from *G. thermodenitrificans*, FlhG from *S. putrefaciens* interacts with the C-ring component FliM. The third C-ring component in *B. subtilis*, FliY, displays an unusual domain architecture compared to its orthologue FliN (**Figure 39**). FliY and FliN share a highly conserved C-terminal domain (FliN-homology domain), but FliY comprises an additionally N-terminal ‘EIDAL’ motif and a globular middle domain (CheC-like phosphatase domain). *In vitro* interaction assays have shown that the interaction between FlhG and FliM/FliN is mediated by the N-terminal ‘EIDAL’ motif of FliM (Chapter 2.2.4). In *G. thermodenitrificans* the interaction between FliM/FliY and FlhG is also mediated through the N-terminal ‘EIDAL’ motif but from FliY instead of FliM (89). Moreover, it could be observed in *in vivo* and *in vitro* studies that *S. putrefaciens* FlhG does not stay associated with the FliM/FliN/FliG complex in contrast to the situation in *B. subtilis* (see above). This is the first molecular evidence of differences of an FlhG-dependent coordination of C-ring assembly between the peritrichously flagellated *G. thermodenitrificans* and the monotrichously flagellated *S. putrefaciens*. Additionally, this work shows that the FlhG interaction with the C-ring of *S. putrefaciens* is restricted to the primary (polar) flagellar-system and does not interact with the secondary lateral flagellar-system (Chapter 2.2.3).

Interestingly, the ‘EIDAL’ motif of FliM mediates also the interaction with CheY. This protein belongs to the chemotaxis system controlling the motor switch of flagellar rotation. FliM from the secondary lateral system lacks this EIDAL motif and is thus independent of the FlhF-FlhG mediated flagella formation and the chemotaxis system and represents a completely different system (73).

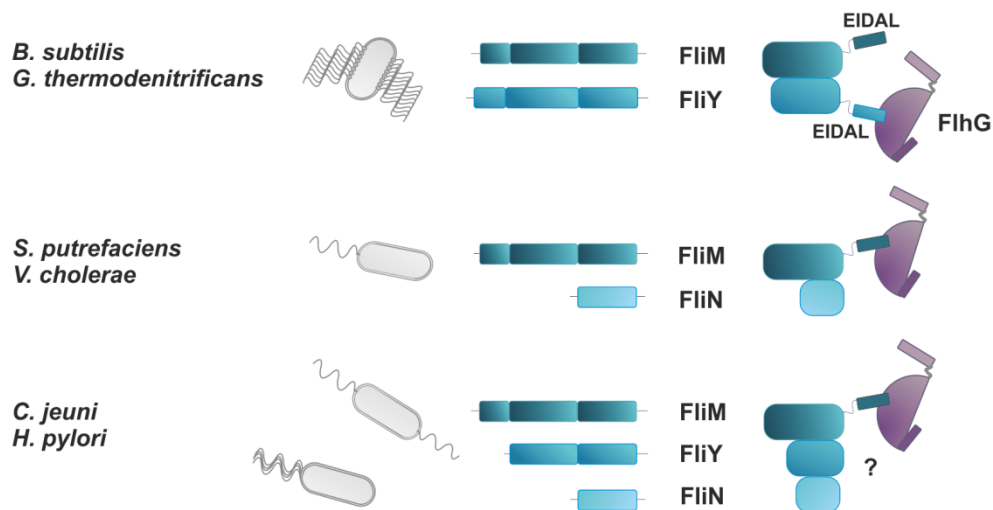


**Figure 40: C-ring composition in different organisms.** Schematic overview of the different C-ring compositions from differently flagellated bacteria. Interactions of FlhG (purple) with the corresponding C-ring component via the ‘EIDAL’ motif are indicated.

Special roles in this case play the  $\epsilon$ -proteobacteria *Campylobacter* and *Helicobacter*, which comprise both FliN and FliY at different loci at their genome (50) (**Figure 24**). In contrast to *B.subtilis* and *G. thermodenitrificans*, FliY lacks the N-terminal ‘EIDAL’ motif. Initial interaction studies have shown an interaction of FlhG with FliM from *C. jejuni* and an interaction between FliY and FliN (Chapter 2.2.5). However, no direct interaction between FliM and FliY and FliN could be observed and requires further attention. However, it can be assumed that the potential interaction partner of FliM in *C. jejuni* is FliY, because *fliY* is localized in the genome close to *fliM*. Furthermore, it seems that FlhG influences spatial parameters of division, because an deletion of *flhG* results in a significant formation of mini cells (64). In many bacteria the spatial regulation of the cell division including the Z-ring formation is controlled by the Min-system. *Campylobacter* species lack genes for the Min-system (64). The crystal structure of *C. jejuni* FlhG solved in this work confirmed that FlhG exhibits some properties common to MinD, which raise the possibility that *Campylobacter* species have adapted FlhG to influence inhibition of division at poles (Chapter 2.2.1, (84)).

### 3.2.1 Bifunctional role of FlhG

Based on our *in vivo* and *in vitro* data combined with literature reports two possible models with the involvement of FlhG during C-ring assembly are taken into consideration (**Figure 40**):

In the first scenario, FlhG might function as a spacer between the basal bodies and promotes the assembly of the flagellar C-ring biogenesis. Here it is assumed, that the monomeric FlhG interacts with FliM/FliY complex in the cytoplasm arriving together to the nascent basal body. Whether FlhG delivers FliM/FliY complex to the nascent basal body or *vice versa* is not clear so far. At the nascent basal body FlhG supports the assembly of FliM/FliY to FliG in an ATP-dependent manner. Previous data demonstrate that lipids and FliG trigger the ATP-dependent dimerization of FlhG. This requires further FlhG/FliM/FliY complexes and result in a complete C-ring formation (89,122). Possibly during and after the C-ring assembly, FlhG remains at the C-ring. This raises the possibility that the ATP-bound FlhG homodimer could function as spacer between the basal bodies (**Figure 40A**). This is in line with observations in *B. subtilis*, where an *flhG* deletion results in aggregated basal bodies. How FlhG is inactivated is not known.

In the second scenario which is mainly based on data of polar flagellated bacteria, FlhG acts as negative flagellar regulator (**Figure 40B**). In this scenario FlhG binds FliM/FliN, this ternary complex arrives at the future basal body structure. Whether FlhG recruits FliM/FliN to FliG or *vice versa* is not clear. In contrast to FlhG from *B. subtilis*, FlhG does not remain at the C-ring neither it builds a quaternary complex with FliM/FliN/FliG. Possibly, the association of FliM/FliN into the nascent C-ring recruits FlhG close to the membrane and FlhF. With the completion of the C-ring the basal body is complete and FlhF as a putative recruiter for early flagella components is no longer needed. Therefore, FlhG inactivates FlhF and serves as a control point, so that no further basal bodies can be formed. This fits with the observation that a deletion of *flhG* deletion in polar flagellated bacteria results in hyper-flagellated cells. Furthermore in *P. aeruginosa* and *V. cholerae* it was shown that FlhG interacts with the main flagellar regulator FlhQ (also FlrA) and inhibits its ATPase activity, which might result in downregulation of flagellar gene expression. Moreover, in *S. putrefaciens* recent have experiments demonstrated that FlrA interacts with FlhG stimulates its ATPase activity and serves as potential release factor of FlhG (Mrusek, Steinchen & Bange, unpublished data). This FlrA/FlhG interaction directly links localization to control of transcription and might be required for the numerical control of

flagella. FlrA is restricted to the monotrichously flagellated species and is a further difference of the FlhF-FlhG directed flagella formation of monotrichously flagellated and peritrichous flagellated species.

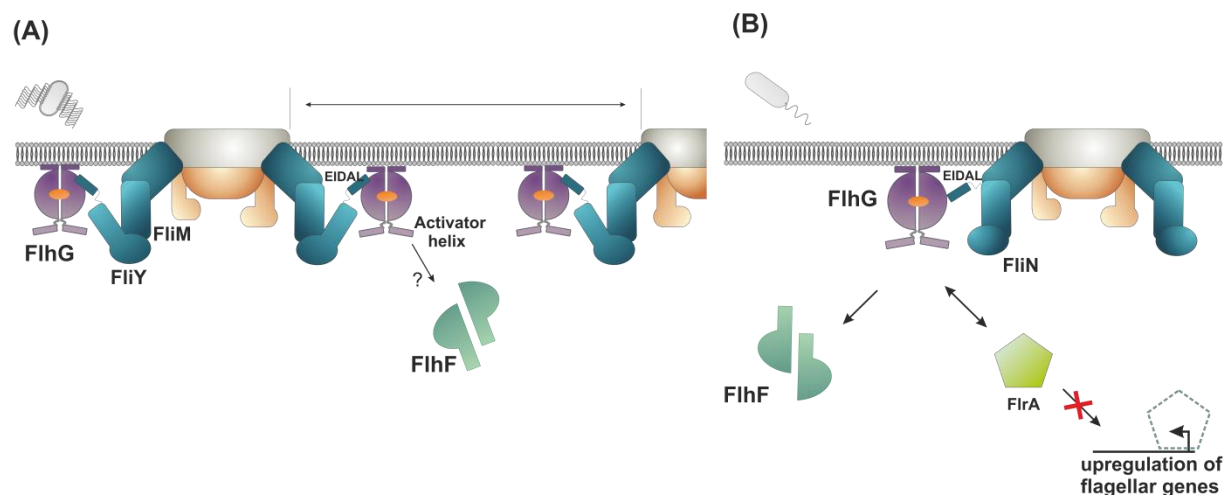


**Figure 41: The Working hypothesis of FlhG during formation of polar and peritrichous flagella patterns.** (A) Schematic model of FlhG in peritrichously flagellated bacteria. FlhG interacts with the FliM/FliY complex via the ‘EIDAL’ motif of FliY and support the assembly of the FliM/FliY complex into the C-ring. The ATP-bound FlhG homodimer remains bound to FliM/FliY and could therefore acts as a spacer to ensure minimal distances between flagella. The consequences of the FlhF-FlhG interaction are still not clear and marked by a question mark (B) FlhG acts as negative regulator in polar flagellated bacteria. FlhG interacts with the FliM/FliN complex via the ‘EIDAL’ motif of FliM to promote C-ring assembly. In close proximity to FlhF, FlhG stimulates the GTPase activity of FlhF. FlhF enters into the inactive state and dissociates from the membrane. FlhG interacts with the master transcription regulator FlrA, which results in the downregulation of flagellar genes. FlrA interaction with FlhG might also stimulate the release of FlhG from the membrane.

The main task of FlhG seems to differentiate between monotrichously flagellated bacteria and peritrichously flagellated bacteria. In monotrichously flagellated bacteria, FlhG must ensure that only one flagellum is formed. Therefore FlhG inactivates FlhF and interacts with the master regulator FlrA, which results in an inactivation of FlrA, downregulation of flagellar gene expression and finally inactivation of FlhG. The interaction with the C-ring could serve as a

temporal checkpoint. The interaction with the C-ring possibly signals the completion of the basal body and FlhF is no longer required.

In peritrichously flagellated bacteria FlhG supports the C-ring assembly and serves as a spacer to prevent basal body aggregation. Little is known about the stimulation of FlhF by FlhG in peritrichously flagellated bacteria and it seems that deletions of *flhF* or *flhG* in *B. subtilis* have only minor influence on the flagellation pattern and do not impair swimming or swarming motility. The FlhF/FlhG-mediated orchestration of lophotrichous flagellation pattern such as *H. pylori* is fairly unknown. A deletion of *flhG* in *H. pylori* leads to non-flagellated cells indicating an opposite effect of FlhG on the number of flagella and a different mechanism of counting (65). Furthermore the amphitrichously flagellated bacterium *C. jejuni*, FlhG seems to be involved in cell division. It is remarkable, how such a highly conserved protein which shows only little variations in its structure along the bacteria, controls a wide spectrum of features depending on the respective interaction network and requires more attention for better understanding

### 3.3 The mysterious role of FlhF

FlhF consists of three domains named the B-, N- and G-domain. While the B-domain is natively unfolded, the N- and G-domains form a structurally and functionally coupled unit (86). Notably, all three domains of FlhF are required for spatio-numerical regulation of flagellation and motility (16, 91, 117).

The NG-domain shares high structural homology with the well-characterized SRP-GTPases Ffh and FtsY. Structural and biochemical analysis have shown that the NG-domain of FlhF forms a homodimer in the presence of GTP that shares significant homology to the well-characterized Ffh/FtsY NG-domain heterodimer that regulates the co-translational insertion of transmembrane protein in all living organisms (86) (compare also to chapters 1.5 and 1.6).

Sequence alignments of FlhF proteins from different bacterial species reveal significant differences in their length between FlhF proteins from different bacterial species. While the NG-domain shows a high degree of conservation, the B-domain is generally less conserved. The strongest degree of conservation between different B-domains is found within the N-terminal 40 residues of FlhF proteins (123).



The precise molecular function of FlhF remains enigmatic. It is clear that the protein is required for the correct localization of flagella. Therefore, it is assumed that FlhF targets early flagellar components to the future flagella assembly site. However, an exact mechanism is far from being demonstrated. *In vivo* data of monotrichously flagellated bacteria suggested that FlhF can localize to the cell pole independent of other flagellar proteins. However, no transmembrane binding region for FlhF has been identified so far. Furthermore, it was shown that FlhF from *V. cholerae* is important for the polar localization of the earliest flagellar structural component, the inner-membrane MS-ring protein FliF (16). Moreover, it seems that the N-domain of FlhF is important for the polar localization, while the B- and G-domain are responsible for recruitment of FliF to the cell pole. Interestingly, in the monotrichously flagellated *Shewanella oneidensis*, it was shown that the G-domain of FlhF is necessary for its placement, contrasting the N-domain of *V. cholerae* FlhF (123).

In this study, I have identified novel interaction partners of FlhF providing hints towards a better understanding of the biological role of FlhF. In the following chapters, I will summarize what we know on the interaction partners of the B- and NG-domain of FlhF and what their presence allows us to conclude about the function of the mysterious protein FlhF.

### **3.3.1 The B-domain of FlhF: a platform for multiple interactions**

I could show that *S. putrefaciens* FlhF associates with ribosomes whereby the first N-terminal residues of the B-domain seem to play a crucial role (Chapter 2.5.3). Moreover, it was shown that the absence of the first 10 amino acids impairs the interaction with the ribosomes. Additionally, *in vivo* studies demonstrated that deletion of the first ten amino acids of FlhF has the same negative effect on swimming as a deletion of the whole gene (Chapter 2.5.2).

The association of FlhF with ribosomes might be not surprising as FlhF is the third member of the SRP-GTPase family. The two other members FtsY and Ffh are well characterized for their important role in mediating the transfer of ribosomes-nascent chain complexes (RNC) to the translocon within the membrane. An interesting idea about the function of FlhF could be inspired by recent data on the SRP-receptor FtsY. In *E.coli*, FtsY is targeted to the membrane during its own production via its N-domain (108). It is assumed that after targeting of FtsY to the membrane, the ribosome or its large subunit remains membrane-bound. The integral membrane

protein-encoding mRNA targets to the ribosome and forms a translation initiation complex, followed by the recognition through the SRP after emerging of the nascent hydrophobic peptide. A detailed overview about the novel model of the SRP receptor-mediated ribosome targeting pathway is described in the introduction (Chapter 1.6).

As such, it is conceivable to speculate that FlhF could target the ribosome in a way comparable to FtsY. In such a scenario, the N-domain would guide ribosomes to the membrane. Since it was shown that the N-terminal region of the B-domain was able and sufficient to bind ribosomal proteins, it is possible that FlhF attaches to the ribosome via its B-domain close to the membrane (Chapter 2.5). How and whether the SRP system may be involved in this process, is still unclear. In this work no direct interaction between FlhF and FtsY or Ffh was observed, but could be due to poor stability of full-length FlhF from *S. putrefaciens*. *In vitro* interaction assays revealed that the N-terminal region of the B-domain is also able to bind the SRP-RNA. Whether a specific interaction between the SRP-RNA and FlhF as observed in this study is true or not, has to be further illuminated (Chapter 2.5.4). However, recent *in vitro* studies with FlhF and FtsY from *B. subtilis* indicate an interaction between both proteins (Bange, unpublished data). It is also possible that FlhF acts as a counterpart to the SRP-System (e.g.; FtsY) to control the recruitment of integral flagellar proteins to the right position. However, no congruent model can be derived from these data at this point and requires further attention.

Furthermore, I was able to demonstrate that the B-domain of FlhF interacts with the flagellar C-ring. *In vitro* interaction assays demonstrated the FlhF from *S. putrefaciens* and *B. subtilis* is able to bind FliN(Y) and FliN(Y)/FliM (Chapter 2.5.5). Again the N-terminal 40 residues of the B-domain are required for the interaction of FlhF with the flagellar C-ring proteins. Moreover, it could be observed that FlhF of *S. putrefaciens* is also able interact with FliY of *B. subtilis* and *vice versa*. This compatibility of the C-ring components suggests that the interaction interface of the cognate C-ring protein might be located in the FliN-homology domain. This suggests that the natively disordered B-domain of FlhF serves as platform for multiple interactions partners and might be responsible for the spatiotemporal coordination of basal body assembly.

### 3.4 Species independent and species dependent interaction partners of FlhG and FlhF

A well-documented interaction partner of FlhF is the MinD-like ATPase FlhG (89). FlhG interacts with FlhF via its conserved N-terminus (also named: activator helix) and stimulates the GTPase activity of FlhF (see chapter 2.2.1). This feature marks the central interconnection between the regulatory circuits of FlhF and FlhG. The FlhF/FlhG interaction has been characterized in peritrichous and amphitrichous as well as in polar flagellated species (82, 88, 115)

Interestingly, FlhF and FlhG are able to bind to C-ring components. While FliG and FliM are highly conserved, the third C-ring member FliN(Y) differs in size and domain architecture. FlhF from both *B. subtilis* and *S. putrefaciens* is able to bind FliN(Y). FlhG interacts in *B. subtilis* as well as *S. putrefaciens* with the C-ring but it interacts with different components of the C-ring in both species. The difference in the C-ring composition and the variation in the FlhG binding site with the C-ring is probably an important hint in its role to maintain different flagellation patterns. The association of FlhF with the ribosome has been only observed in *S. putrefaciens*, but it is easy to imagine that this interaction occurs in other organisms, especially with the involvement of the conserved N-terminal region of the B-domain.

Besides components of the basal body, FlhF and FlhG interact with proteins, which are limited to bacterial species or families. Therefore two proteins are described, which are restricted mainly to monotrichously flagellated bacteria like *Pseudomonas*, *Vibrio* and *Shewanella* species, the master regulator of flagellar gene transcription FleQ/FlrA and the polar landmark protein HubP. Both, FlhF and FlhG interact with HubP (81), and it was at first assumed that HubP marks the initial placement of the flagellum. But FlhF locates independently of HubP to the cell pole, which suggests HubP is not necessary for the localization of the flagellum. Interestingly, *hubP*-deleted cells show a hyper-flagellated phenotype like  $\Delta flhG$  cells. Because of the plethora of interaction partners of HubP, it could be possible that HubP serves as gathering place including FlhF and FlhG, which implies an important role of HubP during different cell processes such as chromosome partitioning, chemotaxis and flagellation pattern control.

In *Pseudomonas*, FlhG (also: FleN) interacts with the DNA binding domain of master regulatory transcription factor of flagellar biogenesis, FleQ (also: FlrA) (63). Moreover, FlhG inhibits the ATPase activity of FleQ, which might result in downregulation of flagellar gene expression (100,102). Recent studies in our workgroup confirmed that FlhG interacts with the master regulator FlrA in *S. putrefaciens* and demonstrate that the DNA-binding domain of FlrA interacts with FlhG in the ATP-bound state (dimer) and stimulates its ATPase activity (Mrusek, Steinchen & Bange, unpublished data). This regulatory interaction between FlhG and FlrA could represent the basis to restrict flagellar biosynthesis to one flagellum in monotrichously flagellated bacteria. This idea is supported by the fact that FleQ/FlrA homologues are missing in bacteria exhibiting more than one flagellum such as the lophotrichous *Helicobacter* and amphitrichous *Campylobacter* species. However, further evidence is needed to support this idea.

### 3.5 Conclusion & Open questions

Based on the available data, I would like to propose a (very speculative) hypothesis in which FlhF serves as an ‘alternative’ SRP-receptor dedicated to directing the massive amount of flagellar transmembrane proteins to the correct future assembly site (**Figure 41**).

I would inspire a thinking in which FlhF targets a ribosome to the membrane during its own production (**Figure 42A**). How FlhF recognizes the future flagellar site (e.g.; the cell pole) remains puzzling. One idea might be that FlhF is able to recognize specific lipid compositions such as enriched cardiolipin at the cell pole (125). Another way would be the presence of specific landmark proteins enabling the ‘first contact’ of the FlhF-ribosome complex with the future assembly site. For the polar-flagellated bacteria, the landmark protein HubP seems to be a promising candidate and several experiments support that notion (reviewed in (83)).

Another unresolved issue is whether and how the SRP system is involved in this pathway. Considering the fact that spontaneous membrane insertion of transmembrane proteins is error-prone and extremely unlikely, the probability seems high that FtsY and SRP are involved in this process. FlhF recruits, possibly in complex with ribosomes, flagellar proteins to the flagellar assembly site. So far only the recruitment of the earliest component FliF was observed, but FlhF could perform a similar function for other flagellar integral membrane proteins (e.g.; components

of the type III export apparatus such as FliOPQR, FlhA, or FlhB) (**Figure 41B**). The function of the novel interaction between FlhF and the C-ring is not completely understood and can only be at most speculated. One option could be: FlhF binds the FliM/FliN complex as the last missing component of the basal body and together with the landmark protein HubP recruits FlhG in close proximity to the membrane (**Figure 41C**). Now, FlhG locates close to FlhF, triggers its GTPase activity and takes over the FliM/FliN complex. The FlhF dimer falls apart and is released from the membrane. The accumulation of FlhG close to the membrane and the nascent flagellum leads to ATP-dependent dimerization. The membrane-bound FlhG promotes the assembly of FliM/FliN into the C-ring and prevents further polar localization of FlhF. After assembly of the basal body, FlhG interacts with FlrA, which is thought to possess two functions (**Figure 42D**): At first, FlhG inactivates FlrA and represses expression of flagellar genes and secondly stimulates of the ATPase activity which subsequently releases FlhG from the membrane.

These examples illustrate how diverse the interaction network of FlhG/FlhF between bacterial species can be and provide an idea how a conserved molecular switch may control different flagellation patterns.

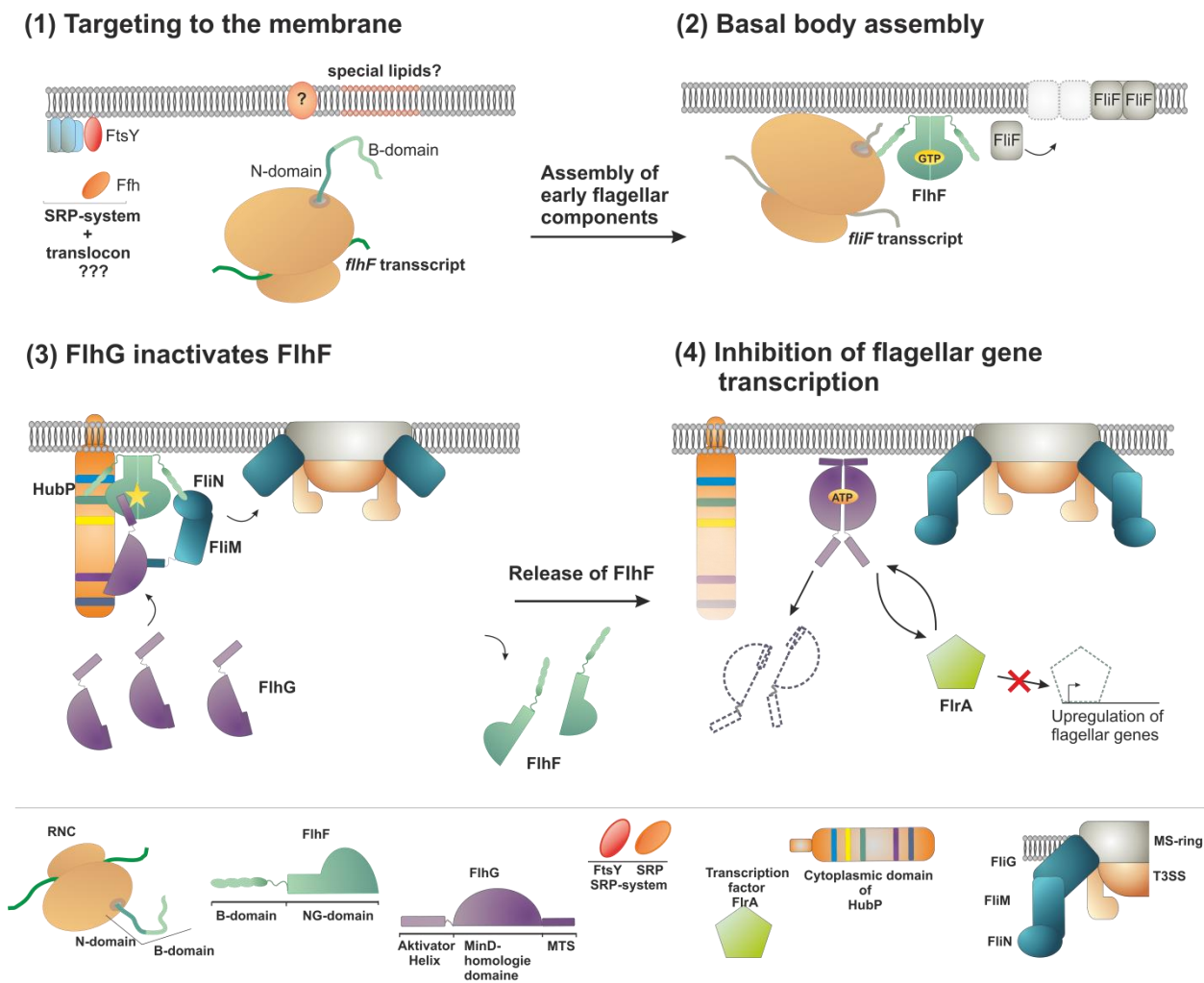


**Figure 42: Working hypothesis of polar flagellation patterning determined by FlhF and FlhG.** (1) FlhF targets to the future flagellar assembly site in a co-translational process. The ribosome remains membrane-bound and close to the future assembly site for further flagellar components (especially membrane proteins). (2) FlhF might support the assembly of flagellar proteins into the basal body. The last components of the basal body are the C-ring components FliM and FliN. (3) The landmark protein HubP together with FlhF and FliM/FliN promotes the accumulation of FlhG close to the flagellar assembly site. In close proximity, FlhG stimulates the GTPase activity of FlhF and takes over the FliM/FliN complex. FlhF falls apart and disassembles from the membrane. FlhG might assist the assembly of FliM/FliN in the C-ring (4). The interaction of FlhG with the master regulator of flagellar gene transcription FlrA has several effects: 1. FlhG inhibits the ATPase activity, which might result in downregulation of flagella genes. 2. FlrA stimulates ATPase activity of FlhG and serves as release factor of FlhG.

## 4. Material and methods

### 4.1 Materials

#### 4.1.1 Chemicals

Chemicals were purchased from Sigma Aldrich, Roth and AppliChem in highest purity available. Chemicals were used as received without further purification unless states otherwise.

Consumable supplies (1.5/2.0 ml reaction tubes, 15/50 ml Falcon tubes, pipette tips as well as syringes) were purchased from Sarstedt and Braun. Other equipment (pipettes, heating block, vortexers and power supplies) were from Neolab.

#### 4.1.2 Bacterial strains and plasmids.

Large-scale protein production for crystallography and biochemical assays was carried out in phage-resistant, chemically competent *E. coli* BL21 (DE3) (Life technologies) and Rosetta (Novagen). For plasmid amplification, chemically competent *E. coli* DH5 $\alpha$  (Life technologies) were employed. For ribosome purification and preparation of *S. putrefaciens* lysates, strain *Shewanella putrefaciens* CN-32 was used (gifted from the Thormann group, (73)).

##### 4.1.2.1 Plasmids

Various plasmids were used in the scope of this work for different purposes. pET24d(+) and pET16b (both Novagen) served as vectors for protein production of (His)<sub>6</sub>-tagged proteins, which also allowed co-production of different proteins due to different resistance markers. N-terminal GST-fusion proteins were generated using pGAT3 (J. Peränen and M. Hyvönen, unpublished).

**Table 1: Vectors used in this work**

<b>Vector</b>	<b>Insert</b>	<b>Org</b>	<b>Cloning sites</b>	<b>Tag</b>	<b>Reference</b>
pET24d	FlhF dN152	<i>Sp</i>	PciI/BamHI	N-His	This study
pET24d	FlhF dN152/dC20	<i>Sp</i>	PciI/BamHI	N-His	This study
pET24d	FlhF (fl)	<i>Sp</i>	PciI/BamHI	N-His	This study
pGEX	FlhF (fl)	<i>Sp</i>	BamHI/EcoRI	N-His, N-GST	This study
pEM-Gb1	FlhF	<i>Sp</i>	BspHI/BamHI	N-His	This study
pET24d	FlhF dN10	<i>Sp</i>	PciI/BamHI	N-His	This study
pET24d	FlhF B-dom	<i>Sp</i>	PciI/BamHI	N-His	This study
pGEX	FlhF B-dom	<i>Sp</i>	BamHI/EcoRI	N-His, N-GST	This study
pET16b	FlhF B-dom	<i>Sp</i>	PciI/BamHI	No His	This study
pGAT3	FlhF N32	<i>Sp</i>	NcoI/Xho	N-His, N-GST	This study
PGAT3	FlhF N11-32	<i>Sp</i>	NcoI/Xho	N-His, N-GST	This study
pET24d	FlhF_R285A	<i>Sp</i>	PciI/BamHI	N-His	This study
pET24d	FlhF_dN10_D390A	<i>Sp</i>	PciI/BamHI	N-His	This study
pET24d	FlhF_dN10_R285A	<i>Sp</i>	PciI/BamHI	N-His	This study
pET24d	FlhG (fl)	<i>Sp</i>	NcoI/Xho	N-His	This study
pGAT3	FlhG-GST	<i>Sp</i>	NcoI/Xho	N-His, N-GST	This study
pET24d	FlhG dN16	<i>Sp</i>	NcoI/Xho	N-His	This study
pGAT3	FlhG N20	<i>Sp</i>	NcoI/Xho	N-His, N-GST	This study
pET24d	FtsY	<i>Sp</i>	NcoI/Xho	N-His	This study
pET16b	FtsY	<i>Sp</i>	NcoI/Xho	N-His	This study
pGAT3	FtsY	<i>Sp</i>	NcoI/Xho	N-His, N-GST	This study
pGAT3	FtsY N32	<i>Sp</i>	NcoI/Xho	N-His, N-GST	This study
pGAT3	FtsY N11-32	<i>Sp</i>	NcoI/Xho	N-His, N-GST	This study
pET24d	Ffh -NG	<i>Sp</i>	PciI/BamHI	N-His	This study
pET16b	Ffh -NG	<i>Sp</i>	PciI/BamHI	N-His	This study
pET24d	Ffh	<i>Sp</i>	PciI/BamHI	His	Bange Lab
pET24d	Ffh	<i>Sp</i>	PciI/BamHI	No His	Bange Lab
pET24d	FliM1	<i>Sp</i>	PciI/BamHI	C-His	This study
pET24d	FliM1	<i>Sp</i>	PciI/BamHI	No His	This study
pET24d	FliM1 dEIDALL (1-27)	<i>Sp</i>	PciI/BamHI	C-His	This study
pET24d	FliM1 dEIDALL (1-27)	<i>Sp</i>	PciI/BamHI	No His	This study
pET16b	FliM1 dEIDALL (1-27)	<i>Sp</i>	PciI/BamHI	No His	This study
pET24d	FliN1	<i>Sp</i>	PciI/BamHI	N-His	This study
pET16b	FliN1	<i>Sp</i>	PciI/BamHI	No His	This study
pET24d	FliM2	<i>Sp</i>	NcoI/Xho	No His	This study
pET24d	FliN2	<i>Sp</i>	NcoI/Bam	N-His	This study
pGAT3	FlhG	<i>Cj</i>	NcoI/BamHI	N-His, N-GST	This study
pET24	FliY	<i>Cj</i>	PciI/BamHI	No His	This study
pET16b	FliY	<i>Cj</i>	PciI/BamHI	No His	This study
pET16b	FliM	<i>Cj</i>	NcoI/Bam	C-His	This study
pET24d	FliN	<i>Cj</i>	NcoI/Bam	No His	This study
pMAL-CS2	FliM	<i>Cj</i>		N-MBP	Hendrixson Lab



pQE30	FlhN	<i>Cj</i>	N-His	Hendrixson Lab
pQE30	FlhF	<i>Cj</i>	His	Hendrixson Lab
pQE30	FlhG	<i>Cj</i>	His	Hendrixson Lab
pQE30	FlhF D321A	<i>Cj</i>	His	Hendrixson Lab
pQE30	FlhF R324A	<i>Cj</i>	His	Hendrixson Lab
pET24d	FlhF	<i>Cj</i>	His	Hendrixson Lab
pET24d	FlhG	<i>Cj</i>	His	Hendrixson Lab
pET24d	FlhF, FlhGd4-24	<i>Cj</i>	His, FLAG	Hendrixson Lab
pET24d	FlhF, FlhGQ4A	<i>Cj</i>	His, FLAG	Hendrixson Lab
pET24d	FlhG D61A	<i>Cj</i>	His	Hendrixson Lab
pET24d	FlhG K37A	<i>Cj</i>	His	Hendrixson Lab
pET24d	FlhG Q4A	<i>Cj</i>	His	Hendrixson Lab
pET24d	FlhG d4-24	<i>Cj</i>	His	Hendrixson Lab
	FlhF	<i>Bs</i>		Bange Lab
pGAT3	FlhF B-dom	<i>Bs</i>	N-His, N-GST	Bange Lab
pGAT3	FlhF B 21-111	<i>Bs</i>	N-His, N-GST	Bange Lab
pGAT3	FlhF B 41-111	<i>Bs</i>	N-His, N-GST	Bange Lab
pGAT3	FlhF B 61-111	<i>Bs</i>	N-His, N-GST	Bange Lab
pGAT3	FlhF B 81-111	<i>Bs</i>	N-His, N-GST	Bange Lab
pGAT3	FlhF B 1-47	<i>Bs</i>	N-His, N-GST	Bange Lab
pGAT3	FlhF B 21-47	<i>Bs</i>	N-His, N-GST	Bange Lab
pET24d	FlhG	<i>Gt</i>	N-His	Bange Lab
pET24d	FliM	<i>Gt</i>	C-His	Bange Lab
pET24d	FliY	<i>Gt</i>	C-His	Bange Lab
pET16b	FliY	<i>Gt</i>	C-His	Bange Lab

### 4.1.3 Oligonucleotides

The oligonucleotides used in this work were obtained from Sigma-Aldrich and are listed in table 2.

**Table 2: Oligonucleotides used in this work**

Primer	Sequence	Organism
SheFlhFdN152-6HP	ctctaaacatgtcacaccatcaccatcaccatgctgatattgaagccatg	<i>S. putrefaciens</i>
SheFlhFdN185-6HP	ctctaaacatgtcacaccatcaccatcaccatcccgttgccgctatgctg	<i>S. putrefaciens</i>
SheFlhF-Bam-R	ttaaggatccttactcaaatgcacaggcc	<i>S. putrefaciens</i>
SheFlhFdN109-PciI	ttaaaccatgtctcaccatcaccatcaccatcagcaacctgaggccg	<i>S. putrefaciens</i>
SheFlhFdN88-PciI	ttaaaccatgtctcaccatcaccatcaccatccagcagattcattacaagc	<i>S. putrefaciens</i>
SpFlhFdN10_PciI	ttaaaccatgtctcaccatcaccatcaccatgctgcccgtctg	<i>S. putrefaciens</i>
SpFlhF_PciI_HF	ttaaaccatgtctcacgtgaagattaaacga	<i>S. putrefaciens</i>
SheFlhF-dC20-Bam	ttaggatccttaactatctaatgtcgaagcgc	<i>S. putrefaciens</i>
FlhF-N32-Nco6H-F	ttaaccatggggcaccatcaccatcaccatgctgcccgtctg	<i>S. putrefaciens</i>
FlhF-N32-Xho-R	ttaactcgagttattgtttgacatgataa	<i>S. putrefaciens</i>

FlhFdN73-PciI-F	ttaaacaatgtctcaccatcaccatcaccatggaaagcagcctgtg	<i>S. putrefaciens</i>
FlhFdN137-Pci-F	ttaaacaatgtctcaccatcaccatcaccatccggccgcttttgataaaaa g	<i>S. putrefaciens</i>
SpFlhF BamHI-F	taaggatccatgggggcaccatcaccatcaccataagattaacgattt	<i>S. putrefaciens</i>
SpFlhF EcoRI-R	ttaagaattcttactcaaatgcacag	<i>S. putrefaciens</i>
SpFlhF Bdom Pci no His F	ttaaacaatggtggaagattaacgattttttgcc	<i>S. putrefaciens</i>
FlhF-Bdom Bam R	ttaggatccttacggaatgtctc	<i>S. putrefaciens</i>
SpFlhF R285A F	gatcatttatgccattggegccc	<i>S. putrefaciens</i>
SpFlhF R285A R	ggcgccaatggcataatgatc	<i>S. putrefaciens</i>
SpYlxH N20 R		<i>S. putrefaciens</i>
SpYlxH D58A F	cttagtgcttgacgcagcccttgcttagccaatgt	<i>S. putrefaciens</i>
SpYlxH D58A R	gacattggctaagccaagggtgctgctcaagcactaa	<i>S. putrefaciens</i>
SpFlhG Q5A F	accctggatgcagcaagtgg	<i>S. putrefaciens</i>
SpFlhG Q5A R	ccacttgctgcatccagggt	<i>S. putrefaciens</i>
SpFlhG dN16 Nco6H-F	ttaacatggggcaccatcaccatcaccataacgaaaaagtgaaagta a	<i>S. putrefaciens</i>
SpFFH NG Pci6H F	ttaaacaatgtctcaccatcaccatcaccatcaccatcttgagaacctaacc	<i>S. putrefaciens</i>
SpFFH NG BamR	ttaaggatccttagcccaaaatgctggaag	<i>S. putrefaciens</i>
SpFtsY_H6_ Nco F	ttaacatggggcaccatcaccatcaccatgcaagaaaggtttt	<i>S. putrefaciens</i>
SpFtsY_XhoI R	ttaactcgagtttagttatccgctttt	<i>S. putrefaciens</i>
SpFtsYN32-Xho-R	ttaactcgagttaagtatctgtgttgg	<i>S. putrefaciens</i>
SpFtsYdN10-F	ttaacatggggcaccatcaccatcaccatcgtaaagataag	<i>S. putrefaciens</i>
Sp FliMdN15 Pci	ttaaacaatgtctgggggtgatgacgtcg	<i>S. putrefaciens</i>
Sp FliM1 Bam_R	ttaaggatccttataattcagtatctctagc	<i>S. putrefaciens</i>
FliM1dN27 PciI F	ttaaacaatgtctgctgctagccaagatgctgctgacccctac	<i>S. putrefaciens</i>
SpSRP-RNA R1	ttaactgcaggcagattggaggttcc	<i>S. putrefaciens</i>
SpSRP-RNA F1	ttaaggatccctaatacgaactacatacgggtgaccctag	<i>S. putrefaciens</i>
Cj FlhG Nco_F	ttaacatggggcaccatcaccatcaccatattaaccaagcaaat	<i>C. jejuni</i>
Cj FlhG Xho_R	ttaactcgagttaaaatctttcaataatttttc	<i>C. jejuni</i>
CjFlhF Nco_F	ttaacatggggcaccatcaccatcaccatggacaactatacat	<i>C. jejuni</i>
CjFlhF Xho_R	ttaactcgagttattcattatttttcc	<i>C. jejuni</i>
C FlhG K37Q-F	gcgttggaacaaagtacg	<i>C. jejuni</i>
CjFlhG K37Q-R	cgtactttgtccaacgc	<i>C. jejuni</i>
CjFliM NcoI	ttaacatggctgagatactctc	<i>C. jejuni</i>
CjFliM dN26 Nco	ttaacatggcctcaaatcaaa	<i>C. jejuni</i>
CjFliM Bam		<i>C. jejuni</i>
CjFliM Bam-6H	ttaaggatccttaatggtgatggtgatggtgtatttctcatcctcc	<i>C. jejuni</i>
CjFliY Pci	ttaaacaatggtgatcaatgatttttaaaaatggttac	<i>C. jejuni</i>
CjFliY Bam	ttaaggatccttatcttagttgttctaattcttc	<i>C. jejuni</i>
CjFliN Nco	ttaacatggggcagcgatgatatagag	<i>C. jejuni</i>
CjFliN BamHI	ttaaggatccttaatttctttt	<i>C. jejuni</i>

#### **4.1.4. Enzymes and cloning equipment**

Restriction enzymes and further reagents (e.g.; dNTPs, BSA solution, reaction buffers) for molecular cloning and genetic manipulations were purchased from New England Biolabs, Biozym Scientific GmbH and Fermentas. Plasmid preparation and gel extraction of amplified or plasmid DNA were performed using kits from Qiagen (QIAprep spin Miniprep kit and QIAquick Gel Extraction Kit, respectively) according to the manual provided by the manufacturer. As size standard for agarose gels, Quick-Load® Purple 2-log DNA ladder (0.1 -10.0 kb and Gene Ruler™ 1 kb was employed, which was provided by New England Biolabs and Thermo Scientific, respectively. Protein variants were generated by overlapping PCR. All plasmids obtained were sequenced at MWG-Biotech AG.

#### **4.1.5 Protein biochemistry**

Purified proteins were concentrated using Amicon Ultra-15 centrifugal filter units (10 K, 30 K or 50 K molecular weight cut-off) purchased from Merck Millipore. PageRuler™ prestained protein ladder 10-180 kDa, PageRuler™ unstained broad range protein ladder and Pierce unstained protein MW marker from Life technologies as well as Protein Marker EXTended PS13 (5-245 kDa) supplied by GeneOn, were used as size standards for SDS-PAGEs. Ni-NTA agarose and glutathione sepharose 4B were purchased from Qiagen and GE Healthcare, respectively. Spin columns and other equipment for pull down experiments were supplied by MoBiTec.

#### **4.1.6 Crystallization**

Crystallization experiments were performed in SWISSCI MRC 2-well and MRC 3-well crystallization plates with 96 conditions on each plate. The JCSG core suite providing 386 crystallization conditions served as initial screen. Individual fine screens and additive screens were prepared in SWISSCI MRC 2-well and MRC 3-well plates. Crystals were looped and flash frozen with equipment (CrystalWand Magentic, Mounted CryoLoops and CrystalCap HT™ Vial) ordered from Hampton Research.

#### 4.1.6.1 Data collection at the ESRF

Diffraction data of crystals was collected at the ESRF in Grenoble, France at the beamlines ID23-1 and ID23-2.

#### 4.1.7 Growth media and buffers

*E. coli* was cultured in Luria-Bertani (LB) broth medium (20 g/l) and on LB-Agar (16 g/l) ordered as a premix from Roth. LB broth medium and agar were sterilized before usage.

**Table 3: Buffers used in this work**

Lysis Buffer	20 mM HEPES, pH 8.0 250 mM NaCl 20 mM KCl 20 mM MgCl <sub>2</sub> 40 mM imidazole
Ni-NTA elution buffer	20 mM HEPES, pH 8.0 250 mM NaCl 20 mM KCl 20 mM MgCl <sub>2</sub> 500 mM imidazole
SEC-Buffer	20 mM HEPES, pH 7.5 200 mM NaCl 20 mM KCl 20 mM MgCl <sub>2</sub>
10x PBS buffer,	137 mM NaCl 2.7 mM KCl 10 mM Na <sub>2</sub> HPO <sub>4</sub> 1.8 mM KH <sub>2</sub> PO <sub>4</sub>
PBS-T	137 mM NaCl 2.7 mM KCl 10 mM Na <sub>2</sub> HPO <sub>4</sub> 1.8 mM KH <sub>2</sub> PO <sub>4</sub> 0.1% (v/v) Tween 20

Transferbuffer	48 mM Tris 39 mM Glycin 35 mg/ml SDS 20% (v/v) Methanol	
GSH elution buffer	50 mM Tris-HCl, pH 7.9 20 mM glutathione	
SDS separation buffer	1,5M Tris 0.1% (w/v) SDS	pH 8.8
SDS stacking bufer	0.5M Tris-HCl 0.1% (w/v) SDS	pH 6.8
10x SDS running -buffer	0.8M Glcin 0.1M Tris 0.25% (w/v) SDS	pH 8.3
5x SDS loading buffer	100 mM Tris 2 mg/ml SDS 10% (v/v) Glycerol 3% (v/v) $\beta$ -mercaptoethanol 1 mg/ml bromphenol	

### 4.1.8 Antibiotics

**Table 4**

Antibiotic	Stock solution	End concentration	Solvent
Ampicillin-sodium salt	100mg/ml	100 $\mu$ g/ml	ddH <sub>2</sub> O
Kanamycin sulfate	50mg/ml	50 $\mu$ g/ml	ddH <sub>2</sub> O
Chloramphenicol	34mg/ml	34 $\mu$ g/ml	Ethanol 96% (v/v)

## 4.1.9 Laboratory equipment

Table 5

Equipment	Supplier
<b>FPLC systems</b>	
Äkta purifier	GE Healthcare
Äkta prime	GE Healthcare
<b>Columns</b>	
HiLoad 26/600 Superdex S200 pg	GE Healthcare
HiLoad 26/600 Superdex S75 pg	GE Healthcare
HisTrap FF 1 ml and 5 ml	GE Healthcare
<b>Centrifuges</b>	
Heraeus Pico 21 Centrifuge	Thermo Scientific
Heraeus Fresco 21 Centrifuge	Thermo Scientific
Heraeus Megafuge 40R	Thermo Scientific
Sorvall LYNX 6000 A27-8 x 50 Fixed Angle Rotor Fiberlite™ F9-6 x 1000 LEX Fixed Angle Rotor	Thermo Scientific
Optima XPN-80 Ultracentrifuge JLA-16.250 Rotor (Fixed Angle) SW 40 Ti Rotor (Swinging Bucket)	Beckmann Coulter
<b>Incubators</b>	
WiseCube Incucell	Wisd Laboratory Instruments
Shaking Incubator WIS-20	Wisd Laboratory Instruments
Western-Blot equipment	Biorad
SDS-PAGE equipment	Biorad
Agarose gel equipment	Cleaver Scientific
Photometer	Amersham biosciences
T 100TM Thermo Cycler	Biorad
M-110L Microfluidizer	Microfluidics
GEL iX20 Imager	Intas
ChemiDoc MP Imaging System	Biorad

Gryphon LCP	ARI-Art Robbins Instruments
Peristaltic pump	Gilson
NanoDrop Lite	Thermo Scientific

## 4.2 Methods

### 4.2.1 Molecular cloning

The genes encoding for the proteins (FlhF, FlhG, FliM, FliG, FliN, FliN(Y), Ffh, FtsY, (**Table 6**) used in this study were amplified from *S. putrefaciens* CN-32, *B. subtilis* PY79 and *C. jejuni* 81-176 genomic DNA by polymerase chain reaction (PCR) using Q5 High-Fidelity DNA Polymerase (New England Biolabs) according to the manufacturer's manual. Most forward primers encoded a hexahistidine tag in-frame with the DNA sequence of the corresponding gene. Protein variants were generated by overlapping PCR. A list of primer and plasmid used in this work is provided with table 1 and table 2.

**Table 6**

Protein	<i>S. putrefaciens</i> CN-32	<i>C. jejuni</i> 81-176
FlhF	Sputcn32_2561	CJJ81176_0102
FlhG	Sputcn32_2560	CJJ81176_0101
FliM	Sputcn32_2569	CJJ81176_0098
FliY		CJJ81176_0097
FliN	Sputcn32_2568	CJJ81176_0375
FliM1	Sputcn32_3479	
FliM2	Sputcn32_3480	
Ffh	Sputcn32_1167	
FtsY	Sputcn32_0289	

### 4.2.2 Isolation of plasmid DNA from *E. coli*

Plasmid DNA was extracted from 4 ml overnight cultures of *E. coli* DH5 $\alpha$ . The plasmid preparations were carried out using the QIAprep Spin Miniprep Kit (Qiagen, Germany) according to the instructions of the manufacturer. Therefore, the cells were harvested by centrifugation by 4000 rpm for 10 min at 4°C. Upon lysis of the cells through alkaline conditions, the sample was neutralized and centrifuged (13 000 rpm, 10 min, and 4 °C) to remove the cell debris. The supernatant was transferred to a spin column and eluted with ddH<sub>2</sub>O.

### 4.2.3 Agarose gel electrophoresis

The quality of PCR reactions and analysis of DNA restriction enzyme digests were assessed by agarose gel electrophoresis. The gels were prepared in TB-buffer containing 1-2 % (w/v) agarose depending on the size of the analyzed DNA fragment. The agarose was dissolved in TB-buffer (100 mM Tris, 100 mM boric acid and 2 mM EDTA, pH 8.3) by heating and poured into horizontal gel casts. The DNA samples were mixed with 6 x loading dye (300 mM boric acid, 300 mM Tris, 20% (v/v) glycerol and 0.5 mg/ml bromphenolblue) and loaded on the gel. After running at 100V for 30 minutes, the DNA was stained with ethidium bromide (Roth) and visualized using a GEL iX20 Imager. Amplified DNA was extracted from agarose gels using the QIAquick Gel Extraction kit (Qiagen) according to the manufacturer's manual.

### 4.2.4 Purification of recombinant proteins

For recombinant expression of proteins from *S. putrefaciens*, *C. jejuni* and *B.subtilis*, *E. coli* BL21 (DE3), transformed with the respective plasmids, and were grown in LB broth in the presence of appropriate antibiotics kanamycin or ampicillin in final concentrations of 50 or 100  $\mu$ g/ml, respectively. Large-scale protein production was mainly performed under autoinduction conditions. Therefore, 12.5 g/l D-(+)-lactose-monohydrate was added to the culture followed by incubation at 30 °C for ~16-20 h under constant shaking (180 rpm). If necessary, proteins were produced following induction with IPTG. In brief, 1 mM IPTG was added to a cell culture with an optical density ( $A_{600\text{ nm}}$ ) of approximately 0.6 - 0.8. After further incubation (typically 2-3h at 37°C under constant shaking at 180 rpm), the cells were harvested by centrifugation (2,000 x g, 20 min, 4°C). The cells were resuspended in lysis buffer and subsequently lysed using the M-



110L Microfluidizer (Microfluidics). To clarify the lysate from cell debris, the sample was centrifuged at 47,850 x *g* for 20 min at 4°C. The clear supernatant was loaded on a 1 ml HisTrap FF column equilibrated with 10 column volumes (CV) of lysis buffer. After washing the column with 50 ml lysis buffer, the proteins were eluted using 15 ml Ni-NTA elution buffer. The eluted protein fractions were concentrated using Amicon Ultra-15 centrifugal filter units and subsequently applied to SEC, equilibrated with SEC buffer. Fractions were analysed using SDS-PAGE. Protein-containing fractions were pooled and concentrated up to a concentration fitting the experimental requirements. The concentration was determined by spectrophotometer.

#### 4.2.5.1 Ribosome purification

The ribosome purifications were prepared either using the protocol of Bommer and co-workers (121). Mid-log-phase cultures of *S. putrefaciens* CN-32 strain grown at the temperature 37 °C. Harvested cultures were resuspended in 10 ml buffer 1 (20 mM HEPES, 6 mM MgCl<sub>2</sub> and 100 mM NaCl). After opening the cells with the Microfluidizer the cells were again centrifuged for 30 min at 27,000 x *g* and 4°C. The cells were diluted in 1.5 ml buffer 1 and layered onto a 10-40 % (w/v) sucrose gradient in a centrifuge tube with an end volume of 12 ml. This was spin down in an Ultracentrifuge in a swinging-bucket rotor for 12 h by 4°C and 80,000 x *g*. After centrifugation, the gradient was collected by hand from the top to the bottom in 0.8 ml fractions. The samples were analyzed by SDS-PAGE and Western blotting.

#### 4.2.5.2 Ribosome high and low salt wash

*S. putrefaciens* CN-32 was grown in LB-medium at 37 °C and vigorous shaking until mid-logarithmic phase. The cells were harvested by centrifugation (3,500 x *g*, 20 min, 4°C), suspended in 10 ml ribosome lysis buffer (20 mM HEPES, 60 mM K-acetate, 1 M Mg-acetate, 5 mM DTT and 1 mM PMSF) and subsequently lysed using the M-110L Microfluidizer (Microfluidics). Following cell lysis three centrifugation steps are applied: For clarifying the cell lysate from cell debris, the sample was centrifuged for 15 min by 29,900 x *g* at 4°C. The cleared lysate was transferred to a new tube and centrifuged for 30 min at 81,000 x *g* at 4°C. The resulting supernatant was then centrifuged at 207,000 x *g* for 2h at 4°C. The pellet with the ribosomes was resuspended in 2ml of ribosome lysis buffer and laid over a cushion of 25 % (m/v) sucrose in lysis buffer supplied with 100 mM K-acetate for low salt wash or 800 mM for high salt wash, respectively. The samples were centrifuged at 247,000 x *g* for 2h at 4°C. The supernatant

was precipitated with 50% trichloroacetic acid. Samples were taken at all relevant purification steps and analyzed by SDS-Page and Western blotting.

#### **4.2.6 SDS-Page**

The visualization of protein samples was carried out with Sodium-dodecylsulfate polyacrylamide gel electrophoresis (SDS-PAGE) and self-prepared polyacrylamide gels of 10 %, 12.5 % or 15 %. The gels were cast in a Mini-PROTEAN 3 Multi-Casting Chamber (Biorad). The protein samples were mixed with 5x SDS loading buffer and loaded on the gel. Electrophoresis was carried out in a Mini-PROTEAN® Tetra Cell with 240-260 V for 30-40 min. The gels were stained with Coomassie Brilliant Blue R-250 (3.2 g dissolved in ddH<sub>2</sub>O/ethanol/acetic acid in 5:5:1 ratio) and destained with a mixture of ddH<sub>2</sub>O, ethanol and acetic acid (6:3:1).

#### **4.2.7 Western blotting and immunodetection**

The identification of a specific protein was verified by Western blotting. After SDS-Page, proteins were transferred to a nitrocellulose membrane (Protran, Ge Healthcare) using the semi-dry Western blotting protocol. Therefore, whatman paper was soaked with transfer buffer and the nitrocellulose membrane was activated in ddH<sub>2</sub>O. The polyacrylamide gel was laid over the nitrocellulose membrane and sandwiched between blotting papers. The electrotransfer was conducted for 90 min at 0.8 mA per cm<sup>2</sup> of gel area using an electro-blotting apparatus (Biorad).

After the transfer of proteins onto a nitrocellulose membrane, the membrane was incubated for 2h in blocking solution (PBST- buffer containing 5% (w/v) skimmed milk). The membrane was washed 3 times with PBST, followed by incubation with blocking solution containing FlhF-antiserum (1: 2000 dilution) over night at 4 °C. After rinsing with PBST, the membrane was incubated for 2 h in blocking solution containing the secondary antibody (horseradish peroxidase-conjugated goat anti-rabbit IgG; 1:20000 dilution). The immunoblot was developed using LumiSensor™ Chemiluminescent HRP-substrate (Genscript) and the ChemiDoc MP Imaging System.

## 4.2.8 Protein interaction assays

### 4.2.8.1 Glutathione-S-transferase (GST)

GST-pull-down assays were performed in PBS buffer at 4 °C or room temperature depending on the proteins investigated. Typically, one nmol of purified GST-protein was immobilized on 20 µl Glutathione-Sepharose 4B in small filter columns by incubation for 10 minutes. Putative binding partners (typically 5-10 nmol) and 2.5 mM of appropriate nucleotides were added and incubated for 20 min at the respective temperature, except if stated differently in the experiment. After centrifugation (1500 x g, 1 min, 4 °C), the column was washed 3 times with PBS buffer. Proteins were eluted with 40 µl of GSH elution buffer and analyzed by Coomassie-stained SDS-PAGE.

### 4.2.8.1 Ni-NTA affinity

Ni-NTA affinity pull-down assays from expression cultures were performed in lysis buffer on ice. Therefore, 100-200 ml culture of hexahistidine-tagged proteins ('bait protein') and untagged proteins ('prey protein') were mixed and harvested. The cells were lysed by using the M-110L Microfluidizer and centrifuged (45850 x g, 20 min, 4 °C). The clarified cell lysate was incubated with 200 µl of Ni-NTA agarose (Qiagen) for 15 min. After incubation, the samples were centrifuged at 1500 x g for 10 min at 4°C. Subsequently, the Ni-NTA agarose was washed 3 times with lysis buffer. Proteins bound to the Ni-NTA agarose were eluted with 200 µl Ni-NTA elution buffer and analyzed by Coomassie-stained SDS-PAGE.

## 4.2.9 Protein crystallization

All crystallization experiments were carried out by the sitting-drop method at room temperature using the JCSG core suite. The reservoir volume was 50 µl and the drop volume was 1 µl, with a 1:1 mixture of protein and crystallization solution. Crystals of *CjFlhG* were obtained from a 23 mg/ml solution after ~ 16h in 0.2 M ammoniumfluoride and 20 % (w/v) PEG 3350. Crystals of dimeric *SpFliN* were obtained from a 21 mg/ml solution after one week from 0.2 M lithium sulfate, 0.1M Tris pH 8.5 and 40% (w/v) PEG400.

### 4.2.9.1 Data collection

Prior to data collection, crystals were flash-frozen in liquid nitrogen after a short incubation in a cryo-protecting solution that consisted of mother-liquor supplemented with 20 % (v/v) glycerol.

Data collection was performed at the ESRF in Grenoble, France under cryogenic conditions at beamlines ID23-1 (*CjFlhG*) and ID23-2 (*SpFlhN*). Data were recorded with a DECTRIS PILATUS 6M detector and processed using iMosflm (113) as well as the CCP4-implemented program SCALA (114). The structures were solved by MR with CCP4-integrated PHASER (115), built in COOT and refined using PHENIX refine (117). Figures containing crystal structures or superimpositions of crystal structures were generated with PyMol ([www.pymol.org](http://www.pymol.org)).

#### 4.2.10 GTPase/ATPase assays

The GTPase activity of FlhF and the ATPase activity of FlhG were monitored by high-pressure liquid-chromatography (HPLC). Typically, 100  $\mu$ M of protein (as indicated in figures and text) was incubated together with 1 mM GTP/ATP in SEC-buffer for 30 min at 37 °C. Reactions were stopped by flash-freezing with liquid nitrogen and stored at -20 °C until measurement. HPLC measurements were performed with an Agilent 1100 Series HPLC system (Agilent Technologies) and a C18 column (EC 250/4.6 Nucleodur HTec 3 $\mu$ m; Macherey-Nagel). GDP/ADP and GTP/ATP were eluted with a buffer containing 50 mM KH<sub>2</sub>PO<sub>4</sub>, 50 mM K<sub>2</sub>HPO<sub>4</sub>, 10 mM tetrapentylammonium bromide and 15% (v/v) acetonitrile at 0.8 ml/min flow rate and detected at a wavelength of 253 nm for GTP and 260 nm for ATP in agreement with standards. GDP/ADP originating from non-enzymatic hydrolysis of GTP/ATP was determined by triplicate measurement of 1 mM GTP/ATP treated similar as the enzymatic reactions and subtracted from the quantified GDP/ADP. In addition, a kinetic analysis of the ATPase activity of *CjFlhG* was monitored by HPLC as described above. Therefore, 100  $\mu$ M *CjFlhG* were incubated at 37°C in the presence of varying amounts of ATP (i.e., 0.25, 0.5, 1, 2.5, 3.5, 5, 7.5, 10 mM). For each ATP concentration, five different time points (i.e., 5/10/15/20/30 minutes) were measured. The velocity of ATP-hydrolysis for each concentration of ATP was obtained by linear regression of quantified ADP at different time points. The slope of the regression curve representing the velocity of ATP-hydrolysis was plotted against the concentration of ATP (see also **Figure 16**). The  $K_m$  and  $V_{max}$  values  $\pm$  SD of ATP-hydrolysis were obtained from a Michaelis-Menten fit of the  $v/S$  characteristic using the equation  $v = V_{max} S / (K_m + S)$ . Kinetic data analysis was performed using GraphPad Prism version 6.04 for Windows (GraphPad Software).

## 5. Literatur

1. Jarrell KF, McBride MJ. The surprisingly diverse ways that prokaryotes move. *Nat Rev Microbiol.* 2008;6(6):466–76.
2. Kearns DB, Losick R. Swarming motility in undomesticated *Bacillus subtilis*. *Mol Microbiol.* 2003;49(3):581–90.
3. Overhage J, Bains M, Brazas MD, Hancock REW. Swarming of *Pseudomonas aeruginosa* is a complex adaptation leading to increased production of virulence factors and antibiotic resistance. *J Bacteriol.* 2008;190(8):2671–9.
4. Duan Q, Zhou M, Zhu L, Zhu G. Flagella and bacterial pathogenicity. *J Basic Microbiol.* 2013;53(1):1–8.
5. Chaban B, Hughes HV, Beeby M. The flagellum in bacterial pathogens: For motility and a whole lot more. Vol. 46, *Seminars in Cell and Developmental Biology.* Academic Press; 2015. p. 91–103.
6. Zhao X, Norris SJ, Liu J. Molecular architecture of the bacterial flagellar motor in cells. *Biochemistry.* American Chemical Society; 2014;53(27):4323–33.
7. Miyata M. Unique centipede mechanism of *Mycoplasma* gliding. *Annu Rev Microbiol.* 2010;64:519–37.
8. Kearns DB. A field guide to bacterial swarming motility. *Nat Rev Microbiol.* 2010;8(9):634–44.
9. Muramoto K, Kawagishi I, Kudo S, Magariyama Y, Imae Y, Homma M. High-speed rotation and speed stability of the sodium-driven flagellar motor in *Vibrio alginolyticus*. *J Mol Biol.* 1995;251(1):50–8.
10. Fenchel T, Thar R. “*Candidatus Ovobacter propellens*”: A large conspicuous prokaryote with an unusual motility behaviour. *FEMS Microbiol Ecol.* 2004;48(2):231–8.
11. Sourjik V, Wingreen NS. Responding to chemical gradients: Bacterial chemotaxis. Vol. 24, *Current Opinion in Cell Biology.* 2012. p. 262–8.
12. Chevance FF V, Hughes KT. Coordinating assembly of a bacterial macromolecular machine. *Nat Rev Microbiol.* 2008 Jun [cited 2013 Jun 2];6(6):455–65.
13. Morimoto Y V., Ito M, Hiraoka KD, Che YS, Bai F, Kami-ike N, et al. Assembly and stoichiometry of FliF and FlhA in *Salmonella* flagellar basal body. *Mol Microbiol.* 2014;91(6):1214–26.
14. Ueno T, Oosawa K, Aizawa SI. M ring, S ring and proximal rod of the flagellar basal body of *Salmonella typhimurium* are composed of subunits of a single protein, FliF. *J Mol Biol.* 1992;227(3):672–7.
15. Bange G, Kümmerer N, Engel C, Bozkurt G, Wild K, Sinning I. FlhA provides the adaptor for coordinated delivery of late flagella building blocks to the type III secretion system. *Proc Natl Acad Sci U S A.* 2010;107(25):11295–300.
16. Green JCD, Kahramanoglou C, Rahman A, Pender AMC, Charbonnel N, Fraser GM. Recruitment of the earliest component of the bacterial flagellum to the old cell division pole by a membrane-associated signal recognition particle family GTP-binding protein. *J Mol Biol.* Elsevier Ltd; 2009;391(4):679–90.

17. Macnab RM. HOW BACTERIA ASSEMBLE FLAGELLA - Annual Review of Microbiology, 57(1):77. Annu Rev Microbiol. 2003;
18. Altegoer F, Bange G. Undiscovered regions on the molecular landscape of flagellar assembly. *Curr Opin Microbiol*. Elsevier Ltd; 2015;28:98–105.
19. Minamino T, Imada K, Namba K. Molecular motors of the bacterial flagella. Vol. 18, *Current Opinion in Structural Biology*. 2008. p. 693–701.
20. Lee LK, Ginsburg M a, Crovace C, Donohoe M, Stock D. Structure of the torque ring of the flagellar motor and the molecular basis for rotational switching. *Nature*. Nature Publishing Group; 2010;466(7309):996–1000.
21. Dyer CM, Vartanian AS, Zhou H, Dahlquist FW. A Molecular Mechanism of Bacterial Flagellar Motor Switching. *J Mol Biol*. 2009;388(1):71–84.
22. Minamino T, Imada K. The bacterial flagellar motor and its structural diversity. *Trends Microbiol*. Elsevier Ltd; 2015;23(5):267–74.
23. Delalez NJ, Berry RM, Armitage JP. Stoichiometry and turnover of the bacterial flagellar switch protein FliN. *MBio*. 2014;5(4):1–5.
24. Sircar R, Borbat PP, Lynch MJ, Bhatnagar J, Beyersdorf MS, Halkides CJ, et al. Assembly states of FliM and FliG within the flagellar switch complex. *J Mol Biol*. Elsevier Ltd; 2015;427(4):867–86.
25. Brown PN, Terrazas M, Paul K, Blair DF. Mutational analysis of the flagellar protein FliG: Sites of interaction with FliM and implications for organization of the switch complex. *J Bacteriol*. 2007;189(2):305–12.
26. Toker a S, Macnab RM. Distinct regions of bacterial flagellar switch protein FliM interact with FliG, FliN and CheY. *J Mol Biol*. 1997;273(3):623–34.
27. Paul K, Gonzalez-Bonet G, Bilwes AM, Crane BR, Blair D. Architecture of the flagellar rotor. *EMBO J*. Nature Publishing Group; 2011;30(14):2962–71.
28. Mathews MA, Tang HL, Blair DF. Domain analysis of the FliM protein of *Escherichia coli*. *J Bacteriol*. 1998;180(21):5580–90. A
29. Park S-Y, Lowder B, Bilwes AM, Blair DF, Crane BR. Structure of FliM provides insight into assembly of the switch complex in the bacterial flagella motor. *Proc Natl Acad Sci U S A*. 2006;103(32):11886–91.
30. Bren a, Eisenbach M. The N terminus of the flagellar switch protein, FliM, is the binding domain for the chemotactic response regulator, CheY. *J Mol Biol*. 1998;278(3):507–14.
31. Welch M, Oosawa K, Aizawa S, Eisenbach M. Phosphorylation-dependent binding of a signal molecule to the flagellar switch of bacteria. *Proc Natl Acad Sci U S A*. 1993;90(October):8787–91.
32. Berg HC. Bacterial flagellar motor. *Curr Biol*. 2008;18(16):103–32.
33. Lam KH, Ip WS, Lam YW, Chan SO, Ling TKW, Au SWN. Multiple conformations of the FliG C-terminal domain provide insight into flagellar motor switching. *Structure*. 2012;20(2):315–25.
34. Zhou J, Lloyd SA, Blair DF. Electrostatic interactions between rotor and stator in the bacterial flagellar motor. *Proc Natl Acad Sci*. 1998;95(11):6436–41.

35. Lam KH, Lam WWL, Wong JYK, Chan LC, Kotaka M, Ling TKW, et al. Structural basis of FliG-FliM interaction in *Helicobacter pylori*. *Mol Microbiol.* 2013;88(4):798–812.
36. Berg HC. The rotary motor of bacterial flagella. *Annu Rev Biochem. Annual Reviews* 4139 El Camino Way, P.O. Box 10139, Palo Alto, CA 94303-0139, USA; 2003;72(1):19–54.
37. Berg HC, Brown D a. Chemotaxis in *Escherichia coli* analysed by three-dimensional tracking. *Nature.* 1972;239(5374):500–4.
38. Bischoff DS, Ordal GW. Identification and characterization of FliY, a novel component of the *Bacillus subtilis* flagellar switch complex. *Mol Microbiol.* 1992;6(18):2715–23.
39. Sarkar MK, Paul K, Blair D. Chemotaxis signaling protein CheY binds to the rotor protein FliN to control the direction of flagellar rotation in *Escherichia coli*. *Proc Natl Acad Sci U S A.* 2010;107(20):9370–5.
40. González-Pedrajo B, Minamino T, Kihara M, Namba K. Interactions between C ring proteins and export apparatus components: A possible mechanism for facilitating type III protein export. *Mol Microbiol.* 2006;60(4):984–98.
41. McMurry JL, Murphy JW, González-Pedrajo B. The FliN-FliH interaction mediates localization of flagellar export ATPase FliI to the C ring complex. *Biochemistry.* 2006;45(39):11790–8.
42. Minamino T. Protein export through the bacterial flagellar type III export pathway. *Biochim Biophys Acta - Mol Cell Res.* 2013;
43. Thomas D, Morgan DG, DeRosier DJ. Structures of bacterial flagellar motors from two FliF-FliG gene fusion mutants. *J Bacteriol.* 2001;183(21):6404–12.
44. Liu X, Matsumura P. The FlhD/FlhC complex, a transcriptional activator of the *Escherichia coli* flagellar class II operons. *J Bacteriol.* 1994;176(23):7345–51.
45. Iino T, Komeda Y, Kutsukake K, Macnab RM, Matsumura P, Parkinson JS, et al. New unified nomenclature for the flagellar genes of *Escherichia coli* and *Salmonella typhimurium*. *Microbiol Rev.* 1988;52(4):533–5.
46. Hughes KT, Gillen KL, Semon MJ, Karlinsey JE. Sensing structural intermediates in bacterial flagellar assembly by export of a negative regulator. *Science (80- ).* 1993;262(5137):1277–80.
47. Wu J, Newton A. Regulation of the *Caulobacter* flagellar gene hierarchy; not just for motility. *Mol Microbiol.* 1997;24(2):233–9.
48. Kim Y-K, McCarter LL. Analysis of the polar flagellar gene system of *Vibrio parahaemolyticus*. *J Bacteriol. American Society for Microbiology;* 2000;182(13):3693–704.
49. Syed KA, Beyhan S, Correa N, Queen J, Liu J, Peng F, et al. The *Vibrio cholerae* flagellar regulatory hierarchy controls expression of virulence factors. *J Bacteriol.* 2009;191(21):6555–70.
50. Gilbreath JJ, Cody WL, Merrell DS, Hendrixson DR. Change is good: variations in common biological mechanisms in the epsilonproteobacterial genera *Campylobacter* and *Helicobacter*. *Microbiol Mol Biol Rev.* 2011 Mar [cited 2013 Jul 16];75(1):84–132. =abstract
51. Aldridge P, Hughes KT. Regulation of flagellar assembly. Vol. 5, *Current Opinion in Microbiology.* 2002. p. 160–5.
52. Anderson JK, Smith TG, Hoover TR. Sense and sensibility: flagellum-mediated gene regulation.

- Trends Microbiol. 2010;18(1):30–7.
53. Kutsukake K, Ohya Y, Iino T. Transcriptional analysis of the flagellar regulon of *Salmonella typhimurium*. *J Bacteriol.* 1990;172(2):741–7.
  54. Chilcott GS, Hughes KT. Coupling of Flagellar Gene Expression to Flagellar Assembly in *Salmonella enterica* Serovar Typhimurium and *Escherichia coli*. *Microbiol Mol Biol Rev.* 2000;64(4):694–708.
  55. Yokoseki T, Iino T, Kutsukake K. Negative regulation by FliD, FliS, and FliT of the export of the flagellum-specific anti-sigma factor, FlgM, in *Salmonella typhimurium*. *J Bacteriol.* 1996;178(3):899–901.
  56. Prouty MG, Correa NE, Klose KE. The novel sigma54- and sigma28-dependent flagellar gene transcription hierarchy of *Vibrio cholerae*. *Mol Microbiol.* 2001;39(6):1595–609.
  57. Correa NE, Barker JR, Klose KE. The *vibrio cholerae* FlgM homologue is an anti- $\sigma^{28}$  factor that is secreted through the sheathed polar flagellum. *J Bacteriol.* 2004;186(14):4613–9.
  58. Spohn G, Scarlato V. Motility, Chemotaxis, and Flagella. *Helicobacter pylori: Physiology and Genetics.* 2001.
  59. Tsang J, Hoover TR. Themes and Variations: Regulation of RpoN-Dependent Flagellar Genes across Diverse Bacterial Species. *Scientifica (Cairo).* 2014;2014:1–14.
  60. Guttenplan SB, Shaw S, Kearns DB. The cell biology of peritrichous flagella in *Bacillus subtilis*. *Mol Microbiol [Internet].* 2013 Jan [cited 2014 Feb 4];87(1):211–29.
  61. Ping L. The asymmetric flagellar distribution and motility of *Escherichia coli*. *J Mol Biol.* 2010;397(4):906–16.
  62. González-Pedrajo B, Ballado T, Campos A, Sockett RE, Camarena L, Dreyfus G. Structural and genetic analysis of a mutant of *Rhodobacter sphaeroides* WS8 deficient in hook length control. *J Bacteriol.* 1997;179(21):6581–8.
  63. Dasgupta N, Arora SK, Ramphal R. fleN, a gene that regulates flagellar number in *Pseudomonas aeruginosa*. *J Bacteriol. American Society for Microbiology;* 2000;182(2):357–64.
  64. Balaban M, Hendrixson DR. Polar flagellar biosynthesis and a regulator of flagellar number influence spatial parameters of cell division in *Campylobacter jejuni*. *PLoS Pathog.* 2011 Dec [cited 2013 Jun 5];7(12):e1002420.
  65. Van Amsterdam K, Van Der Ende A. *Helicobacter pylori* HP1034 (ylxH) is required for motility. Vol. 9, *Helicobacter.* 2004. p. 387–95.
  66. McCarter LL. Dual flagellar systems enable motility under different circumstances. *J Mol Microbiol Biotechnol.* 2004;7(1–2):18–29.
  67. Merino S, Shaw JG, Tomás JM. Bacterial lateral flagella: An inducible flagella system. *FEMS Microbiol Lett.* 2006;263(2):127–35.
  68. Kawagishi I, Maekawa Y, Atsumi T, Homma M, Imae Y. Isolation of the polar and lateral flagellum-defective mutants in *Vibrio alginolyticus* and identification of their flagellar driving energy sources. *J Bacteriol.* 1995;177(17):5158–60.
  69. McClain J, Rollo DR, Rushing BG, Bauer CE. *Rhodospirillum centenum* utilizes separate motor



- and switch components to control lateral and polar flagellum rotation. *J Bacteriol.* 2002;184(9):2429–38.
70. Canals R, Altarriba M, Vilches S, Shaw JG, Tomás JM, Horsburgh G, et al. Analysis of the Lateral Flagellar Gene System of *Aeromonas hydrophila* AH-3. *J Bacteriol.* 2006;188(3):852–62.
  71. Stewart BJ, McCarter LL. Lateral flagellar gene system of *Vibrio parahaemolyticus*. *J Bacteriol.* 2003;185(15):4508–18.
  72. Bubendorfer S, Held S, Windel N, Paulick A, Klingl A, Thormann KM. Specificity of motor components in the dual flagellar system of *Shewanella putrefaciens* CN-32. *Mol Microbiol.* 2012;83(2):335–50.
  73. Bubendorfer S, Koltai M, Rossmann F, Sourjik V, Thormann KM. Secondary bacterial flagellar system improves bacterial spreading by increasing the directional persistence of swimming. *Proc Natl Acad Sci U S A.* 2014;111(31):11485–90.
  74. Lam H, Schofield WB, Jacobs-Wagner C. A landmark protein essential for establishing and perpetuating the polarity of a bacterial cell. *Cell.* 2006;124(5):1011–23.
  75. Ebersbach G, Briegel A, Jensen GJ, Jacobs-Wagner C. A Self-Associating Protein Critical for Chromosome Attachment, Division, and Polar Organization in *Caulobacter*. *Cell.* 2008;134(6):956–68.
  76. Ramamurthi KS, Losick R. Grasping at Origins. Vol. 134, *Cell.* 2008. p. 916–8.
  77. Jenal U. The role of proteolysis in the *Caulobacter crescentus* cell cycle and development. *Res Microbiol.* 2009;160(9):687–95.
  78. England JC, Gober JW. Cell cycle control of cell morphogenesis in *Caulobacter*. *Curr Opin Microbiol.* 2001;4(6):674–80.
  79. Curtis PD, Brun Y V. Getting in the loop: regulation of development in *Caulobacter crescentus*. *Microbiol Mol Biol Rev.* 2010;74(1):13–41.
  80. Huitema E, Pritchard S, Matteson D, Radhakrishnan SK, Viollier PH. Bacterial birth scar proteins mark future flagellum assembly site. *Cell.* 2006;124(5):1025–37.
  81. Yamaichi Y, Bruckner R, Ringgaard S, Möll A, Ewen Cameron D, Briegel A, et al. A multidomain hub anchors the chromosome segregation and chemotactic machinery to the bacterial pole. *Genes Dev.* 2012;26(20):2348–60.
  82. Rossmann F, Brenzinger S, Knauer C, Driessens AK, Bubendorfer S, Ruppert U, et al. The role of FlhF and HubP as polar landmark proteins in *Shewanella putrefaciens* CN-32. *Mol Microbiol.* 2015;98(4):727–42.
  83. Schuhmacher JS, Thormann KM, Bange G. How bacteria maintain location and number of flagella? *FEMS Microbiol Rev.* 2015;39(6):812–22.
  84. Kazmierczak BI, Hendrixson DR. Spatial and numerical regulation of flagellar biosynthesis in polarly flagellated bacteria. *Mol Microbiol* [Internet]. 2013 May [cited 2014 Jan 29];88(4):655–63. Available from: <http://www.ncbi.nlm.nih.gov/pubmed/23600726>
  85. Leipe DD, Wolf YI, Koonin E V, Aravind L. Classification and evolution of P-loop GTPases and

- related ATPases. *J Mol Biol.* 2002;317(1):41–72.
86. Bange G, Petzold G, Wild K, Parlitz RO, Sinning I. The crystal structure of the third signal-recognition particle GTPase FlhF reveals a homodimer with bound GTP. *Proc Natl Acad Sci U S A.* National Academy of Sciences; 2007;104(34):13621–5.
  87. Walter P, Ibrahimi I, Blobel G. Translocation of proteins across the endoplasmic reticulum. I. Signal recognition protein (SRP) binds to in-vitro-assembled polysomes synthesizing secretory protein. *J Cell Biol.* 1981;91(2 I):545–50.
  88. Grudnik P, Bange G, Sinning I. Protein targeting by the signal recognition particle. *Biol Chem.* 2009;390(8):775–82.
  89. Schuhmacher JS, Rossmann F, Dempwolff F, Knauer C, Altegoer F, Steinchen W, et al. MinD-like ATPase FlhG effects location and number of bacterial flagella during C-ring assembly. *Proc Natl Acad Sci U S A.* 2015;112(10):3092–7.
  90. Rowlett VW, Margolin W. The Min system and other nucleoid-independent regulators of Z ring positioning. *Front Microbiol.* 2015;6(MAY):1–10.
  91. Lutkenhaus J. NIH Public Access. 2013;20(9):411–8.
  92. Lutkenhaus J. Assembly dynamics of the bacterial MinCDE system and spatial regulation of the Z ring. *Annu Rev Biochem.* 2007;76(1):539–62.
  93. Bange G, Kümmerer N, Grudnik P, Lindner R, Petzold G, Kressler D, et al. Structural basis for the molecular evolution of SRP-GTPase activation by protein. *Nat Struct Mol Biol.* Nature Publishing Group; 2011;18(November):1376–80.
  94. Murray TS, Kazmierczak BI. FlhF Is required for swimming and swarming in *Pseudomonas aeruginosa*. *J Bacteriol.* 2006;188(19):6995–7004.
  95. Schniederberend M, Abdurachim K, Murray TS, Kazmierczak BI. The GTPase Activity of FlhF Is Dispensable for Flagellar Localization, but Not Motility, in *Pseudomonas aeruginosa*. *J Bacteriol.* 2013;195(5):1051–60.
  96. Pandza S, Baetens M, Park CH, Au T, Keyhan M, Matin A. The G-protein FlhF has a role in polar flagellar placement and general stress response induction in *Pseudomonas putida*. *Mol Microbiol.* 2000;36(2):414–23.
  97. Kitaoka M, Nishigaki T, Ihara K, Nishioka N, Kojima S, Homma M. A novel dnaJ family gene, sfLA, encodes an inhibitor of flagellation in marine vibrio species. *J Bacteriol.* 2013;195(4):816–22.
  98. Kusumoto A, Nishioka N, Kojima S, Homma M. Mutational analysis of the GTP-binding motif of FlhF which regulates the number and placement of the polar flagellum in *vibrio alginolyticus*. *J Biochem.* 2009;146(5):643–50.
  99. Kusumoto A, Shinohara A, Terashima H, Kojima S, Yakushi T, Homma M. Collaboration of FlhF and FlhG to regulate polarflagella number and localization in *Vibrio alginolyticus*. *Microbiology.* 2008;154(5):1390–9.
  100. Baraquet C, Harwood CS. Cyclic diguanosine monophosphate represses bacterial flagella synthesis by interacting with the Walker A motif of the enhancer-binding protein FleQ. *Proc Natl Acad Sci U S A.* 2013;110(46):18478–83.

101. Correa NE, Peng F, Klose KE. Roles of the Regulatory Proteins FlhF and FlhG in the *Vibrio cholerae* Flagellar Transcription Hierarchy. *J Bacteriol. American Society for Microbiology*; 2005;187(18):6324–32.
102. Dasgupta N, Ramphal R. Interaction of the antiactivator FleN with the transcriptional activator FleQ regulates flagellar number in *Pseudomonas aeruginosa*. Vol. 183, *Journal Of Bacteriology*. 2001. p. 6636–44.
103. Kusumoto A, Shinohara A, Terashima H, Kojima S, Yakushi T, Homma M. Collaboration of FlhF and FlhG to regulate polar-flagella number and localization in *Vibrio alginolyticus*. *Microbiology*. 2008;154(Pt 5):1390–9.
104. Cowles KN, Moser TS, Siryaporn A, Nyakudarika N, Dixon W, Turner JJ, et al. The putative Poc complex controls two distinct *Pseudomonas aeruginosa* polar motility mechanisms. *Mol Microbiol*. 2013;90(5):923–38.
105. Salvetti S, Ghelardi E, Celandroni F, Ceragioli M, Giannessi F, Senesi S. FlhF, a signal recognition particle-like GTPase, is involved in the regulation of flagellar arrangement, motility behaviour and protein secretion in *Bacillus cereus*. *Microbiology*. 2007;153(8):2541–52.
106. Wild K, Bange G, Motiejunas D, Kribelbauer J, Hendricks A, Segnitz B, et al. Structural Basis for Conserved Regulation and Adaptation of the Signal Recognition Particle Targeting Complex. *J Mol Biol. Elsevier Ltd*; 2016;428(14):2880–97.
107. Bibi E. Early targeting events during membrane protein biogenesis in *Escherichia coli*. *Biochim Biophys Acta - Biomembr* [Internet]. Elsevier B.V.; 2011;1808(3):841–50. Available from: <http://dx.doi.org/10.1016/j.bbmem.2010.07.025>
108. Bercovich-Kinori A, Bibi E. Co-translational membrane association of the *Escherichia coli* SRP receptor. *J Cell Sc*. 2015;128(7):1444–52.
109. Bibi E. Is there a twist in the *Escherichia coli* signal recognition particle pathway? *Trends Biochem Sci. Elsevier Ltd*; 2012;37(1):1–6.
110. Voigts-Hoffmann F, Schmitz N, Shen K, Shan S-O, Ataide SF, Ban N. The structural basis of FtsY recruitment and GTPase activation by SRP RNA. *Mol Cell. Elsevier Inc.*; 2013 Dec 12 [cited 2014 Feb 4];52(5):643–54.
111. von Loeffelholz O, Knoops K, Ariosa A, Zhang X, Karuppasamy M, Huard K, et al. Structural basis of signal sequence surveillance and selection by the SRP-FtsY complex. *Nat Struct Mol Biol. Nature Publishing Group*; 2013 May [cited 2014 Jan 21];20(5):604–10. A
112. Estrozi LF, Boehringer D, Shan S-O, Ban N, Schaffitzel C. Cryo-EM structure of the *E. coli* translating ribosome in complex with SRP and its receptor. *Nat Struct Mol Biol. Nature Publishing Group*; 2011;18(1):88–90.
113. Batty TGG, Kontogiannis L, Johnson O, Powell HR, Leslie AGW. iMOSFLM: A new graphical interface for diffraction-image processing with MOSFLM. *Acta Crystallogr Sect D Biol Crystallogr*. 2011;67(4):271–81.
114. Winn MD, Ballard CC, Cowtan KD, Dodson EJ, Emsley P, Evans PR, et al. Overview of the CCP4 suite and current developments. Vol. 67, *Acta Crystallographica Section D: Biological Crystallography*. 2011. p. 235–42.
115. McCoy AJ, Grosse-Kunstleve RW, Adams PD, Winn MD, Storoni LC, Read RJ. Phaser

- crystallographic software. *J Appl Crystallogr.* 2007;40(4):658–74.
116. Emsley P, Cowtan K. Coot: Model-building tools for molecular graphics. *Acta Crystallogr Sect D Biol Crystallogr.* 2004;60(12 I):2126–32.
  117. Adams PD, Afonine P V., Bunkóczi G, Chen VB, Davis IW, Echols N, et al. PHENIX: A comprehensive Python-based system for macromolecular structure solution. *Acta Crystallogr Sect D Biol Crystallogr.* 2010;66(2):213–21.
  118. Gulbranson CJ, Ribardo DA, Balaban M, Knauer C, Bange G, Hendrixson DR. FlhG employs diverse intrinsic domains and influences FlhF GTPase activity to numerically regulate polar flagellar biogenesis in *Campylobacter jejuni*. *Mol Microbiol.* 2016;99(2):291–306.
  119. Bennett B, Kimball E, Gao M. Absolute metabolite concentrations and implied enzyme active site occupancy in *Escherichia coli*. *Nat Chem.* 2009;5(8):593–9.
  120. Steinchen W, Schuhmacher JS, Altegoer F, Fage CD, Srinivasan V, Linne U, et al. Catalytic mechanism and allosteric regulation of an oligomeric (p)ppGpp synthetase by an alarmone. *Proc Natl Acad Sci U S A.* 2015;112(43):13348–53.
  121. U. A. Bommer R. Jonemann, C. M. Spahn, F. J. Triana-Alonso, K. H. Nierhaus NB. Ribosomes and polysomes. *Subcell fractionation A Pract approach.* 1996;301:271–301.
  122. Schuhmacher JS. Investigating the Function and the Interaction Network of the Flagellare Regulator ATPase FlhG (Dissertation). 2015;
  123. Gao T, Shi M, Ju L, Gao H. Investigation into FlhFG reveals distinct features of FlhF in regulating flagellum polarity in *Shewanella oneidensis*. *Mol Microbiol.* 2015;98(3):571–85.
  124. Gulbranson CJ, Ribardo DA, Balaban M, Knauer C, Bange G, Hendrixson DR. FlhG Employs Diverse Intrinsic Domains and Influences FlhF GTPase Activity to Numerically Regulate Polar Flagellar Biogenesis in *Campylobacter jejuni*. *Mol Microbiol.* 2015;(2015):n/a-n/a.
  125. Matsumoto K, Kusaka J, Nishibori A, Hara H. Lipid domains in bacterial membranes. *Mol Microbiol.* 2006;61(5):1110–7.

## 6. Apendix

### Supplementary table

Table S1: Crystallographic table

	<i>Sp</i> FlhN1	<i>Cj</i> FlhG-ADP
<b>Data collection</b>		
Space group	C222 <sub>1</sub>	P6 <sub>1</sub> 22
Cell dimensions		
<i>a</i> , <i>b</i> , <i>c</i> (Å)	35.97 110.59 101.33	124.70 124.70 104.16
<i>a</i> , <i>b</i> , <i>g</i> (°)	90.00 90.00 90.00	90.00 90.00 120.00
Energy (keV)		
Resolution (Å)	48.54 - 2.00 (2.072 – 2.0)	47.94 - 2.8 (2.9 – 2.8)
<i>R</i> <sub>merge</sub>	0.05117 (0.620)	0.154 (0.894)
<i>I</i> / $\sigma I$	19.06 (3.05)	8.71 (1.58)
Completeness (%)	1.00 (1.00)	0.99 (1.00)
Redundancy	6.6 (6.8)	5.4 (5.3)
<b>Refinement</b>		
Resolution (Å)	48.54 – 2.00	47.94 – 2.8
No. reflections	14089	12183
<i>R</i> <sub>work</sub> / <i>R</i> <sub>free</sub>	21.8 26.0	21.4 23.8
No. atoms	1225	2104
Protein	1190	2037
Ligand	0	27
Water	35	40
R.m.s deviations		
Bond lengths (Å)	0.006	0.006
Bond angles (°)	0.79	0.75
Ramachandran (%)		
Preferred	99.00	94.50
Allowed	0.65	4.30
Outliers	0.35	1.20

**Table S2: Proteins found after Ni-NTA chromatography of *SpFlhF***

Protein	Coverage
30S ribosomal protein S4	37%
50S ribosomal protein L24	37%
50S ribosomal protein L18	25%
50S ribosomal protein L19	23%
50S ribosomal protein L4	18%

## Table of figures

Figure 1: Bacterial motility. Flagella mediated motility includes	1
Figure 2: Bacterial flagellum and Basal Body	3
Figure 3: The flagellar C-ring.	6
Figure 4: Flagellar gene transcription hierarchies	7
Figure 5: Bacterial flagellation patterns	8
Figure 6: Dual flagella system of <i>S. putrefaciens</i>	10
Figure 7: Domain architecture of FlhF and FlhG	14
Figure 8: Schematic model of the FlhF/FlhG cycle	15
Figure 9: Regulation of polar flagella number	17
Figure 10: Two models of the SRP-pathway targeting	20
Figure 11: Schematic regulation of the SRP-system during protein	21
Figure 12: Domains architecture und sequence alignments of FlhG	23
Figure 13: Purification of <i>Cj</i> FlhG and <i>Sp</i> FlhG	24
Figure 14: Crystal structure of <i>Cj</i> FlhG	26
Figure 15: ADP coordination	27
Figure 16: MTS of <i>Cj</i> FlhG	28
Figure 17: ATPase activity of FlhG from <i>S. putrefaciens</i> and <i>C. jejuni</i>	30
Figure 18: v/S characteristic of ATP-hydrolysis by <i>Cj</i> FlhG	31
Figure 19: Interaction of FlhF and FlhG from <i>C. jejuni</i> and <i>S. putrefaciens</i>	33
Figure 20: GTPase activity of FlhF	34

Figure 21: Interaction of <i>Sp</i> FliM and <i>Sp</i> FliN from the lateral and polar flagellar C-ring of <i>S. putrefaciens</i>	36
Figure 22: Interaction of <i>Sp</i> FlhG with the FliM <sub>1</sub> /FliN <sub>1</sub> complex	37
Figure 23: Interactions between FlhG and FliM <sub>1</sub> /FliN <sub>1</sub> is mediated by the ‘EIDAL’ motif.	38
Figure 24: Localisation of <i>fliM</i> , <i>fliY</i> and <i>fliN</i> genes in <i>C. jejuni</i> .	39
Figure 25: Interaction of FlhG, FliM, FliY and FliN from <i>C.jejuni</i>	40
Figure 26: Crystallization of FliN <sub>1</sub>	41
Figure 27: Crystallization of FliN <sub>1</sub>	42
Figure 28: Domain organization of FlhF	43
Figure 29: Purification of FlhF variants	45
Figure 30: Influence of <i>flhFΔN10</i> on the motility of <i>S. putrefaciens</i>	46
Figure 31: Interaction of FlhF-N32 with ribosomal proteins	47
Figure 32: FlhF associates with ribosomes in <i>S. putrefaciens</i>	48
Figure 33: The N-terminal 32 residues of FlhF interact with the SRP-RNA	49
Figure 34: The N-terminal residues of FlhF bind SRP-RNA	51
Figure 35: The B-domain of FlhF interacts with FliY and FliM/FliY	52
Figure 36: Compatibility of flagellar components from different organisms	53
Figure 37: Schematic overview of flagellation patterns determined by FlhG and FlhF	54
Figure 38: Regulatory cycle of FlhF and FlhF	56
Figure 39: C-ring composition in different organisms	58
Figure 40: The Working hypothesis of FlhG during formation of polar and peritrichous flagella patterns.	64
Figure 41: Working hypothesis of polar flagellation patterning determined by FlhF and FlhG	67



## Abbreviations

Standardized abbreviations, such as chemical symbols, SI units as well as the one- and three-letter code for amino acids and x for any amino acid as well as h for hydrophobic amino acid residues are used without further reference. All other abbreviations employed in this work are listed in the following. Bacterial species mentioned in the thesis are listed separately.

Å	Ångström ( $10^{-10}$ m)
ADP	adenosine diphosphate
ATP	adenosine triphosphate
Au	Absorption unit
au	atomic unit
c-di-GMP	cyclic diguanosine monophosphate
CCW	counter clockwise
CV	column volume
Da	Dalton ( $1.660538 \times 10^{-27}$ kg)
DNA	desoxyribonucleic acid
ESRF	European Synchrotron Radiation Facility
GAP	GTPase-activating protein
GEF	Guanine nucleotide exchange factor
GDP	guanosine diphosphate
GST	glutathione S-transferase
GTP	guanosine triphosphate
h	hours
HEPES	4-(2-hydroxyethyl)-1-piperazineethanesulfonic acid

HPLC	high performance liquid chromatography
IM	inner membrane
IPTG	isopropyl $\beta$ -D-1-thiogalactopyranoside
JCSG	Joint Center for Structural Genomics
LB broth	lysogeny broth
M	mol/litre
min	minute
MR	molecular replacement
MTS	membrane targeting sequence
NTA	nitrilotiracetic acid
OD	optical density
OM	outer membrane
PBS	phosphate buffered saline polymerase
PCR	polymerase chain reaction
PDB	protein data bank
PEG	polyethylene glycol
PM	plasma membrane
PMF	proton motive force
RNA	ribonucleic acid
RNC	ribosome-nascent chain complex
rpm	revelations per minute
SDS-PAGE	Sodium dodecylsulfate polyacrylamide gel electrophoresis
SEC	size exclusion chromatography

SIMIBI	<u>S</u> ignal recognition particle, <u>M</u> inD and <u>B</u> ioD,
SR	signal recognition receptor
SRP	signal recognition particle
T3SS	type III secretion system
TCA	trichloroacetic acid
TRIS	Tris(hydroxymethyl)aminomethane
UV	ultraviolet

# Acknowledgments

First of all, I would like to thank Dr. Gert Bange for not only giving me the opportunity to pursue my PhD in his group, but also for his continuous support and encouragement throughout my work.

I am very grateful for collaborations with Prof. Dr. Kai Thormann from the (Department of Microbiology, Justus-Liebig University, Gießen) and Prof. Dr. David Hendrixson (Department of Microbiology, UT Southwestern Texas).

I am very thankful to Jan Schuhmacher and Wieland Steinchen for their support and contribution to the project and for a collaborative atmosphere and work during my time in the lab.

I also thank to the whole Bange group: Magdalena Rackwalska-Bange, Wieland Steinchen, Florian Altegoer, Patrick Pausch, Jan Schuhmacher and Devid Mrusek for a nice working atmosphere, many exciting discussions and events in, around and outside the lab. Furthermore, I would like to thank all present and former members of the Graumann group for their friendly atmosphere during my PhD time.

Many thanks go to Wieland Steinchen and Patricia Bedrunka for proofreading.

